Development of Novel Acoustic Emission Based Methodology and Tools for Bearing Fault Diagnostics

BY

BRANDON EDWARD VAN HECKE
B.S., University of Illinois at Chicago, IL, 2010

THESIS

Submitted as partial fulfillment of the requirements
for the degree of Doctor of Philosophy in Industrial Engineering and Operations Research
in the Graduate College of the
University of Illinois at Chicago, 2015

Defense Committee:

David He, Chair and Advisor
Jeremiah Abiade, Mechanical and Industrial Engineering
Eric Bechhoefer, Green Power Monitoring Systems, LLC
Houshang Darabi, Mechanical and Industrial Engineering
Lin Li, Mechanical and Industrial Engineering

This dissertation is dedicated to my parents, Edward and Cynthia, for their love and support, and always instilling the importance of higher education.

ACKNOWLEDGMENTS

I would like to thank my advisor, Dr. David He, for his guidance and support throughout the duration of my graduate studies. His expertise, technical, and editorial advice was essential to my success as a graduate student and completion of my dissertation and various publications.

Additionally, I want to convey gratitude to my committee members – Dr. Jeremiah Abiade, Dr. Houshang Darabi, and Dr. Lin Li – for their unwavering support, suggestions and assistance. I also want to thank Dr. Eric Bechhoefer, for the technical suggestions that helped improve and concretize my ideas in the inceptive stages of my research.

Lastly, I want to express appreciation to my colleagues, Dr. Yongzhi Qu, Dr. Jae Yoon, and Dr. Junda Zhu for the countless of hours of help with data collection and intellectual conversations that aided in the implementation of some of the results and ideas presented herein.

BVH

CONTRIBUTION OF AUTHORS

Chapter 1 is an introduction to bearings, condition-based maintenance and acoustic emission. Chapter 2 is a literature review covering the state of the art techniques available for bearing fault diagnostics. Chapter 3 provides motivation for the research presented herein. Chapter 4 presents the methodology used for the results shown in Chapter 6. The majority of the content is composed of previously published work (Van Hecke, B., Qu, Y., and He, D., 2014, "Bearing fault diagnosis based on a new acoustic emission sensor technique", *Proceedings of the Institution of Mechanical Engineers Part O: Journal of Risk and Reliability*, Vol. 229, No. 2, DOI: 10.1177/1748006X14558900.; Van Hecke, B., He, D., and Qu, Y., 2014, "On the use of spectral averaging of acoustic emission signals for bearing fault diagnostics", *ASME Journal of Vibration and Acoustics*, Vol. 136, No. 6, DOI: 10.1115/1.4028322.) for which I was the first author. My advisor, Dr. David He supervised the research and edited the manuscripts and Dr. Yongzhi Qu aided in collection of the data. Chapter 5 presents the experimental setup for the research presented in this dissertation. Chapter 6 presents the results of multiple case studies. Section 6.1 and 6.2 present the data used for the results in this dissertation. Section 6.3, 6.5 and 6.6 are results from the aforementioned publications and section 6.4 presents results from another previously published manuscript (Van Hecke, B., Qu, Y., He, D., and Bechhoefer, E., 2014, "A new spectral average-based bearing fault diagnostic approach", *Journal of Failure Analysis and Prevention*, Vol. 14, No. 3, pp. 354– 362.) in which Dr. David He supervised the research and edited the manuscript, Dr. Yongzhi Qu assisted in data collection and Dr. Eric Bechhoefer suggested the investigation of Welch's method. Section 6.7 and 6.8 are unpublished investigations on low speed bearing diagnostics using AE sensors and planet gear carrier fatigue crack detection on a UH-60A helicopter using accelerometer data. Finally, Chapter 7 provides a synthesis of the research presented in this dissertation.

TABLE OF CONTENTS

LIST OF TABLES

LIST OF FIGURES

SUMMARY

Acoustic emission (AE) has proven to be an effective nondestructive technique to investigate the behavior of material under mechanical stress. Compared with vibration techniques, AE offers several advantages. For example, AE techniques are capable of incipient fault detection. Additionally, it is sensitive to fault location, allowing its use for fault location detection. When applied to rolling element bearings, it has been shown that AE techniques can detect faults earlier than other technologies (Mba and Rao, 2006; Yoshioka and Fujiwara, 1982). However, there are a number of challenges in the implementation of AE techniques. Namely, in comparison with vibration sensors, AE sensors require a much higher sampling rate. Additionally, it requires significant storage and imposes a computational burden when the volume of data is large. Lastly, the non-stationary behaviors of AE signals make traditional frequency analysis methods ineffective.

In this research, novel AE based methodology and tools are developed that combine a heterodyned based frequency reduction technique, time synchronous resampling, and spectral averaging for bearing fault diagnostics. AE signals from seeded fault bearings are acquired simultaneously with a tachometer signal using a frequency reduction technique on a bearing test rig. Using the crossing times of the tachometer, the signal is time synchronously resampled and spectrally averaged. Finally, after computation of several condition indicators (CIs), bearing fault diagnosis can be achieved.

SUMMARY (continued)

For experimental purposes, a data acquisition system was developed to enable the testing of the proposed methodology. For validation, steel type 6205-2RS bearings were seeded with inner race, outer race, cage, and ball faults for data collection. Then, both AE and accelerometer data was acquired and processed to validate the fault diagnosis capability of the proposed methodology. The results indicate that the proposed signal processing technique efficiently and effectively detects all of the various bearing fault types at both high and low shaft speed ranges. The outcome of this research is effective and efficient methodology and tools that extract bearing fault features for bearing fault diagnosis with validation using the AE and accelerometer signals of seeded fault bearings.

The contributions of this research include:

(1) Development of effective physics based methodology and tools for bearing fault diagnostics using AE sensors. This methodology is developed based on spectral averaging and is the first attempt in applying a synchronous resampling based spectral averaging approach to quantify the AE signals for bearing fault diagnostics. Additionally, Current AE based bearing fault diagnostic methods are mainly based on data-driven approaches (He *et al.*, 2011; Li *et al.*, 2012).

(2) Development of efficient AE based bearing fault diagnostic methodology and tools. This methodology allows the AE signals to be sampled at a low sampling rate that is comparable to vibration techniques. Current AE based fault diagnostic methodologies use high sampling rates up to 10 MHz.

SUMMARY (continued)

(3) Validation of the developed AE based bearing fault diagnostic methodology and tools using steel bearings tested at low (2 – 10 Hz) and high speed (> 10 Hz) applications. The diagnosis of all 4 bearing fault types in the low shaft speed range has not been reported in literature.

(4) The methodology is validated for all 4 types of bearing faults: inner race, outer race, cage, and ball. The current averaging based bearing diagnostic literature reported only inner race or outer race fault detection (McFadden and Toozhy, 2000; Siegel *et al*., 2012).

(5) Current TSA based bearing fault diagnostic literature requires the need for multiple TSAs (McFadden and Toozhy, 2000; Siegel *et al*., 2012). By implementing a spectral averaging approach, the need for multiple TSAs is eliminated and potential bearing slippage and fluctuations in shaft speed are accounted for.

(6) The methodology has been extended and validated for high speed bearing fault diagnosis using accelerometer data. A comparison on the effectiveness of the methodology using AE and vibration data has been conducted which has not been reported in literature.

(7) The methodology has been extended and validated for vibration based planet gear carrier fatigue crack detection for test cell and on-aircraft UH-60A helicopter data. Successful results for on-aircraft data have not been presented in literature.

1. INTRODUCTION

1.1 Rolling Element Bearings – A Brief Introduction

A rolling element bearing is a bearing in which rolling elements, typically in the form of rolling balls, are confined between two bearing rings called the inner and outer races. Rolling element bearings typically consist of the inner and outer raceways, the rolling balls, and the cage which limits the balls from sliding from their intended path. Figure 1.1 presents the components of a rolling bearing. Rolling bearings are constructed in such a way, that the balls can rotate with little resistance, while keeping them in their designated path. One of the earliest known applications of rolling element bearings consisted of a set of logs below a large sheet of stone. As the stone was moved, the logs would rotate, allowing the effective relocation of very heavy objects. Bearings can be found in numerous mechanical devices from the wheels of cars to virtually any mechanical object that has any type of rotational motion.

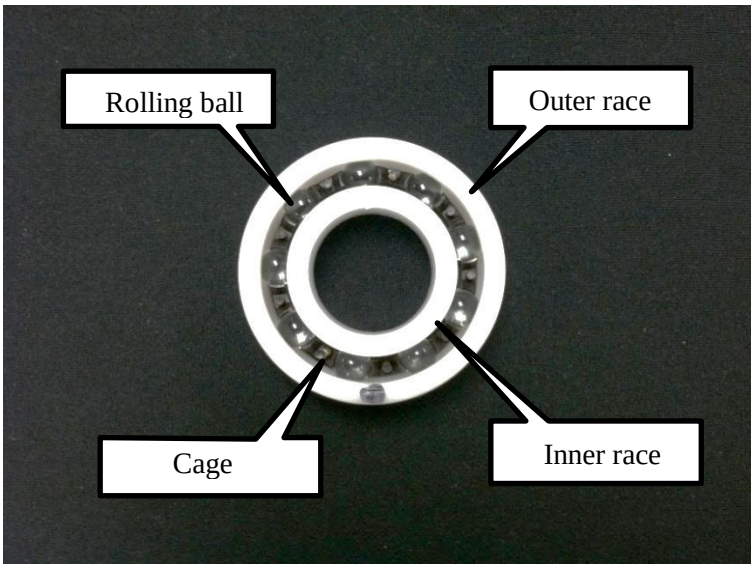

Figure 1.1. Components of a rolling bearing

Rolling element bearings can be found in different forms, varying the size, weight, load capacity, durability, frictional capacity, etc. They typically are designed to find the proper tradeoff of the above features that allow the job they are intended to accomplish to be achieved efficiently. Such bearings are composed of many different materials such as plastic, steel, ceramic, or even hybrids of the above. Additionally, rolling element bearings can contain lubricants such as oil to reduce heat and friction. However, bearings such as the type 6205-RS plastic bearings used in the food industry do not contain such lubricants. The material composition and parameter design is selected based on the intended use of the bearing. For example, steel bearings are commonly used in automobiles and heavy machinery while plastic bearings have common uses in the food and medical industries.

Rolling element bearings can vary in size and load capacity. The inner and outer races are typically designed with grooves such that rolling balls have a slightly loose fit. They are designed this way to keep them in a narrow path, but simultaneously limiting the ball contacts to limit friction. Additionally, cages are often implemented to prevent the balls from rubbing against one another. Besides preventing the contact between other balls, cages also reduce friction, wear, and increase the useful life of the bearing.

1.2 Bearing Fault Diagnosis and Condition-Based Maintenance

Most machines and mechanical devices that have any moving components are likely to contain at least some type of bearing. Over time, these bearings can fail for varying reasons from both natural causes and user related issues. In fact, it has been reported that roughly 40-50% of bearing failure is the result of improper lubrication, 25-30% improper mounting, 20% from other causes, and less than 10% from reaching the natural fatigue limit (Applied Industrial

Technologies, 2009). This clearly indicates that the majority of bearing failures are caused by the user and other modes of failure that are not the result of the intended design, resulting in numerous instances where failure could have been prevented. More recently, it was reported that the global demand for bearings is projected to rise 7.3% annually to $104.5 billion in 2018 (bearing-news, 2014). Considering the above, it is clear that there is both a significant global demand for bearings, and a major source of failure is due to improper maintenance or the lack of. Thus, if bearings could be monitored and maintained, the remaining useful life could be maximized, possibly resulting in the reduction of significant repair/replacement expenditures. Hence, the development of methodology and tools that facilitate the maintenance and detection of bearing faults in the propagation stage has the potential to make a global impact in the industry.

Because rolling element bearings typically are implemented in non-ideal working environments, minor problems can occur that can cause them to fail much quicker than designed. Such harsh conditions include various factors such as fatigue, wear, improper use or installation, lack of lubrication, harsh environmental conditions, etc. The introduction of such harsh conditions can equate to the development of abrasion, fatigue, and other types of bearing faults. Abrasion can occur when contaminants enter the inside of the bearing or get mixed in the lubricant. When this occurs, such contaminants can scrape any of the interior components of the bearing. Although bearings are designed to have a specific lifespan, the introduction of harsh conditions can cause the parts of the bearing to wear out or fatigue. When this occurs, the bearing can fail much earlier than intended. Such conditions can cause failure or fault development in one or more of the bearing components.

Much research has been developed concerning the fault detection and diagnosis of rolling element bearings. One successful implemented strategy in the field of machine fault diagnosis is condition-based maintenance (CBM). In CBM, the health condition of the machine is observed via a health monitoring system. The output of the health monitoring schedule can suggest when maintenance on a given machine is required. However, before CBM can be implemented, efficient and effective fault diagnosis tools need to be developed. Thus, the development of such tools is the focus of this research.

To develop fault diagnostic tools, a number of tasks need to be accomplished. The first is data acquisition. This is typically accomplished through the use of sensors that can collect parameters such as acoustic emission, vibration, temperature, pressure, and so on. For bearing fault diagnosis, traditional sensors include vibration and speed sensors. Recently, newer sensors such as the acoustic emission sensor have gained attention. This research focuses on AE signals and their use for bearing fault diagnosis.

Once the data is acquired, the next step is to extract and process the signals. In a working environment, the acquired signals typically contain a lot of noise. To extract the fault signal, various techniques have been utilized. Such developed techniques include the Hilbert transform, power spectral density, time synchronous averaging (TSA), and wavelet analysis among others. Various techniques have been applied to both vibration and acoustic signals.

Lastly, after the data is acquired, and useful signal extracted, the condition of the bearing needs to be determined. Many data-driven methods such as data mining and neural networks have been shown to be effective for bearing fault diagnosis (He *et al.*, 2011a). However, these methods require a significant amount of training data for their successful implementation. A

different approach would be to move in the direction of online fault diagnosis, in which the condition can be determined without the need to train a model with known faulty information. To move in this direction, physics based approaches such as TSA can be investigated.

To date, most bearing fault diagnosis systems are based on vibration signals, although other approaches have been investigated. A detailed literature review of vibration, AE and other bearing fault diagnostic techniques is provided in section 2.

1.3 AE Detection and Challenges

Acoustic emission (AE) has proven to be an effective nondestructive technique to investigate the behavior of material under mechanical stress. AE is commonly defined as transient elastic waves within materials that are caused by localized stress energy. These waves are short lived bursts of energy that are caused by a sudden internal change of state within a material. All materials have specific elastic properties. Any imposed force on a material can cause strain or compression and the elastic properties determine how that material will return to its original condition. When a crack propagates, a rapid release of energy called an AE event occurs. This AE event corresponds to an AE burst signal in the collected data. Figure 1.2 presents some AE bursts excited by a bearing seeded with a cage fault at a shaft speed of 15 Hz.

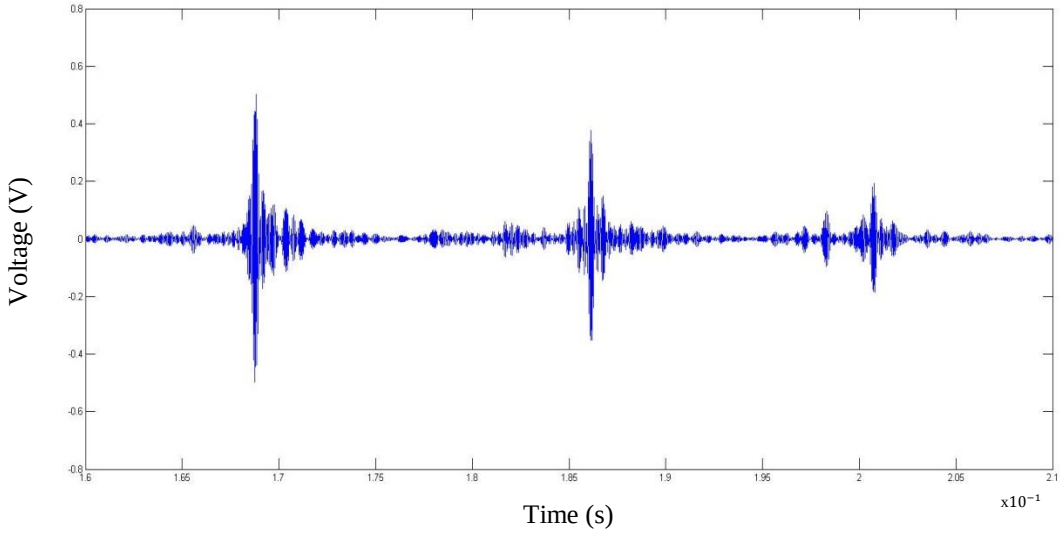

Figure 1.2. Example of an AE burst signal

The defects caused under stress are what generate the AE event. Using an AE sensor, the AE events can be measured, recorded, and processed for analysis. Typically, an AE system contains an AE sensor, preamplifier, and a data acquisition (DAQ) board. The AE sensor converts the mechanical movement of the material into an electrical voltage signal. The preamplifier amplifies the voltage output before the signal is fed to the DAQ board, and is also intended to reduce the background noise. The location of the sensor results in a delay, or arrival time, of the AE burst. By measuring this delay and the amplitude of the burst, the burst location can be approximated. Figure 1.3 shows the typical AE signal features used for analysis. Amplitude is the greatest measured voltage of the waveform. Rise time is the time interval between the first threshold crossing and the peak of the signal. The duration is the time between the first and last threshold crossings. Lastly, counts refer to the number of times the signal amplitude is greater than the threshold.

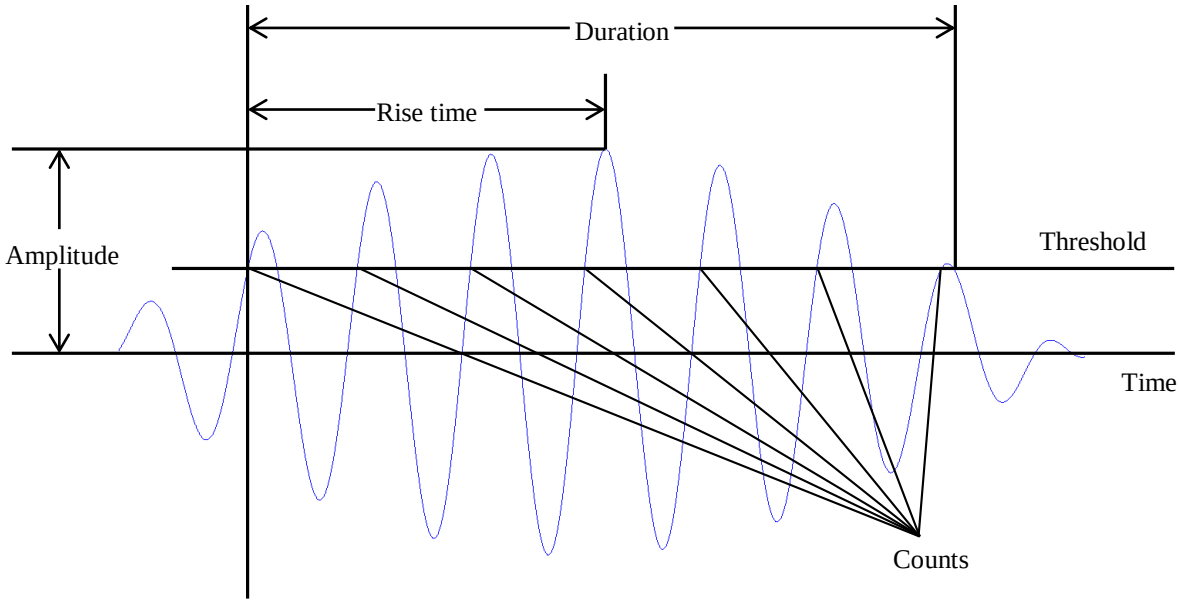

Figure 1.3. AE signal features

When applied to rolling element bearings, it has been shown that AE techniques can detect faults earlier than other technologies (Mba and Rao, 2006; Yoshioka and Fujiwara, 1982). Compared with vibration centered approaches, AE offers several advantages. For example, AE techniques are capable of incipient fault detection. Additionally, it is sensitive to fault location, allowing its use for fault location detection. Also, AE sensors can retrieve information in frequencies that are much higher than vibration signals. However, there are a number of difficulties in the implementation of AE techniques. Namely, in comparison with vibration sensors, AE sensors require a much higher sampling rate (typically above 1MHz). Additionally, it requires significant storage and imposes a computational burden when the volume of data is large. Lastly, the non-stationary behaviors of AE signals make traditional frequency analysis methods ineffective.

1.4 Objective

This research is emphasized on the development of AE based bearing fault diagnostic tools explores the potential of future applications of AE based techniques for bearing fault diagnosis in industry. These tools are developed with the goal of creating efficient and low cost diagnostic techniques that could be realistically applied in a commercial environment.

For experimental purposes, a bearing test rig was developed and constructed in the Intelligent Systems Modeling and Development Laboratory. Moreover, a data acquisition system was designed to enable the testing of the proposed methodology. Multiple type 6205-2RS steel bearings were seeded with the various fault types that have been observed and established in prior research and industry. Additionally, AE and accelerometer data was acquired and processed to validate the fault detection and diagnostic ability of the implemented methodology. The results indicate that the proposed signal processing technique efficiently and effectively detects all of the various bearing fault types, allowing fault diagnosis to be accomplished. The outcome of this research is effective and efficient methodology and tools that extract bearing fault features for bearing fault diagnosis with validation using the AE and accelerometer signals of seeded fault bearings. Validation was conducted at both low (2 – 10 Hz) and high (> 10 Hz) shaft speed ranges. Additionally, this research determined the quantitative relationship between the features of the various fault types that are common amongst instances of bearing failure as well as completed a comparative evaluation of AE against vibration centered techniques. This research was also extended for planet gear carrier fatigue crack detection for the UH-60A helicopter using test cell and on-aircraft vibration data.

1.5 Outline

The remainder of this dissertation is structured as follows. Section 2 provides a detailed literature review of the current state of the art AE based bearing fault diagnostic techniques as well as vibration and microphone centered approaches and a review on low speed bearing analysis. Also, a review on UH-60A helicopter planet gear carrier fatigue crack detection techniques using vibration sensors is provided. Section 3 presents the motivation as to why this research should be conducted. In Section 4, the proposed methodology is explained in detail. Section 5 presents the experimental setup and explanation of the data collected. Lastly, section 6 presents the validation results and section 7 concludes this dissertation.

2. LITERATURE REVIEW

2.1 Acoustic Emission Based Bearing Fault Diagnostics

(Parts of the literature review in this chapter were previously published as Van Hecke, B., Qu, Y., and He, D., 2014, "Bearing fault diagnosis based on a new acoustic emission sensor technique", *Proceedings of the Institution of Mechanical Engineers Part O: Journal of Risk and Reliability*, Vol. 229, No. 2, DOI: 10.1177/1748006X14558900. and Van Hecke, B., He, D., and Qu, Y., 2014, "On the use of spectral averaging of acoustic emission signals for bearing fault diagnostics", *ASME Journal of Vibration and Acoustics*, Vol. 136, No. 6, DOI: 10.1115/1.4028322.)

2.1.1 Acoustic Emission – An Alternative to Vibration Analysis

Acoustic emission (AE) is the generation of transient elastic waves resulting from a rapid release of strain energy caused by a deformity or damage propagation within or on the surface of a material under physical stress. Through non-destructive testing, AE has been proven to be a critical tool for condition monitoring, which has resulted in studies that examine the use of AE for the early detection of machine faults. However, the cost and difficulty of analyzing AE data has limited its application in the industry. For years, vibration analysis has long been established in the field of machine condition monitoring. It has successively been applied to the detection of faults, and many approaches of analysis have been validated. As compared with AE data, vibration signals require a much lower sampling rate, making it cheaper to process and interpret. This equates to a lower cost alternative as opposed to the computational burden of AE analysis that is resultant of sampling rates as high as several MHz. Also, one disadvantage of vibration analysis is that by the time a significant change in the signal is observed, the remaining useful life has been significantly depleted. AE covers a wide frequency range (100 kHz to 1 MHz) and has been proven to be effective in the earlier detection of damage propagation. To date, the

analysis of AE signals for machine fault diagnosis is currently a topic of interest in the field of condition based maintenance.

Traditional AE parameters and diagnostic approaches have been well developed and reviewed comprehensively in the literature (Mba and Rao, 2006). In the application to rotating machinery diagnosis, it has been shown that effective AE parameters include amplitude, rms, kurtosis, crest factor, energy, counts, and events (Mathews, 1983). As mentioned previously, the frequency range of AE signals is so vast that it is difficult to analyze and has prevented the widespread success of its use in the field of condition based maintenance. However, the ability for earlier fault detection and non-destructive testing has made AE a current topic of interest among researchers.

2.1.2 Acoustic Emission – A Bearing Diagnostic Tool

Many Studies have been conducted that monitor the AE response of bearings containing defects. When production is complete, and bearings are implemented in industry, various stress factors cause failures and decrease their remaining useful life. Examples of such factors include poor maintenance, improper lubrication schedules, incorrect installation or application, and harsh environmental conditions. These factors can result in bearing failures such as spalling, pitting, bearing seizure, etc. Because AE methods can detect damage at the early stage of development, its use as a bearing diagnostic tool has been a topic of investigation and nearly all research on this topic has been completed through the use of experimental test rigs.

One of the first known studies that applied AE analysis to the detection of incipient failure in bearings utilized the AE counts per unit of time resulting from an experimental rig with bearings containing artificially seeded faults (Balderston, 1969). The investigated fault types were inner race, outer race, and ball defects, as well as the absence of proper lubrication.

Balderston (1969) sought to make the comparison between vibration and AE signals in their respective frequency ranges. He also noted that continuous AE features could be observed in bearings containing a low level of lubrication, and burst AE features could be attributed to the artificially seeded defects on both the inner and outer races as well as the rolling elements. A decade later, AE was applied to investigate the condition of slowly rotating anti-friction bearings utilized on cranes that were implemented for gas production (Rogers, 1979). Due to the low speed of the bearings and the low frequency range of vibration analysis, such techniques were found to be ineffective in that type of implementation, and it was concluded that AE analysis was more informative.

Later, another study made the conclusion that signals obtained in the AE frequency range were indicative of bearing defects as opposed to other problematic sources such as misalignment and improper balance (Catlin Jr., 1983). It was also found that since AE signals diminish rapidly, if the transducer is applied in a location close to the bearing, high frequency content resulting from bearing faults could be detected. Other researchers have shown that AE parameters were able to identify bearing defects before their appearance in the vibration range (Yoshioka and Fujiwara, 1982 and 1984). Additionally, this research combined AE features and vibration signals to afford the ability to measure the duration of crack propagation resulting from bearing fatigue tests. This led to an investigation that used the AE technique for the detection of subsurface cracks resulting from rolling contact fatigue (Yoshioka, 1992). The method provided the ability to determine the position of sub-surface fatigue cracks by relating the crack positions to the location of the AE signal source.

Other researchers have focused on combining AE and pattern recognition techniques for the early detection of bearing faults (Li and Li, 1985). This study was conducted by seeding

faults on the roller and outer race. It was shown that AE events occurring at a rate equivalent to the bearing defect frequency provided enough evidence to determine the presence of a defect. Although the study could not achieve results for the rolling element, results for the outer race were presented. However, it should be noted that this was the first attempt to utilize AE for roller defect diagnosis.

The conclusions of Yoshioka (1982 and 1984) were later validated in a study that also made the observation that AE techniques are able to detect bearing faults earlier than vibration analysis methods (Hawman and Galinaitis, 1988). This study obtained results by applying the transducer directly on the bearing outer race, and the conclusion was made by modulating the high frequency AE bursts that occurred at the defect frequency of the outer race. By the early 90's, there were a number of studies that involved the use of AE analysis as a tool for bearing diagnostics. Bansal *et al*. (1990) sought to investigate the quality of ball bearings using the AE technique, with the goal of making a comparison with the results when using shock impulse testing. The study was concerned with the use of AE analysis as a quality inspection tool to classify new versus reconditioned bearings. The conclusion was made that both methods were suitable for quality inspection purposes and that bearing conditions could be categorized using AE techniques. Additionally, it was shown that the peak to peak amplitude level for both new and reconditioned bearings did not significantly increase as the loading increased; however, it was noted that in some cases, the peak values of reconditioned bearings were five times that of a new bearing.

Another study used a resonant type transducer to investigate outer race faults by utilizing the peak amplitude and AE count parameters (Tandon and Nakra, 1990). This study incorporated the use of increasing loads and rotational speeds, and it was found that AE counts

were only capable for fault detection when defects were less than 250μm. However, it was also shown that peak amplitude could be utilized for this purpose regardless of the size of the defect. Around the same time period, another study developed a variation of the AE count parameter for fault diagnosis of different sized ball bearings (Tan, 1990). This study not only established a threshold level for AE counts, but also showed that the value of the count is dependent on the AE signals frequency and that the rate of the count is reliant on the amplitudes of AE pulses.

The aforementioned research led to a study that compared the use of current vibration and AE techniques for bearing fault identification (Tandon and Nakra, 1992). It was shown that inner race defects were best identified by measuring AE counts when compared to using the AE peak amplitude or vibration envelope methods. However, it was also noted that AE counts from inner race defects decrease rapidly as the bearing load is increased. For outer race detection, the envelope method provided the best results for high loading conditions, and in the case of low rotational speeds AE counts is the dominant method. Lastly, for ball defect detection, it was shown the best results were achieved using the AE peak amplitude technique. This comparison was later updated by comparing additional diagnostic developments such as vibration methods in both the time and frequency domains, alternate signal processing methods such as the high-frequency resonance technique, as well as AE measurement techniques and newer developments such as wavelet transforms (Tandon and Choudhury, 1999). This study presented the strengths and weaknesses of the various methods, with emphasis on vibration methods which have been widely accepted in the industry. In regards to AE analysis, the reiteration that some studies have shown the ability to detect faults before vibration analysis was noted. Also suggested was the use of demodulated AE signals for bearing defect detection and that the direction of the research has shifted towards a focus on pattern recognition methods and other data driven techniques.

Around the same time period, Yoshioka *et al.* (1999) developed a method to measure the time intervals of acoustic emission generation for the diagnostics of rolling bearings. It was found that the AE counts per minute began to increase hours before a significant increase in vibration rms levels was observed. However, the AE count method was found to be highly dependent on the threshold set by the experimenter. A year later, another study simulated faults in the roller and inner race using the spark erosion method (Choudhury and Tandon, 2000). This investigation looked at both healthy and defective bearings of various sizes. It was shown that for small defect sizes, ringdown counts of the AE signal provided the ability for fault detection on both the inner race and roller of the tested bearings. However, it was also observed that counts ceased to increase after a certain defect size, and thus, counts could no longer provide any information on the progression of the fault. It was also found that as fault size increases, more events occur and both peak amplitudes and ringdown counts also tend to increase.

Another study modified an experimental test rig so that artificially seeded faults could be applied to both the inner and outer races of the test bearing (Morhain and Mba, 2003; Mba, 2003). The modified rig contained a significant amount of acoustic emission noise which provided a realistic atmosphere for diagnostic testing. The diagnostic features used for this study included amplitude, rms, energy, and AE counts. The results of the study concluded that rms and count values were robust methods capable of bearing fault detection. It was also noted that rms and energy tended to correlate with increases in speed, load, and the size of the fault. Additionally, it was validated that although AE maximum amplitude tended to increase with speed, it did not correlate with load and defect size. It was also noted that the threshold level should be at least 30 percent of the lowest speed and operating conditions; however, it was suggested that there is no threshold level that can be applied successfully for all operating

conditions. In addition to validating the work of Choudhury and Tandon (2000), the results contradicted the conclusions of Tandon and Nakra (1990). It was concluded that AE counts could be used for fault detection for lengths up to 15 mm and widths of 1 mm.

Later, a study was conducted that focused on the use of the AE technique for the determination of defect sizes within radially loaded bearings (Mba, 2008). This study focused on bearings with outer race seeded defects of various sizes. The contribution was the relation of fault size with AE burst duration. The conclusion was made that as the length of the fault was increased, an increase in burst duration was observed. Another study focused on the extraction of the characteristic frequency of the bearing from the AE signal (He *et al.*, 2009). This study explored the used of standard parameters of the signals to explore the source characteristics and sensitivity of the bearing faults. Then, another study was conducted that investigated bearing fault diagnosis of machines rotating at 100 rpm or less (Sako and Yoshie, 2010). This research proposed methods for on-site fault diagnostics based on the AE envelope waveform. It was shown that the proposed method was successful at speeds as low as 1 rpm.

By 2011, the cyclostationarity vibration analysis technique, a method based on statistical moments, had been validated to be advantageous for bearing defect diagnosis. A study was conducted that investigated the cyclostationarity of AE signals observed from a faulty bearing (Kilundu *et al.*, 2011). Using a tool that determines the presence of cyclostationarity called cyclic spectral correlation, a comparison was made to the traditional envelope spectrum technique. The results indicated that cyclic spectral correlation was most efficient for small outer race defects and ineffective for inner race defect detection. It was also proposed that the cyclostationarity method was more sensitive when compared to traditional features such as rms, kurtosis, and crest factor.

In the same year, another study was conducted that compared the applicability of AE and vibration technologies for the monitoring of rolling bearing degradation (Eftekharnejad *et al.*, 2011). This was the first know attempt to compare the use of the kurtogram and spectral kurtosis in both AE and vibration data from a faulty bearing. It was concluded that AE was more sensitive for incipient fault detection when compared to vibration. Also, the application of spectral kurtosis analysis and the use of the kurtogram were both shown to be effective for AE and vibration signals.

Other research has also made the vibration and AE comparison by testing the same defective bearing under three rotary speeds (Liu *et al.*, 2011). This research utilized the envelope analysis method for fault diagnosis. It was shown that as the rotation speed was reduced, the quality of the AE signal decreased much quicker than the vibration signal. It was also noted that before an AE sensor is implemented to industrial machinery, comes the need to reduce the amplitude of the high frequency component of the AE signal. The research also resulted in the conclusion that the AE method is superior to vibration at high speeds; however, vibration may be a better alternative in low speed applications.

Other researchers have focused on the application of AE technology as a diagnostic tool for full ceramic bearings. Previously, research in the area had mainly focused on steel ball bearings. This research resulted in the development of AE based condition indicators (CI) for full ceramic bearing fault detection and diagnosis (He *et al.*, 2011a; He *et al.*, 2011b; Li *et al.*, 2012). This method, based on the Hilbert Huang transform (HHT), extracted AE features using the empirical mode decomposition (EMD) method to obtain intrinsic mode functions (IMF) and develop CIs from AE burst signals (He *et al.*, 2011b). Then, the CIs were used to establish a data mining based fault classifier utilizing the *k*-nearest neighbor (KNN) algorithm. Full ceramic

bearings were seeded with outer race, inner race, ball, and cage faults. The AE features used in this research were rms, kurtosis, and peak value. These features were extracted from the IMFs created from the EMD method. The results indicated that the group average of kurtosis provided the lowest classification error; however, no individual CI was able to achieve classification accuracy over 90%. Additionally, it was found that classification accuracy can be significantly improved if a combination of individual CIs is utilized. The best combination found was the group average of rms and standard deviation of rms, resulting in classification accuracy over 92%. It was also noted that the new technique was comparable to the performance of a neural network based algorithm.

More recently, a study was conducted that developed parameters in order to reduce the required amount of data (Nienhaus *et al.*, 2012). The goal of the research was to reduce the necessary amount of data such that the online monitoring of slowly rotating roller bearings could be managed more efficiently. Using the AE parameters rise time and fall time, a threshold level was established and AE burst information was retained while making a significant reduction in the size of the data file. Then, utilizing the normalized regression curve of an AE burst, the new parameter was developed. It was shown that using the two characteristics, it is possible to separate inner race from outer race damage, and the maintenance of slow rotating machines using the method is achievable.

Another study developed an intelligence diagnostic method for bearing fault detection using a combination of principal component analysis, rough sets, and a back propagated neural network (Pan *et al.*, 2012). Using a normalized AE signal, 15 symptom parameters such as mean value, rms, etc. were calculated. Then, principal component analysis was implemented on the symptom matrix to reduce the number of parameters, and rough set theory applied to establish

classification rules. Lastly, a back propagated neural network was implemented to accurately distinguish between the various bearing fault types. More recently, another study investigated the approximate entropy analysis of the AE from various defects in rolling element bearings (He and Zhang, 2012). The results provided an effective feature parameter of the AE signal to use for bearing defect detection.

2.2 Vibration Based Bearing Fault Diagnostics

2.2.1 Vibration Analysis

Presently, the quantification of vibration sensor output is the industry standard for bearing fault detection and diagnosis. This area of research has resulted in many advances in the bearing fault diagnostic field. For example, it has been shown that both wavelet analysis and the Fast Fourier Transform (FFT) combined with envelope detection can efficiently detect some of the known types of bearing faults (Tse *et al.*, 2001). Moreover, the combination of wavelet analysis with the Fourier transform has been shown to be more effective than either method employed alone (Yan *et. al.*, 2009). Other data driven methods such as empirical mode decomposition (EMD) has also resulted in the successful extraction of bearing fault features using a series of intrinsic mode functions (IMFs) (Lei *et al.*, 2008; He *et al.*, 2012b). Some researchers have sought to investigate the integration of different bearing fault diagnostic techniques and have shown improvements in both diagnostic accuracy and robustness of the diagnosis system (Wei and Zhan-Sheng, 2009). More recently, Mutual information based feature selection has also been shown to yield promising bearing fault classification results (Kappaganthu and Nataraj, 2011) and another study used kurtosis-based adaptive bandstop filtering to achieve bearing fault diagnosis results for low signal-to-noise and signal-to-interference environments (Zhang, *et al.*, 2013). In addition to the advancement of diagnostic algorithms, some researched have sought to improve the sensors used to collect the bearing

signals. For example, one study developed a new accelerometer that was proven effective for low speed roller bearing monitoring (Hou *et al.*, 2010).

Recently, a new version of the Lempel-Ziv complexity was developed based on the continuous wavelet transform (Hong and Liang, 2009). This technique was shown to effectively measure the severity of both inner and outer race faults. Another study presented a rolling bearing fault diagnosis technique based on correlation matching (Liu *et al*., 2012). In this study, the method parameters were optimized using maximum kurtosis criteria and minima smoothness index. It was shown that although the approach is effective in the extraction of bearing fault impulses from noisy bearing vibration signals, it was unsuitable for the vibration signal at varying rotating speeds. The research methodology presented in this dissertation is shown to achieve bearing fault diagnosis while accounting for fluctuations in shaft speed. In (Cui *et al.*, 2014), matching pursuit, and its use for roller bearing vibration signal processing and fault diagnosis was also discussed. In this paper, an adaptive matching pursuit algorithm that utilizes a novel impulse dictionary was introduced. The new dictionary model improved the original model by incorporating the rotational speed of the bearing, fault size, bearing dimension, and other parameters.

Another recent development used an integrated autoregressive/autoregressive conditional heteroscedasticity model to characterize faulty bearing vibration signals (Wang *et al.*, 2012). The authors used the normalized model coefficients as feature vectors to allow the use of clustering for bearing fault classification. More recently, dynamic load analysis of a rotor-bearing system was used to develop a roller bearing fault signal model (Cong *et al.*, 2013). In this study, inner and outer race faults were investigated, and it was shown that the precision of a bearing fault signal model could be improved by incorporating the rotor system influence factor. An adaptive

wavelet stripping algorithm to extract simulated fault impact transients from an original bearing fault signal was proposed in (Wang *et al.*, 2013). The methodology presented in this paper was shown to extract the transients from fault signals with both low and high signal to noise ratios while reducing the computation time of the original wavelet stripping algorithm.

Recently, there have been several developments on the detection and diagnosis of bearing faults. One recent study presented a rolling bearing fault diagnosis approach using neural networks and a time/frequency-domain vibration approach (Li, B. *et al.*, 2000). This study showed that neural networks can aid in the diagnosis of various motor bearing faults using vibration data generated from a bearing test rig. Neural networks have also been shown to be effective for condition monitoring when using statistical-time features (Prieto *et al.*, 2013). Another study focused on rotating machinery in general and used a model-based approach for the detection and diagnosis of mechanical faults (Loparo *et al.*, 2000). This research developed a nonlinear filtering technique to address complex nonlinear vibration responses due to factors such as unbalance, changes in stiffness, and damping of the rotor bearing system. Validation of the aforementioned technique was accomplished via the use low signal-to-noise environment simulations. Another investigation presented a fault detection approach based on stator current monitoring for *in situ* bearing faults (Zhou *et al.*, 2008). In this paper, bearing fault features were extracted using a combination of noise cancellation and statistical process control techniques to detect out of control samples due to the degradation of lubrication starved bearings. Other research has presented a two-step data mining approach to classify defects in plastic bearings (He *et al.*, 2013). This study effectively used empirical mode decomposition (EMD) to extract time domain condition indicators (CIs) which were used as inputs in a supervised learning algorithm to classify bearing defects. Other studies have presented effective bearing

defect techniques through the use of local and nonlocal preserving projection (Yu, 2012), trace ratio linear discriminant analysis (Jin *et al.*, 2014), or the power spectral density (PSD) analysis of amplitude and frequency current-demodulated bearing signals for direct-drive wind turbines (Gong and Qiao, 2013).

2.2.2 Time Synchronous Average – A Brief Introduction

The field of condition based maintenance (CBM) has resulted in the development of various methods that aid in determining the condition of equipment, allowing maintenance decisions to be made based on that current condition. Development of effective equipment fault diagnostic tools is a key to the success of the CBM. One example of such developments is time synchronous averaging (TSA), a proven technique that extracts periodic waveforms for the analysis of vibration signals (Braun, 1975). The computation of TSA requires the knowledge of either the repetition frequency of interest, or a synchronous signal that is free of noise. Using either the repetition frequency or the synchronous signal, successive periods of the noisy signal can be sampled and averaged.

The application of synchronous averaging to the tooth meshing vibration of gears within a gear box has been well developed (McFadden 1987a; 1987b; 1991). It has been shown that by presenting the vibration signal as a function of the gears angle of rotation, a comparison can be made of healthy and presumably damaged teeth. To perform the TSA on the vibration of a gear, the rotation of the gear is synchronized with a trigger signal. This trigger signal allows for the determination of the zero crossing times needed to calculate the synchronous average. It has been shown that with the aid of the trigger signal, the zero crossing times can be calculated using various interpolation techniques (McFadden, 1989). Approaches of obtaining the trigger signal include the use of a tachometer, as well as a tachometer-less approach. The tachometer-less

approach uses the running speed and number of teeth on the gear to establish the one per revolution angular reference needed to simulate the trigger signal, which provides the zero crossing times and eliminates the need for a speed sensor (Combet and Gelman, 2007). Numerous TSA algorithms have been developed and documented that use alternative methods for establishing the zero crossing times (Bechhoefer and Kingsley, 2009). Additionally, the aforementioned authors have reviewed other TSA techniques, based on which zero crossing time interpolation approach was implemented.

2.2.3 Time Synchronous Average Applied to Bearing Fault Diagnostics

TSA has been widely applied to vibration analysis of gears. However, only a small number of applications to the fault detection of bearings exist. The first application as a diagnostic tool for bearings combined the high frequency resonance technique with synchronous averaging (McFadden and Toozhy, 2000). For a detailed review of the high frequency resonance technique, the readers are referred to the work of McFadden and Smith (1984). McFadden and Toozhy (2000) related the shaft rotation frequency f_r and bearing defect frequency f_i resulting from an inner race spall by:

$$f_i = [Z/2][1 + (D_e/D_p)\cos(ß)]\, f_r = Z(f_r - f_c) \tag{2.1}$$

where Z is the number of rolling elements, D_e the diameter of each rolling element, D_p the diameter of the pitch circle, ß the contact angle, and the cage rotation frequency represented by f_c.

A fundamental idea presented in the paper is that the envelope spectrum f of the signal contains lines at frequencies that are harmonics of the inner race defect frequency f_i. Additionally, it has been shown that these lines are surrounded by modulation sidebands that

occur at multiples of the shafts rotation frequency f_r (McFadden, 1984 and 1985). Combining this feature with the former allows for the relation:

$$f = mZ(f_r - f_c) + nf_r \tag{2.2}$$

which suggests that some of the previously mentioned spectral lines will occur at integer multiples of $f_r - f_c$, the rotation frequency of the shaft relative to the bearing cage.

It was also shown that the synchronous average $y(t)$ of a time signal $x(t)$ using a trigger signal with frequency f_t is equivalent to the convolution (McFadden and Toozhy, 2000):

$$y(t) = c(t) * x(t) \tag{2.3}$$

where $c(t)$ is a set of N impulses of amplitude $1/N$. The impulses are spaced at time intervals $T_t = 1/f_t$, and formally defined as:

$$c(t) = (\frac{1}{N}) \sum_{n=0}^{N-1} \delta(t + n\,T_t)\,. \tag{2.4}$$

The equivalent form in the frequency domain is the multiplication of the Fourier transform of $X(f)$ of the time signal by $C(f)$, the Fourier transform of $c(t)$. This is formally represented as:

$$Y(f) = C(f) \cdot X(f) \tag{2.5}$$

where $C(f)$ is a comb filter defined as:

$$C(f) = \left(\frac{1}{N}\right) \frac{sin(\pi N T_t f)}{sin(\pi T_t f)}. \tag{2.6}$$

The results of the study were achieved by the frequency domain synchronous average of the envelope signal with a trigger signal that is synchronized with the rotation frequency of the shaft relative to the cage, i.e. $f_t = f_r - f_c$. By doing so, only frequencies that are integer

multiples of the rotation frequency relative to the cage were passed. It was concluded that the synchronous average of a bearing with Z rolling elements, contained an impulse for each rolling element, and that variations in the impulses could be revealed. Thus, information about the damage distribution on the inner race of the bearing was obtained, and the authors were able to identify up to four spalls on the inner race. It was also noted that if the damage on the inner race is greater than the angular separation between rolling elements, the damage distribution may not be clear, possibly resulting in the inability to determine the location of a spall. Additionally, this study only focused on damage to the inner race, and did not explore the ability to locate faults contained in the other components of the bearing.

Christian *et al*. (2007) expanded on this approach by combining TSA with Support Vector machines (SVM) for the diagnosis of bearing faults. In this study, TSA was obtained by convolving the raw vibration signal with a repeating trigger signal, in order to examine the presence of various bearing defect frequencies. Then, twenty features were extracted from the envelope of the TSA signal using independent component analysis (ICA). These features were input to SVM, a classification technique based on risk minimization, for the use of fault detection. The reader is encouraged to reference the paper for further details on SVM and ICA.

A key contribution was the use of the theoretical bearing fault frequencies (i.e. inner race, outer race, and ball pass roller frequency) as the repeating trigger signal. As opposed to using the shaft rotation frequency, the use of the theoretical bearing fault frequency allowed for the implementation of a tachometer-less approach, that overcomes the limitation of the need for a speed sensor. This resulted in the ability to classify faults in different locations within the bearing. In this study, both drive and fan end faulty bearing signals were used for training. The conclusion was made that when testing signals came from the same end as the training signals,

the classification results were 95% or higher in general. However, performance significantly decreased to between 50% and 70% when training and testing signals came from different ends of the test rig. The authors also examined the performance without the use of ICA as a preprocessing technique, and noted that the results were either quite similar or worse. Thus, it was concluded that the faulty bearing location and signal transmission path are critical for diagnosis, and ICA may not be realistic to use for this type of application.

Most recently, another study made a further contribution by developing a tachometer-less synchronously averaged envelope (TLSAE) signal processing and feature extraction technique that provides the ability to detect bearing degradation at varying levels of damage (Siegel *et al*., 2012). The method begins by first using a narrow band pass filter around a calculated bearing fault frequency of interest, and then takes the derivative of the phase of the Hilbert transform in order to generate a synthesized trigger signal. Next, the envelope of the vibration signal is synchronously averaged by combining the calculated trigger signal with the high frequency envelope method to obtain a defect spectrum that highlights frequency content occurring at harmonics of the calculated fault frequency of interest. This method is another TSA application that does not require a tachometer signal for the shaft or bearing cage.

Interesting results were obtained from the study. To verify the method, six bearings were tested: three normal bearings and three with increasing scratch levels on the outer race. For comparison, the FFT method, traditional envelope method, and the TLSAE were all applied. It was shown that although the traditional envelope method allowed for a clear distinction among levels of damage, the TLSAE proved to be more robust. There was a larger separation amongst damage levels, and the results contained less variability in the calculated feature values. This was further validated upon examining the results at the second harmonic of the ball pass outer

frequency. In this case, the envelope method contained a smaller separation between the first and second damage levels and a significant amount of variability in the case of the third scratch level. When compared with the TLSAE, the separations within damage levels were more distinct and a significant reduction in the variability was noted for the third scratch level. This resulted in better input values for classification algorithms, highlighting the capability of the TLSAE method.

2.3 Microphone Based Bearing Fault Diagnostics

Acoustic signals recorded using microphones have also been investigated as bearing fault diagnostic tools. In (Wang *et al.*, 2014), the time-scale manifold ridge demodulation method using acoustic signals was investigated. This paper presented an improvement to the aforementioned demodulation technique, called exchanged ridge demodulation of the time-scale manifold, for the enhancement of the diagnosis of both bearing defects and gear faults. Another recent study presented an acoustic-based diagnostic technique that was constructed from near-field acoustic holography and the gray level co-occurrence matrix (Lu *et al.*, 2012). Using an FFT based near-field acoustic holography, the sound fields and their corresponding acoustic images for different conditions were obtained. Then, after feature extraction, the support vector machines algorithm was utilized to diagnose various types of rolling element faults. In (He *et al.*, 2013), a Wayside acoustic diagnostic scheme was presented that combines signal resampling and information enhancement. In that study, the authors' technique addressed the two problems of the wayside acoustic signal: Doppler shifting and heavy noise interference.

However, the acoustic signals collected in (Wang *et al.*, 2014; Lu *et al.*, 2012; He *et al.*, 2013) and the acoustic emission signals collected to validate the methodology presented herein

are notably different. For example, the acoustic signals used in (Wang *et al.*, 2014; Lu *et al.*, 2012; He *et al.*, 2013) were all acquired via one or more microphones whereas the acoustic emission signals acquired for the method presented in this paper were collected using a wideband AE sensor. Acoustic emission (AE) sensors are generally piezoelectric devices designed to provide a voltage output when exposed to an ultrasonic motion at the surface to which they are coupled, usually generated from an elastic stress wave resulting from a defect or unwanted mechanism within the structure (Eitzen *et al.*, 1987). Thus, the information collected using an AE sensor is quite different than the microphones used in (Wang *et al.*, 2014; Lu *et al.*, 2012; He *et al.*, 2013), which collect the signal information generated from the sound field produced by the object of interest. Additionally, in (Raharjo *et al.*, 2012), a microphone, vibration sensor, and AE sensor were investigated for scratch detection on a self-aligning spherical journal bearing and the conclusion was drawn that although all three sensors could be used to determine bearing conditions, the AE sensor was the most sensitive for the scratch bearing fault. Another notable difference is that the frequency response range of microphones (20 Hz to 100 kHz) is significantly lower than that of AE sensors (over 100 kHz). Hence, acoustic signals collected via the use of microphones require much lower sampling rates than that of AE sensors. For example, the acoustic signals collected via microphone in (Wang *et al.*, 2014; Lu *et al.*, 2012; He *et al.*, 2013) all used sampling rates that are comparable to vibration based techniques (10 kHz or less) whereas AE sensors usually require sampling rates higher than 1 MHz. In this research, a sampling reduction technique was implemented that downshifts the frequency response range of the AE sensor, allowing AE signals to be sampled at a rate comparable to vibration signals collected from accelerometers or acoustic signals collected using a microphone.

2.4 Low Speed Bearing Fault Detection and Diagnostics

In many industries, the use of low speed rotating machines is a staple for successful operation. Such machines can be found in steel and paper mills, biological applications, and wind turbines. Thus, the monitoring of bearings, shafts and gears in such applications is critical for the proper maintenance of low speed equipment. In the low speed bearing fault diagnosis literature, the low speed has been referred to as in the range from 0.33 Hz to 10 Hz (Canada and Robinson, 1995), whereas significantly lower speed thresholds have been considered as a separate classification range. For example, speeds below 0.5 Hz have been viewed as "ultra low" (Sako and Yoshie, 2010) and if below 0.83 Hz considered "extremely low" (Miettinen and Pataniitty, 1999). In this dissertation, the shaft speed falling within the low speed range described in (Canada and Robinson, 1995) will be addressed.

To date, the condition monitoring of rolling element bearings and other rotating equipment using vibratory analysis is an established technique and the industry standard. One study investigated the use of parametric models of amplitude demodulated vibration signals, and the resulting frequency spectra, for bearing fault detection and diagnosis of roller bearings with defects at a shaft speed of 1 Hz (Mechefske and Mathew, 1992). In that paper, a signal processing technique was first used to detect bearing defects and the frequency spectra were then used to classify the defects. Although effective, this methodology required visual inspection of the frequency spectra to achieve fault diagnosis. Later, another study developed a low speed technology system to measure vibrations resulting from low speed rotating machinery (Canada and Robinson, 1995). This system was centered on separating the high frequency noise of the machine from the low frequency signatures of interest, and validation was presented using results from a low speed rotor and gearbox. More recently, for low speed applications, a general model

of faulty bearing vibration signals has been established and it was shown that envelope-autocorrelation can be observed in a faulty bearing, but not in the healthy bearing case (Wang and Kootsookos, 1998). Others have sought to develop new accelerometers and have shown that with the aid of the resonance demodulation technique, low speed rolling bearing faults can be detected (Hou *et al.*, 2010). However, the successful use of vibrations is limited at low speed applications because the change in energy generated from faults at such speeds may not be detectable using traditional accelerometer based monitoring systems. Thus, researchers have investigated the use of AE sensors and strain gauges for component monitoring at such low speed conditions.

AE based studies have shown promising results for the incipient detection of faults and sensitivity to fault location, and recent studies have explored their use for low speed bearing monitoring. One early investigation looked at the monitoring of bearings at low speeds (Smith, 1982). In this study, results comparing acceleration, shock pulse transducer, acoustic emission and jerk measurements were presented. Among other conclusions drawn, it was mentioned that AE resulted in clear detection of an outer track bearing defect at speeds as low as 0.17 Hz. However, it was also mentioned that the observed AE response could not be explained and that averaging methodologies could not be utilized because the signals did not repeat exactly on a once per revolution basis. Another study reported the use of AE for monitoring rolling element bearings at extremely low shaft speeds from 0.0083 Hz to 0.083 Hz (Miettinen and Pataniitty, 1999). In this study it was found that AE measurement is quite sensitive for detecting bearing faults when the bearing is rotating at an extremely low speed, whereas the acceleration envelope was limited to detecting faults at the lowest shaft speed of 10 Hz. This study utilized an AE pulse count and noted that using such an approach allowed the data to be manageable. In this

paper, an approach that facilitates the use of low sampled AE signals is presented which make the use of continuous AE time signals manageable. Jamaludin and Mba (2001) also explored the application of AE for the low speed monitoring of bearings. This study used K-means clustering to classify line defects on a spherical roller bearing. Although promising results were achieved, the study focused on the frequency range of 100kHz to 1MHz and also relied on a data mining technique which can be time consuming due the large data requirement for training and testing of the models. (Widodo *et al.,* 2009) also relied on a data mining approach, presenting a different classification technique based on relevance vector machines and support vector machines to diagnose bearing faults at shaft speeds ranging from 0.33 Hz to 1.33 Hz. In another study, an AE sensor was used to investigate the incipient fault detection of low speed rolling element bearings in the frequency range up to 100kHz (Kim *et al.,* 2007). This study evaluated a number of time domain condition indicators using different filter bands to determine the best parameters that can distinguish between healthy and inner race faulty bearing signals. However, the goal of this study was to determine effective filter band ranges and time domain condition indicators that can be used to evaluate the acquired AE signals. Moreover, only an inner race fault was observed and the diagnosis of all four bearing fault types could not be confirmed using the respective filter band and CIs presented in the paper. Later, Sako and Yoshie (2010) proposed a diagnostic method using the AE envelope waveform and achieved results at speeds less than 1.67 Hz. This study confirmed that the periodicity of outer ring flaking could be captured at speeds as low as 0.17 Hz. Recently, other studies investigated AE and its use for the condition monitoring of slow speed shafts and thrust ball bearings (Elforjani and Mba, 2010; Elforjani and Mba, 2011). These studies demonstrated the ability to use AE to detect crack initiation and growth and also mainly focused on the investigation of AE source location. Moreover, the aforementioned

experiment focused on a single shaft speed of 1.2Hz and tested bearing condition under loading and starved lubricating conditions.

Nonetheless, the aforementioned high frequency AE signals are accompanied by high sampling rates. Moreover, for low speed bearing fault diagnostic applications, data acquisitions need to be relatively long to capture the mechanical defect frequencies. The combination of high sampling rates with long data samples limits the feasibility of practical application of AE based approaches. In this dissertation, an approach that facilitates the use of low sampled AE signals is presented which make the use of continuous AE time signals manageable. It was found that the combination of a new analysis signal and different condition indicators were effective for the evaluated low shaft speeds from 2 to 10 Hz. The diagnosis of all four bearing fault types at the presented shaft speeds has not been presented in literature. That, in combination with the low sampling rate provides merit for the possibility of a practical implementation of an AE based bearing monitoring approach in industry.

2.5 On-Aircraft Fatigue Crack Detection in a UH-60A Planet Gear Carrier Using Vibration Data

The transmission of the UH-60A helicopter contains a planetary gear train in the final stage of the main rotor gear box. In this configuration, torque is transmitted from the central sun gear through the planets to the planet carrier and from the planet carrier to the main rotor shaft. To ensure the safety of the aircraft and passengers, it is important to have tools to determine the condition of critical components. Although difficult to analyze, one tool that can be used for health assessment of planetary gear trains is vibration. The difficulty of assessing the health of planetary gear trains using vibration arises from many factors such as similar vibrations produced from multiple planet gears, and the various time-varying transmission paths from gear

mesh points to the sensors which are mounted on the gearbox housing. Thus, conventional fault detection algorithms may not be as effective when applied to such complicated gear trains.

In 2002, the main transmissions (2400 series) of two US Army UH-60A Black Hawk helicopters were found to contain fatigue cracks in the planet carriers. When investigating the cause of repeated low transmission oil pressure warnings, a 250 mm hub-to-rim crack in the first carrier was found. An 82 mm crack in the second carrier was found during an inspection. These discoveries resulted in flight restrictions on many US Army UH-60A helicopters, and the investigation into cost effective tests that were capable to diagnosing this type of fault.

A vibration test program was conducted by the US Army on the transmission containing the 82 mm crack. The transmission was installed in a test cell at various torque settings and was also ground-run in a helicopter at 20% and 30% torque settings. Vibration was also acquired from undamaged transmissions.

The vibration data was first analyzed by applying planetary gearbox diagnostics to the time synchronous averages (TSAs) of the data (Keller and Grabill, 2003). In this paper the epicyclic sideband index (SIe) and the epicyclic level factor (SLFe) were found to effectively detect the presence of the fault using test cell data, though neither were effective for the low-torque on-aircraft conditions. The same data was investigated using a combination of wavelet analysis and Morkov modeling (Dong *et al.*, 2004). This method was able distinguish the faulty component data from the healthy component data, though training of the data sets was required. Wu *et al*. (2004; 2005) and Saxena *et al.* (2005) presented crack detection results via frequency and wavelet domain processing of the raw data that was reported to be dependent on the location of the sensor and frequency band. Mclnerny *et al*. (2003) processed the test-cell data similarly to

(Keller and Grabill, 2003) by applying a number of metrics to the TSAs of the data. In this paper, statistics were also presented for the raw data and a new metric measuring the ratio in the planet carrier TSA at multiples of planet-pass frequency with the remaining energy in the average was developed. Mclnerny et al. (2003) was able to detect the crack in the test cell though did not investigate their metrics to the on-aircraft data. In (Blunt and Keller, 2006), two new methods of detecting the fatigue crack were developed. These methods were based on changes to the modulation of the fundamental gear mesh vibration resulting from the crack. These methods were again found effective for the test-cell conditions as reported in (Keller and Grabill, 2003) and (Mclnerny *et al.*, 2003), though ineffective for the on-aircraft conditions.

The results presented in the aforementioned research provided motivation to develop a technique that can effectively detect the fatigue crack in the on-aircraft conditions that would not require the need to train the data sets. The research in this dissertation also involved analyzing the UH-60A vibration on-aircraft data using a TSR based spectral average approach. These results are presented in section 6.8.

3. MOTIVATION

Upon examination of current state of the art AE based bearing fault diagnostic methods, it is apparent that there is a need for effective and efficient AE signal processing techniques that are capable of extracting useful bearing fault features. It has been shown that AE signals are more sensitive which provides the capability of incipient fault detection. Also, AE signals are sensitive to fault location, providing the ability to detect fault positions. However, there are numerous challenges in the application of AE based methods to bearing fault diagnostics. One issue is the need for a high sampling rate due to the frequency range of AE signals. Also, accompanied with a large volume of AE data is the need for a significant storage capacity and an imposed computational burden. Additionally, AE signals contain non-stationary behavior that makes traditional frequency analysis methods ineffective. If effective and efficient AE based diagnostic techniques can be developed, their implementation would allow fault detection in the propagation stage, ensuring the ability to perform maintenance before mechanical failure.

Additionally, most of the current developments only deal with the use of accelerometer signals. Literature to date does not contain any documented cases of synchronous averaging apporaches applied to AE signals for the use of bearing fault diagnostics. Moreover, the current tachometer based TSA bearing applications only present results for inner race fault detection. This approach also requires the need to compute a TSA for each bearing fault type. Therefore, there is significant motivation to explore the use of similar noise reduction averaging methods and their diagnostic ability of multiple bearing fault types. Also, if AE data could be collected and processed efficiently to take advantage of the sensor benefits, it would make a significant contribution to the field of condition based maintenance.

4. METHODOLOGY

(The majority of the content in this chapter is composed of previously published work as Van Hecke, B., Qu, Y., and He, D., 2014, "Bearing fault diagnosis based on a new acoustic emission sensor technique", *Proceedings of the Institution of Mechanical Engineers Part O: Journal of Risk and Reliability*, Vol. 229, No. 2, DOI: 10.1177/1748006X14558900. and Van Hecke, B., He, D., and Qu, Y., 2014, "On the use of spectral averaging of acoustic emission signals for bearing fault diagnostics", *ASME Journal of Vibration and Acoustics*, Vol. 136, No. 6, DOI: 10.1115/1.4028322.)

4.1 Overview of the Proposed Methodology

As previously mentioned, other studies that explored the use of time synchronous averaging as a bearing fault diagnostic tool have focused on the processing of accelerometer signals. McFadden and Toozhy (2000) computed the synchronous average of the vibration signal envelope with a trigger signal that is synchronized with the rotation frequency of the shaft relative to the cage, and were successful in inner race fault detection. This was a successful implementation of synchronous averaging using a tachometer signal for inner race detection; however, the study did not examine the diagnostic ability to detect other typical bearing fault types.

Another successful study on computing the vibration based synchronous averaging for bearing fault detection utilizing a trigger signal was developed based on the theoretical bearing fault frequencies (Christian *et al*., 2007). This research showed the bearing fault diagnostic capability of TSA using a tachometer-less approach, generating trigger signals based on bearing fault frequencies. It was shown that multiple fault types can be detected, however multiple trigger signals need to be determined for each fault frequency type. Siegel *et al*. (2012) also implemented a tachometer-less TSA approach that resulted in higher fault detection accuracy and less variability than other traditional bearing fault diagnostic methods. However, the method

also required the calculation of multiple trigger signals to detect the various bearing fault types and only outer race fault detection results were provided. In fact, literature to date contains no reports presenting the implementation of TSA to diagnose all four bearing fault types.

This research implements a novel signal processing combination of time synchronous resampling and spectral averaging for bearing fault diagnosis seeking the evaluation and comparison by quantifying both AE and accelerometer data. This method was also modified and validated to work for low speed AE bearing analysis and for the detection of UH-60A planet gear carrier fatigue cracks using vibration signals. The result is an effective diagnostic approach that is accomplished via the computation of a single average which has not been presented in literature.

Figure 4.1 and Figure 4.2 present respective overviews of the AE and vibration based signal processing methodology for this research. Also, provided in Figure 4.3 is an overview of the low speed AE based methodology and Figure 4.4 presents the overview of the vibration based UH-60A planet gear carrier fatigue crack detection methodology.

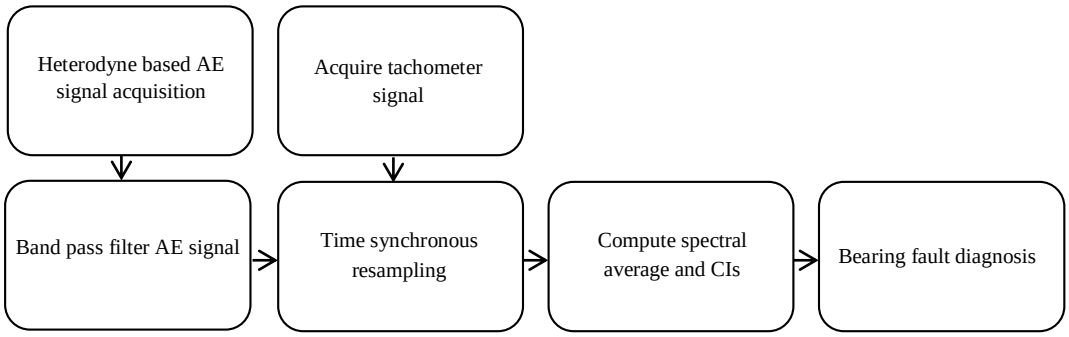

Figure 4.1. The AE based methodology

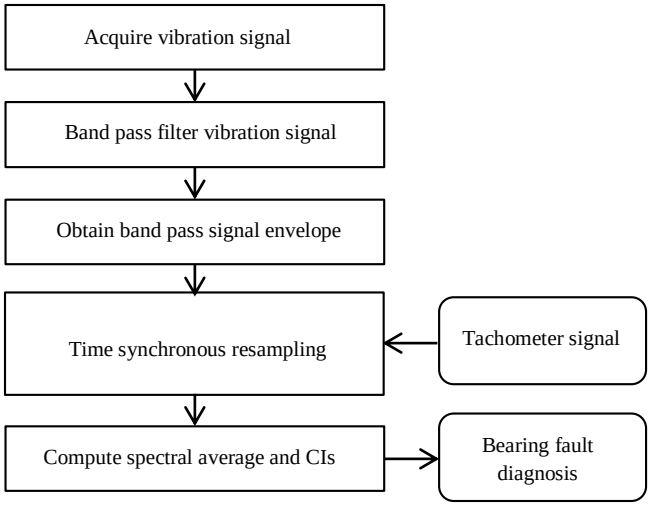

Figure 4.2. The vibration based methodology

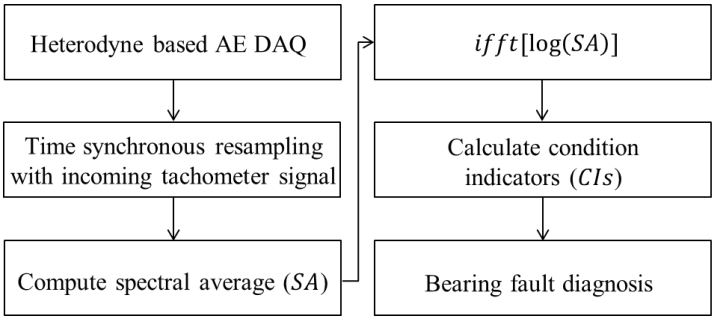

Figure 4.3. The low speed AE methodology

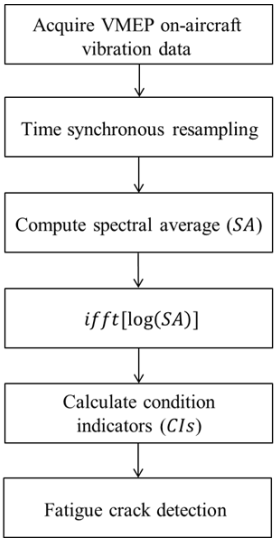

Figure 4.4. The vibration based UH-60A crack detection methodology

4.2 Heterodyne Based AE Signal Sampling and Tachometer Signal Acquisition

The initial step in the methodology is the acquisition of both the tachometer and AE sensor signals from the test rig. The data acquisition procedure is described in detail in the experimental setup section. The tachometer records the rotational shaft speed and real time angle, while the AE sensor provides the AE signal, which is recorded at a sampling rate of 100 kHz. In comparison to other bearing fault diagnostic studies that have focused on AE burst data, this research will focus on the processing of continuous AE signals. The successful implementation of the methodology requires the need to address the large volume of data and non-stationary behavior of the AE signal.

One disadvantage of AE based approaches is the significant computational burden. Because the frequency of the output signal from AE sensors is typically as high as several megahertz, AE based techniques are usually accompanied with sampling rates as high as several to 10MHz. In this dissertation, a heterodyne based sampling frequency reduction technique is employed that down-shifts the energy related to the signal so that a sampling rate comparable to vibration methods can be utilized. This is significant because less data needs to be collected and stored on the computer. Thus, the cost associated with data acquisition is reduced.

The concept of heterodyne has long been utilized in the field of communications. In radio, the carrier signal of typical amplitude modulated (AM) signals are often as high as several megahertz. However, the frequency of the audio signal that is modulated to that carrier signal is often as low as a few kHz. Through demodulation, the AM signal frequency is downshifted, allowing the audio to be sampled at a much lower rate. The result is a reduction in not only the sampling rate, but also the computational power required to process the data.

The AE signal demodulator implemented in this paper works similarly to a radio quadrature demodulator: shifting the carrier frequency to baseband, followed by low-pass filtering. The technique applied here is called heterodyne. Mathematically, heterodyning is based on the trigonometric identity. For two signals with frequency f_1 and f_2 , respectively, it could be written as

$$sin(2\pi f_1 t)\, sin(2\pi f_2 t) = \frac{1}{2}\cos[2\pi(f_1 - f_2)t] - \frac{1}{2}cos[2\pi(f_1 + f_2)t] \tag{4.1}$$

wheref_1 is the AE carrier frequency and f_2 is the reference signal frequency of the demodulator.

For example, let $f_1 = 3$ Hz and $f_2 = 4$ Hz, and note $y_1 = sin(2\pi 3t)$ and $y_2 = sin(2\pi 4t)$. Then, their multiplication $Y = y_1 y_2$., is shown in Figure 4.5.

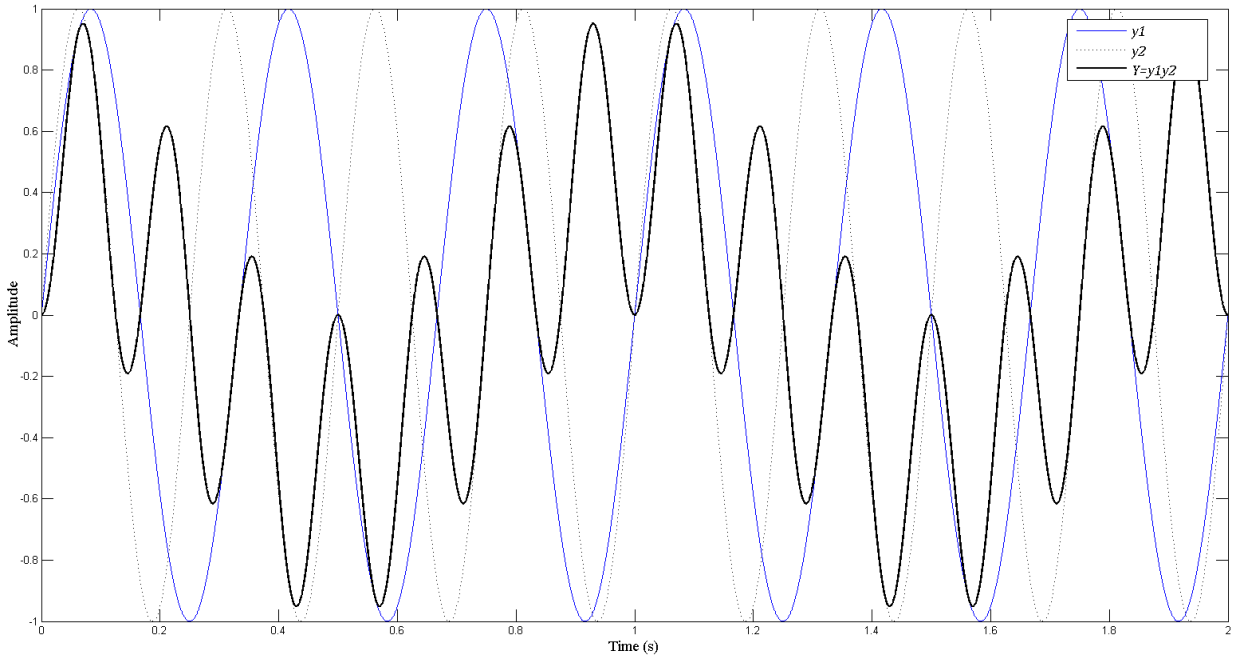

Figure 4.5. The multiplication of two sinusoid signals

Next, as shown in Figure 4.6, the modulated signal is low-pass filtered to reject the high frequency image at frequency $(f_1 + f_2)$.

A detailed discussion of the heterodyne technique applied on the raw AE signal is given next. In general, amplitude modulation is the major modulation form for AE signals. Although frequency modulation and phase modulation are potentially present in the AE signal, they are considered trivial and will not be discussed here. The amplitude modulation function is given in Eq. (4.2).

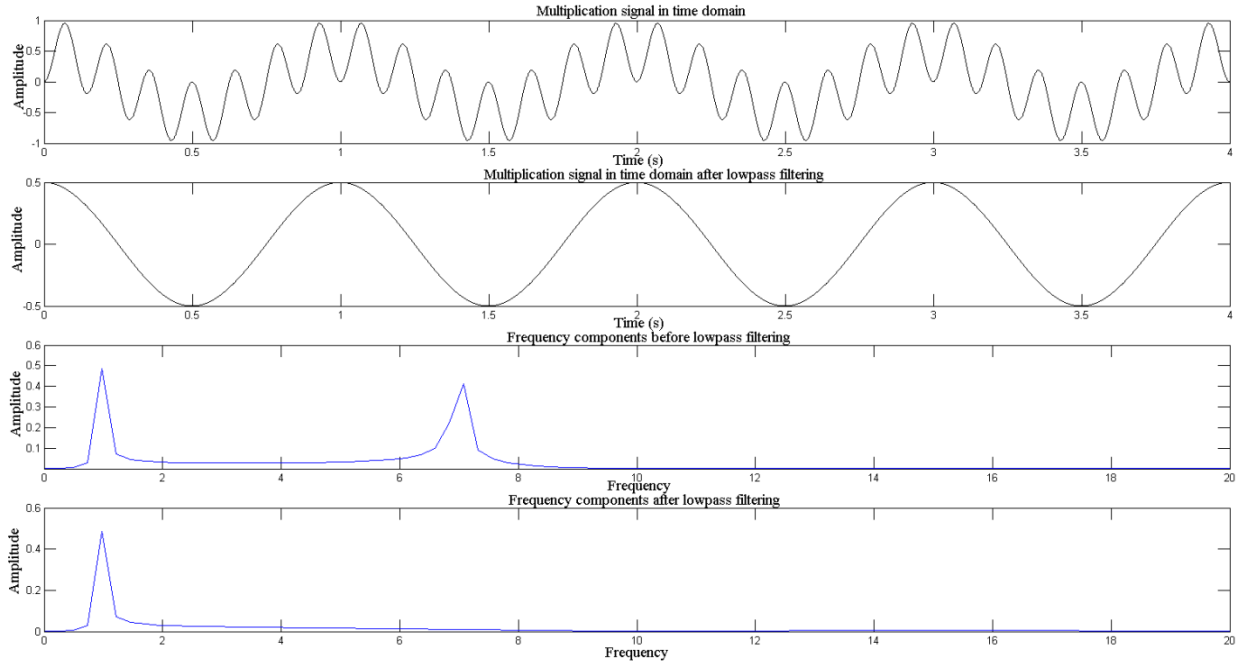

Figure 4.6. The extraction of the heterodyned signal by frequency domain filtering

$$U_a = (U_m + mx)co\,s\,\omega_c t \tag{4.2}$$

where, U_a is the modulated signal, U_m is the carrier signal amplitude, ω_c is the carrier signal frequency, m is the modulation coefficient, and x is the signal of interest. With an amplitude X_m and frequency Ω, assume that x can be expressed as

$$x = X_m cos\Omega t \tag{4.3}$$

Note that it is assumed that the frequency Ω of the signal x is normally much smaller than the frequency ω_c of the carrier signal. Then, with the heterodyne technique, the modulated signal will be multiplied by a unit amplitude reference signal $\cos(\omega_c t)$. The result U_o is given as following:

$$U_o = (U_m + mx)\, cos(\omega_c t)\, cos(\omega_c t) = (U_m + mx)\left[\frac{1}{2} + \frac{1}{2} cos(2\omega_c t)\right] \tag{4.4}$$

Then, after substituting Eq. (4.3) into Eq. (4.4):

$$\begin{aligned} U_o = {} & \frac{1}{2}U_m + \frac{1}{2}mX_m cos\Omega t + \frac{1}{2}U_m cos(2\omega_c t) \\ & + \frac{1}{4}mX_m[cos(2\omega_c + \Omega)t + cos(2\omega_c - \Omega)t] \end{aligned} \tag{4.5}$$

Since U_m does not contain any useful information related to the modulated signal, it can be set as 0, or removed through detrending. From Eq. (4.5), it can be seen that only the part $\frac{1}{2}mX_m cos\Omega t$ which is the signal of interest will be retained after low-pass filtering, and the high-frequency components around frequency $2\omega_c$ will be removed. A critical step in applying the heterodyne technique to AE signals is to select the appropriate frequency of the reference signal. The optimization procedure reported in (Qu *et al.*, 2014) can be used to search for the optimal frequency of the reference signal using a linear chirp function as the demodulation input. The optimization process is to search for the best frequency such that the root mean square (RMS) of the demodulated signal is maximized.

By adding a demodulation step, it can achieve the purpose of reducing the signal frequency to 10s of kHz. This is close to the frequency range of general vibration signals. Thus, any data acquisition board with a low sampling rate should be able to sample the pre-processed AE data.

4.3 Band Pass Filter Selection Procedure

4.3.1 Filter Band Selection Based on Fundamental Defect Frequencies

Upon data acquisition, the next step is to select a proper band pass filter range to extract the signal information related to the bearing fault. Generally, a properly selected band pass filter removes the high frequency components and low frequency contents associated with shaft imbalance (Shirioshi *et al.*, 1997). Hence, when a band pass filter is executed properly, the information associated with the bearing fault is maintained.

In theory, as a bearing rotates at a constant speed, its AE signal can be characterized by a periodical property. In general, there are four fundamental defect frequencies to describe this motion. The four defect frequencies are the fundamental train frequency (FTF), ball spin frequency (BSF), ball pass frequency outer (BPFO), and ball pass frequency inner (BPFI), respectively representing the defect frequencies of the cage, ball, outer race, and inner race (Felten, 2003). Some bearing manufacturers provide these frequencies, or one of them accompanied with multipliers that assist in the calculation of the others. However, if the frequencies are not provided, they can be calculated using the bearing parameters and the rotational speed of the shaft. The required parameters for defect frequency calculations are: the diameter of the rolling elements D_e, the pitch circle diameter D_p, the number of rolling elements Z, the contact angle ß in degrees, and the rotational speed of the shaft in revolutions per second ω. Once the previously mentioned parameters have been acquired, the fundamental fault frequencies can be calculated using the following formulae:

$$FTF = [\omega/2][1 - (D_e/D_p)\cos(ß)] \tag{4.6}$$

$$BSF = [\omega\, D_p/2D_e]\{1 - [(D_e/D_p)\cos(ß)]^2\} \tag{4.7}$$

$$BPFO = [\omega Z/2][1 - (D_e/D_p)\cos(ß)] \quad (4.8)$$

$$BPFI = [\omega Z/2][1 + (D_e/D_p)\cos(ß)] \quad (4.9)$$

If the bearing rotates at a constant shaft speed, the fundamental defect frequencies can be computed by multiplying the defect frequency multipliers by the rotational shaft speed. In the absence of mechanical noise, the fault frequencies could be observed, leading to the selection of a filter band that contains the bearing fundamental defect frequencies.

4.3.2 Filter Band Selection Based on Spectral Analysis

If the fault frequencies cannot be observed in the spectrum due to noise in the system, they cannot be used as the basis for filter band selection. However, upon examination of the spectrum a filter band range can be selected that contains the majority of the spectral content and energy related to the signal. This technique was shown to be effective for the band pass filter selection of bearing vibration signals (Van Hecke *et al.*, 2014c)

4.3.3 Filter Band Selection Based on Highest Entropy

In practice, bearing signals are in the presence of mechanical noise from surrounding mechanical components, which eliminates the possibility of identifying the defect frequencies, and therefore, the ability to select a filter band that encompasses them. Thus, the filter band can be selected based on prior knowledge of the system or by utilizing some other criteria. If a correct filter band is selected, the useful signal information related to the fault is extracted. Consequently, the filter band that can extract the signal information must be determined. In this research, one tool used to select a filter band is Shannon's entropy, which is defined as the average amount of information in a message. To select the proper filter band, different bands can be tested on healthy bearing signals. After filtering with each filter band, the entropy in the resulting signal is measured. Hence, the filtered signal that contains the highest level of

information can be used to select the filter band to implement before further processing. Shannon's entropy is formally defined by:

$$Entropy = -\sum_{i=1}^{n} x_i^2 \ln(x_i^2) \tag{4.10}$$

Where $Entropy$ is the Shannon's entropy, or average amount of information in the dataset x, and x_i is the i^{th} element of the dataset x.

4.4 Spectral Averaging of AE and Accelerometer Signals

In this section, spectral averaging, time synchronous resampling, and their relationship with TSA are discussed. TSA is a proven technique for the extraction of periodic waveforms and has numerous applications to the tooth meshing vibrations for gear fault diagnosis (McFadden 1987, 1991). Additionally, TSA has been effectively implemented in the processing of enveloped vibration signals for bearing fault diagnosis (McFadden and Toozhy, 2000; Siegel *et al.*, 2012). The concept is to compute the ensemble average of successive periods of a waveform of interest, resulting in a significant reduction of noise and an enhanced signal representing one period of the averaged waveform. Braun (1975) formally expressed the TSA $y(nT)$ of a signal $x(t)$ sampled at interval nT by the following:

$$y(nT) = (1/N) \sum_{r=0}^{N-1} x(nT - rmT) \tag{4.11}$$

where the averaged period is denoted by mT. More details concerning TSA can be found in (McFadden, 1987).

The successful implementation of TSA to quantify the vibration signals for bearing fault diagnosis has created interest to use it for the processing of AE signals. The successful

application of TSA requires the knowledge of either the repetition frequency of interest, or a synchronous signal that is free of noise. Thus, two types of approaches have been presented in the literature, namely, the tachometer based TSA, and the tachometer less TSA. When compared to TSA using a tachometer, the tachometer less approach uses the repetition frequency of interest to estimate the angular information from the accelerometer signal. However, in the context of bearing fault diagnosis, this requires the computation of a trigger signal for each fault type. This research applies a tachometer based averaging approach.

Although TSA has been widely applied to gear fault analysis (Bonnardot *et al.*, 2005; Bechhoefer, 2013; Qu *et al.*, 2013a, 2013b), literature to date contains limited implementations for bearing fault diagnosis (McFadden and Toozhy, 2000; Christian *et al.*, 2007; Siegel *et al.*, 2012). Additionally, these applications have all been based on the quantification of vibration signals, and none have reported the ability to diagnose cage fault, only presenting results for inner race, outer race, or ball fault diagnosis. Furthermore, these studies have focused on either multiple spalls of the same fault type or severity of damage and none have shown the ability to diagnose all four of the bearing fault types. Additionally, although it was shown that TSA can result in an improvement upon the envelope analysis technique (Siegel *et al.*, 2012), it still requires the need for multiple averages for each of the investigated bearing fault types. A number of difficulties need to be overcome to successfully apply TSA to quantify AE signals for bearing fault diagnosis. For example, the tachometer signal must be synchronous with all bearing fault types. Additionally, the large data volume and non-stationary behavior of the AE signals make the direct computation of TSA and real time condition monitoring unrealistic. In this dissertation, time synchronous resampling and spectral averaging is used to overcome these challenges and results in the extraction of features that are used for bearing fault diagnostics.

In addition to the time domain TSA approach, frequency domain TSA algorithms have been presented in (Bechhoefer and Kingsley, 2009). One challenge in a time domain TSA approach for bearings is the requirement of four TSAs to account for each bearing fault type. Additionally, bearings could experience fluctuations in speed during industrial operation, and due to slippage, fault rates based on bearing geometries could not be exact. It has also been shown that by using a synchronous resampling technique (TSR) based on shaft revolutions, potential fluctuations in shaft speed can be accounted for, and the effect of spectral smearing reduced (Bechhoefer *et al.*, 2013). Thus, by resampling to an even number of points between trigger signal revolutions, a better FFT result was obtained. In this research, a similar TSR approach is accomplished using the shaft ZCT's and is expressed in the following.

Formally, the resampling process is achieved by interpolating the r number of data points in one shaft revolution, into L number of data points, such that:

$$L = 2^{Ceiling[log2(r)]} \tag{4.12}$$

where L is the number of interpolated points between ZCTs, and r is the average number of points between shaft crossings before resampling. Once L is determined, each segment contains an equal number of data points for FFT computations and the spectral average can be implemented.

The methodology presented in this paper combines the aforementioned TSR approach with spectral averaging to compute a single average which allows the extraction of effective CIs for bearing fault diagnosis. Thus, the computation of a single spectral average eliminates the necessity to compute multiple TSAs. Presented in Figure 4.7, is an overview of the spectral averaging approach. The computation of the spectral average requires the data to be sectioned so

that the Fourier transform of each section can be computed and the ensemble average of the squared magnitude of the segments executed.

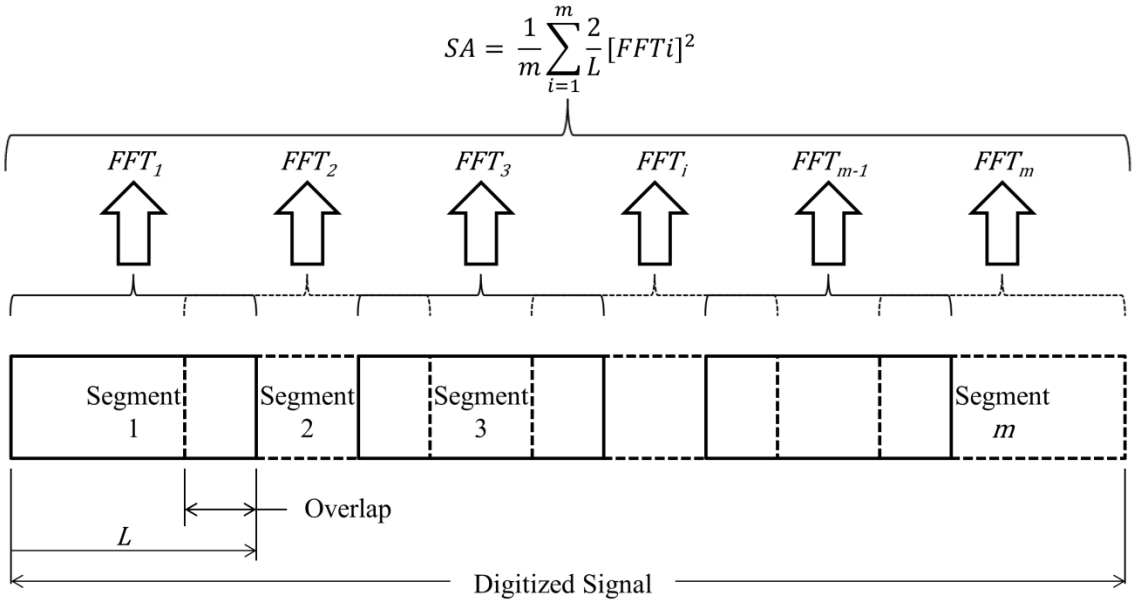

Figure 4.7. The spectral averaging approach

Welch (1967) formally expressed the execution of this approach. First, let $Z(j), for\ j = 0, \ldots, N-1$ be a sample from a stationary, stochastic sequence whose mean is 0 and let $Z(j)$ have a spectral density $P(f), |f| \leq \frac{1}{2}$, where f is the normalized frequency. Then, if one takes several possibly overlapping segments of length L with starting points of the segments M points apart and let $Z_1(j), j = 0, \ldots, L-1$ be the first segment, then,

$$Z_1(j) = Z(j), for\ j = 0, \ldots, L-1. \tag{4.13}$$

Likewise,

$$Z_2(j) = Z(j+M), for\ \ j = 0, \ldots, L-1. \tag{4.14}$$

And finally,

$$Z_K(j) = Z(j+(K-1)M), for\ j = 0, \ldots, L-1. \tag{4.15}$$

The result is K segments, $Z_1(j), \ldots, Z_K(j)$, that cover the entire data sample $Z(j)$. Moreover, $(K-1)M + L = N$.

Next, for each segment of length L we obtain the Fourier transform. In other words, we choose a data window $W(j),\ for\ j = 0, \ldots, L-1$, and take the Fourier transforms $F_1(n), \ldots, F_K(n)$, of the segments $Z_1(j)W(j), \ldots, Z_K(j)W(j)$. This is formally expressed in Eq. (4.16):

$$F_k(n) = \frac{1}{L}\sum_{j=0}^{L-1} Z_k(j)W(j)e^{-2kijn/L} \tag{4.16}$$

where $i = (-1)^{\frac{1}{2}}$. The result is K number of Fourier transforms $B_k(f_n)$, which correspond to the K number of segments:

$$B_k(f_n) = \frac{L}{S}|F_k(n)|^2, for\ k = 1, 2, \ldots, K. \tag{4.17}$$

Where,

$$f_n = \frac{n}{L}, for\ n = 0, \ldots, L/2. \tag{4.18}$$

And,

$$S = \frac{1}{L}\sum_{j=0}^{L-1} W^2(j). \tag{4.19}$$

Finally, the spectral average result, $SA(f_n)$, is obtained by taking the average of the K Fourier transforms:

$$SA(f_n) = \frac{1}{K}\sum_{k=1}^{K} B_k(f_n). \tag{4.20}$$

To implement Welch's method, the signal must first be sectioned. By using the shaft ZCTs to section and resample the AE signal, and then averaging the magnitude squared spectrums of the sections, the spectral average result is obtained. In other words, the duration between shaft revolutions is utilized as the sectioning function to average the AE signal. Moreover, the data segment length L is determined by the number of data points between ZCTs of the shaft after resampling. By resampling the segments to L data points, an equal number of

data points are used for FFT computations. Hence, this methodology uses the ZCTs of shaft rotations to section and resample the AE signals and compute the ensemble average of the squared magnitude Fourier transforms of the sections. This approach affords the ability to compute one spectral average and effectively diagnose any bearing fault that may occur. Moreover, the need to compute a single average also reduces the computational burden on the hardware, making on-line analysis and maintenance decision-making feasible. After the computation of the spectral averaging of the AE signals, various bearing fault features are extracted and evaluated.

4.5 Condition Indicators for Bearing Fault Diagnosis

There are numerous bearing fault condition indicators in the literature that quantify accelerometer signals to aid in bearing fault diagnosis. In addition, studies have developed effective CIs that accomplish bearing fault diagnosis through the quantification of AE signals (He *et al.* 2011a, 2011b). A significant difference among the available CI feature extraction techniques is in the way the CIs are computed, i.e. features can be extracted from both the time and frequency domain. Additionally, features can be extracted from the raw signal or after a signal processing technique such as TSA or spectral averaging. For shaft speeds of 30 Hz and higher, the inverse Fourier transform of the spectral average in combination with the RMS and Peak CIs have been used to successfully diagnose bearing faults for both AE and vibration signals (Van Hecke *et al.*, 2014a, 2014b, 2014c, 2014d). However, because the aforementioned analysis signal and CIs tested in those studies were not effective for low speed analysis, such work was left for future investigation. Thus, the inverse Fourier transform of the log of the spectral average result was used to investigate the potential of new CIs that allow the clear diagnosis of all four bearing fault types for low speed applications. By introducing a log into the

inverse Fourier transform, the signal being analyzed is similar to a power cepstrum that has been utilized in (El Badaoui *et al.*, 2001) for gear analysis. It should also be mentioned that although the introduction of the log was found to be effective for the low speed application, it was not effective for the high speed data used in (Van Hecke *et al.*, 2014a, 2014b, 2014c, 2014d). Moreover, the CIs used for the high speed investigations (RMS and Peak) were not effective for the low speed data. Also, some of the low speed bearing CIs used in (Kim *et al.*, 2007) were not effective for the high speed applications, but were found to work for the tested low shaft speeds when combined with the new analysis signal which takes the inverse Fourier transform of the log of the spectral average. The respective time domain input signals used for CI computation for high speed and low speed analysis are formally obtained by Eq. (4.21) and Eq. (4.22):

$$x = ifft[SA(f_n)] \tag{4.21}$$

where x is the time domain signal used for CI computations and $ifft[SA(f_n)]$ is the inverse Fourier transform of the spectral average result $SA(f_n)$ obtained by Eq. (4.20).

As previously mentioned, for low speed AE analysis, the time domain signal used for CI computation is obtained by the following:

$$x = ifft\{\log[SA(f_n)]\} \tag{4.22}$$

where x is time domain signal used for CI computations and $ifft\{\log[SA(f_n)]\}$ is the inverse Fourier transform of the log of the spectral average result $SA(f_n)$ obtained by Eq. (4.20).

Additionally, CIs were evaluated using the energy operator (EO) of the spectral average results. The EO is a type of residual of the autocorrelation function (Teager, 1992). In discretized form, the mathematical formula is given as:

$$EO[x_i] = x_i^2 - x_{i-1} \cdot x_{i+1} \tag{4.23}$$

Where $EO[x_i]$ is the i^{th} element in the EO, and x_i is the i^{th} element of dataset x acquired using either Eq. (4.21) or Eq. (4.22).

The CIs are also computed using the amplitude modulation (AM) signal, or Hilbert envelope of the signal obtained in Eq. (4.21) or Eq. (4.22). The AM signal is formally obtained by the following:

$$AM = abs[hilbert(x)] \tag{4.24}$$

where $abs[hilbert(x)]$is the Hilbert envelope of the dataset x acquired using either Eq. (4.21) or Eq. (4.22).

In this research, a number of feasible CIs were explored for bearing fault diagnosis. Provided in

Table **4.1** is the definitions of the investigated CIs. Presented is the definition for root mean square (*RMS*), peak, crest factor (CF), kurtosis ($Kurt$), skewness ($Skew$), Peak to peak (*p2p*), *Shannon's entropy, Log entropy,* Histogram upper bound (*UB*), and Histogram lower bound (*LB*). Each CI is evaluated on the signals computed using Eq. (4.21) through (4.24).

Table 4.1. The definitions of the CIs

CI	Description / Equation	Signal y used to computed the CIs: Input signal (x)	EO of input signal (x)	AM of input signal (x)
Root mean square (*RMS*)	$\sqrt{(\frac{1}{N})\sum_{i=1}^{N} y_i^2}$	RMS: statistical measure of the magnitude of a varying quantity.		
peak	$\frac{(y_{max} - y_{min})}{2}$	$peak$: maximum value in the dataset.		
Crest factor (*CF*)	$\frac{y_{peak}}{y_{rms}}$	CF: the ratio of peak to RMS; describes how extreme the peaks are in a waveform.		
Kurtosis (*Kurt*)	$\frac{N\sum_{i=1}^{N}(y_i - \bar{y})^4}{[\sum_{i=1}^{N}(y_i - \bar{y})^2]^2}$	$Kurt$: describes the peakedness or smoothness of the dataset.		
Skewness (*Skew*)	$\frac{(\frac{1}{N})\sum_{i=1}^{N}(y_i - \bar{y})^3}{[\sqrt{(\frac{1}{N})\sum_{i=1}^{N}(y_i - \bar{y})^2}]^3}$	$Skew$: measures the asymmetry of the data around its sample mean. A negative or positive value of *Skew* implies the data is spread to the left or right of the mean respectively.		
Peak to peak (*p2p*)	$(y_{max} - y_{min})$	*p2p:* measures the distance between the maximum and minimum value in the dataset.		
Shannon's entropy	$-\sum_{i=1}^{n} y_i^2 \ln(y_i^2)$	*Shannon's entropy:* average amount of information in the dataset.		
Log entropy	$\sum_{i=1}^{n} \ln(y_i^2)$	*Log entropy:* log energy entropy in the dataset.		
Histogram upper bound (*UB*)	$y_{max} + \frac{1}{2}[\frac{(y_{max} - y_{min})}{(N-1)}]$	*UB:* Highest frequency bin value in the dataset.		
Histogram lower bound (*LB*)	$y_{min} - \frac{1}{2}[\frac{(y_{max} - y_{min})}{(N-1)}]$	*LB:* Lowest frequency bin value in the dataset.		

Note: y_i is i^{th} element of the input data y; N is the length of the input data y; y_{max} and y_{min} are the maximum and minimum values in the data y; $\bar{y}$ is the mean value of the input data y defined as $\sum_{i=1}^{N} y_i / N$; y_{peak} and y_{rms} are the peak and RMS of the data y.

4.6 Bearing Fault Diagnosis

Once the spectrally averaged waveform is obtained and CIs computed, bearing fault diagnosis can be accomplished. The diagnosis is facilitated by examining the CI results for the healthy case and all four fault types to determine if differentiation amongst their levels can be observed. If the faulty signals can be separated from the healthy case and from each other, bearing fault diagnosis is accomplished.

5. EXPERIMENTAL SETUP

(Parts of this chapter were previously published as Van Hecke, B., Qu, Y., and He, D., 2014, "Bearing fault diagnosis based on a new acoustic emission sensor technique", *Proceedings of the Institution of Mechanical Engineers Part O: Journal of Risk and Reliability*, Vol. 229, No. 2, DOI: 10.1177/1748006X14558900. and Van Hecke, B., He, D., and Qu, Y., 2014, "On the use of spectral averaging of acoustic emission signals for bearing fault diagnostics", *ASME Journal of Vibration and Acoustics*, Vol. 136, No. 6, DOI: 10.1115/1.4028322.)

This section presents the experimental setup used to validate the proposed AE based bearing fault diagnostic methodology. Figure 5.1 shows the experimental bearing test rig used for data collection along with its main components. The motor controls the shaft which rotates the bearing located in the bearing housing. The rig also contains a hydraulic loading mechanism that affords the ability to apply a lateral load to the bearing housing if needed.

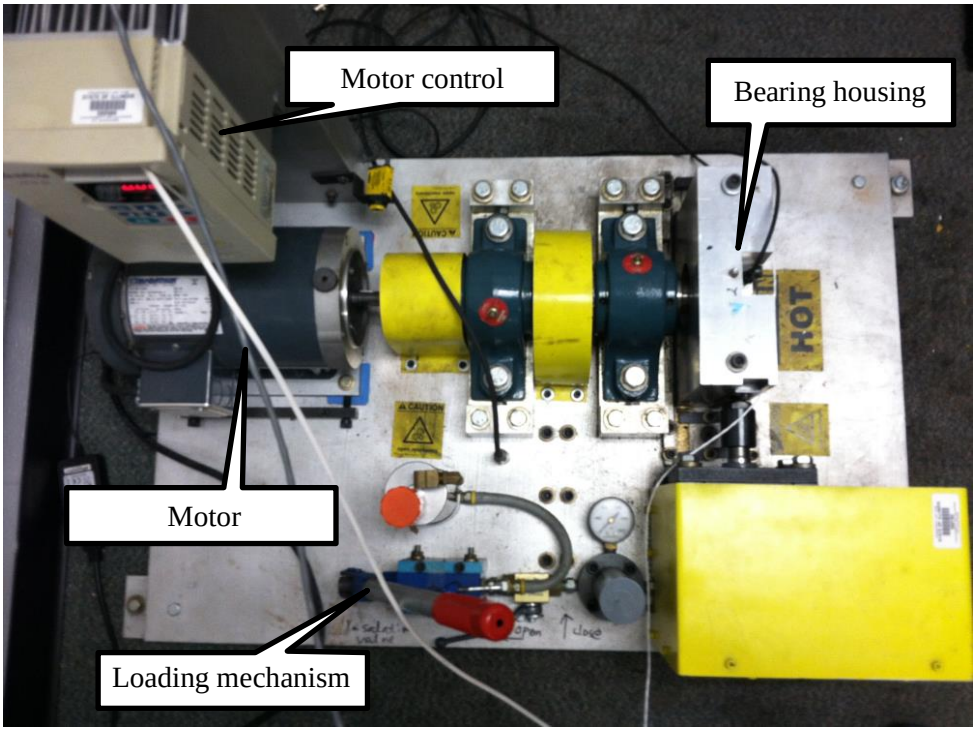

Figure 5.1. The bearing test rig

Figure 5.2 is another view of the test rig that provides a better view of the location of the AE and vibration sensors and tachometer used for data collection. The axially mounted AE sensor and radially mounted accelerometer provide the input signals needed for processing and the tachometer provides the trigger signal required for the synchronous averaging of the AE and vibration signals.

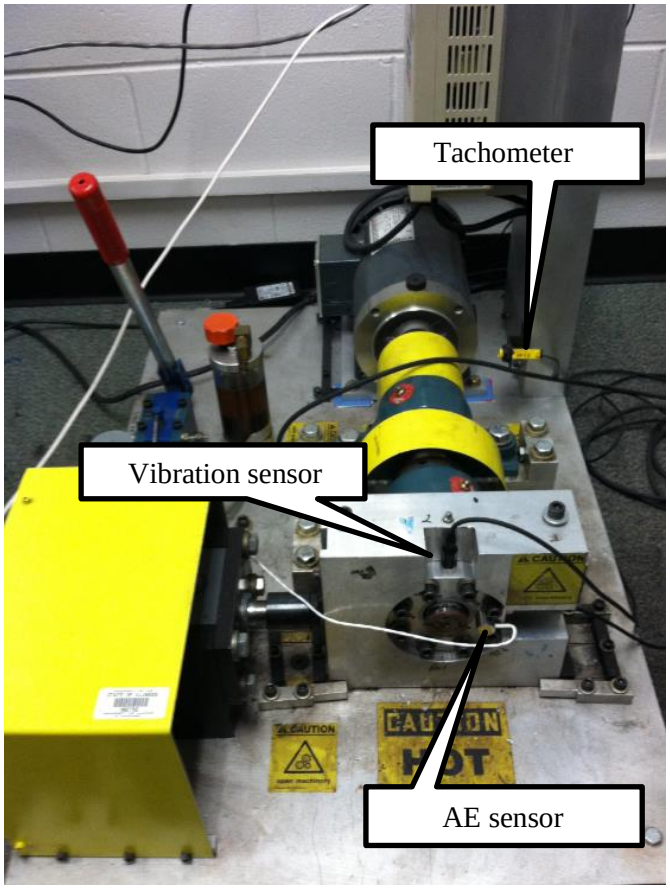

Figure 5.2. AE sensor and tachometer locations on bearing test rig

A Mastech HY3003D DC power supply set at 16 V was implemented to power both the AE sensor and a Physical Acoustics Corporation 2/4/6 preamplifier which is shown in Figure 5.3. The purpose of the preamplifier is to enlarge the AE voltage output before it is fed to the

Analog Devices AD8339 demodulation board. By increasing the voltage output, the desired signal output is increased resulting in an improvement in the signal to noise ratio. For the purpose of data collection, the selected gain was set at 40 dB. Simultaneous with AE signal collection was the signal acquisition of a radially mounted model 608A11 Industrial ICP accelerometer by IMI sensors.

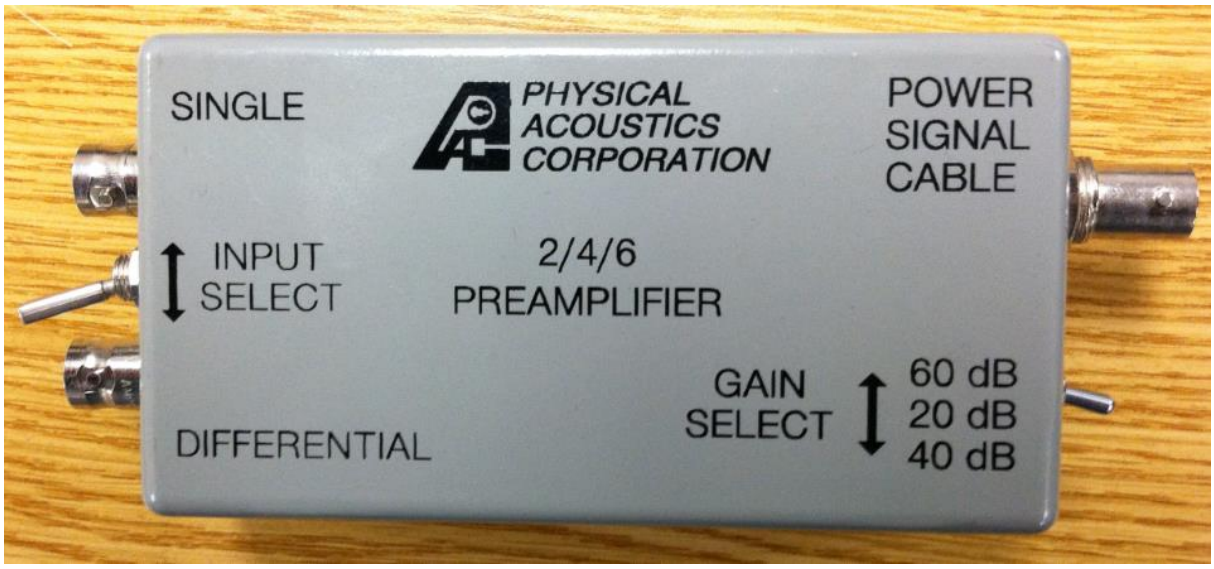

Figure 5.3. Physical acoustics corporation 2/4/6 preamplifier

Figure 5.4 shows the aforementioned AD8339 demodulation board and its power supply, as well as the function generator, and the NI-DAQ 6211 sampling board. The demodulation board is responsible for the multiplication of the AE sensor signal and the reference signal output from the function generator. Both the reference signal and AE sensor signal are the inputs to the board. After filtering out the high frequency components, the output of the demodulation board is fed to the NI-DAQ 6211 sampling board. In order to sample the data at 100 kHz, the AE signal is demodulated to shift the useful signal information below 50kHz. Thus a sampling rate

of 100 kHz can effectively extract the information needed for bearing fault diagnosis. This step is needed because if the signal was not demodulated, the energy related information would remain in the high frequency range and lost when low-pass filtered. To illustrate, consider the multiplication of two signals from different sources with respective frequencies f_1 and f_2 to be modeled by Eq. (4.1), where f_1 is the AE carrier frequency and f_2 is the demodulator's reference signal frequency. The result is two new signals, one at the frequency $f_1 + f_2$ and the other at the frequency $f_1 - f_2$. These new frequencies are called heterodynes, and the process of shifting a signal to a lower frequency range is called the heterodyne process. After proper demodulation, the high frequency content at $f_1 + f_2$ can be removed via a low-pass filter. Thus, the useful fault information is shifted to a lower frequency range. By identifying the AE carrier signal center frequency as 400kHz, it is used as the demodulation reference frequency. Thus, the data can be sampled at 100kHz, while maintaining the necessary information needed for fault diagnosis. The utilization of the demodulation and heterodyne process has been developed and a detailed explanation provided section 4.2.

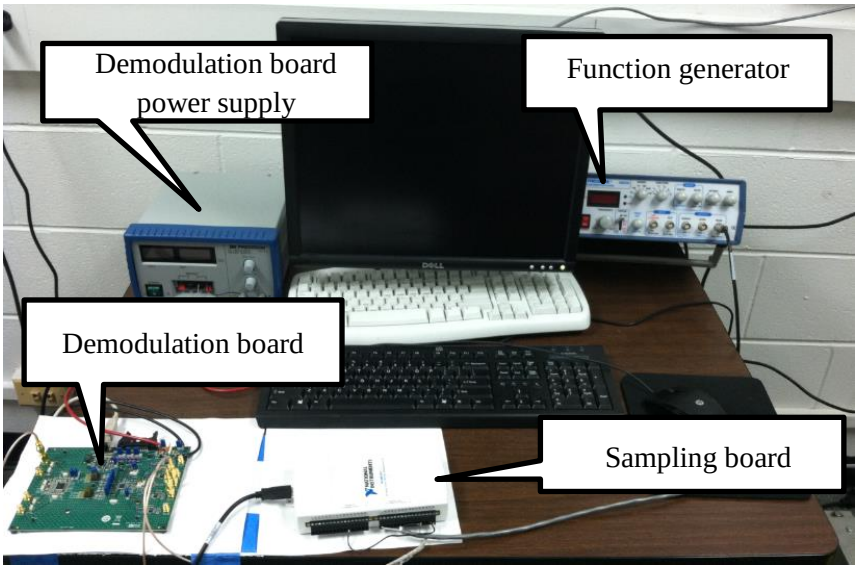

Figure 5.4. Demodulation board, sampling board, and function generator

Data acquisition of the AE signals was accomplished via NI LabVIEW SignalExpress. All AE signals were sampled at 100kHz at varying durations throughout the experiment. A wide band (WD) type AE sensor was mounted on the face of the bearing housing using instant glue. For data acquisition of the accelerometer, VibraQuest Pro by SpectraQuest, Inc. was used to digitize the continuous vibration signals at a sampling rate of 102.4 kHz. An explanation of the data sets is provided in the validation results section. A sample of the LabVIEW software interface for data acquisition is shown in Figure 5.5. The blue signal is the tachometer signal, and the red is the AE signal. Both are the voltage outputs of the sensors.

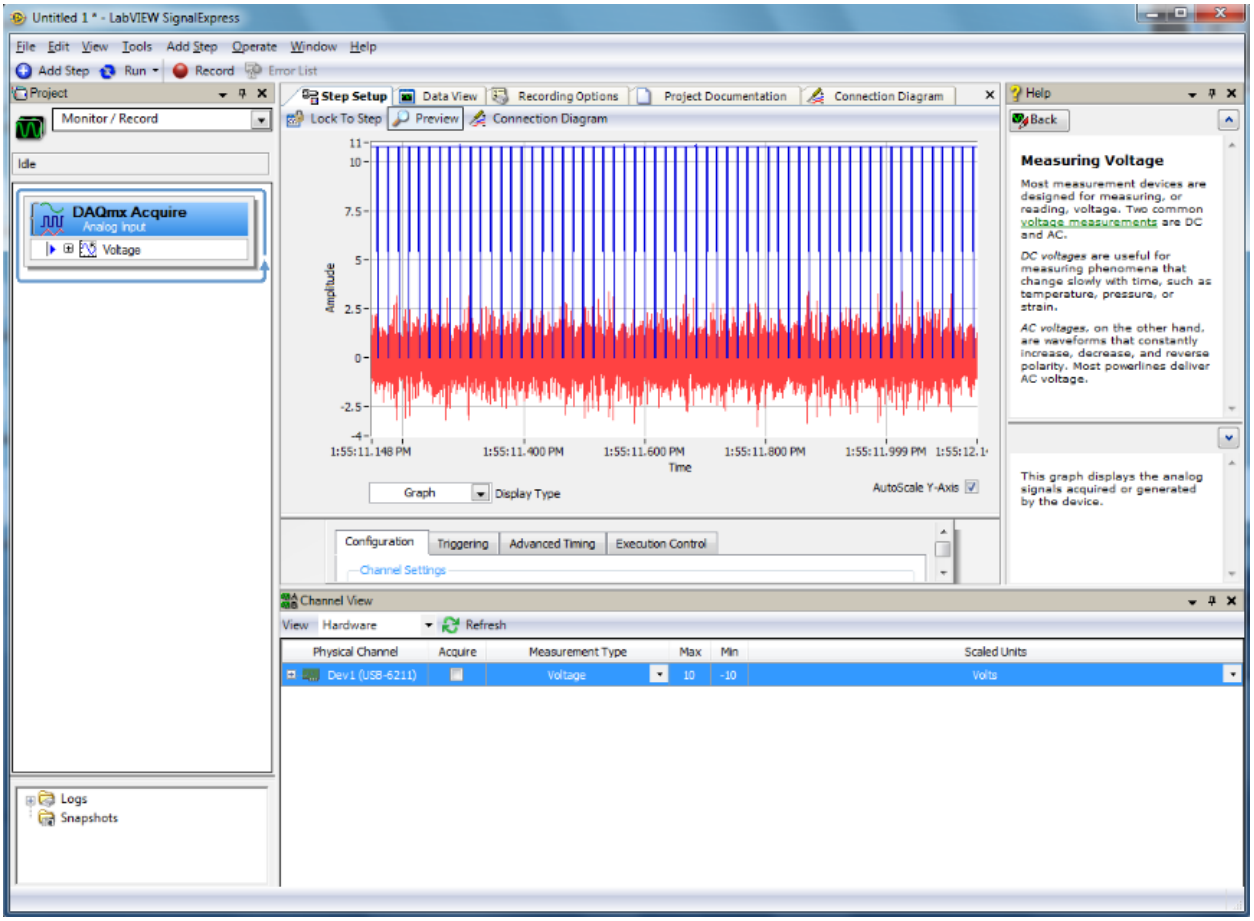

Figure 5.5. Sample LabVIEW software interface for data acquisition

The image in Figure 5.5 presents an example view of the interface during data acquisition. The image is from a bearing seeded with a cage fault with a shaft frequency of 60Hz. Figure 5.6 shows a drawing of the type 6205-2RS bearing used for the experiment.

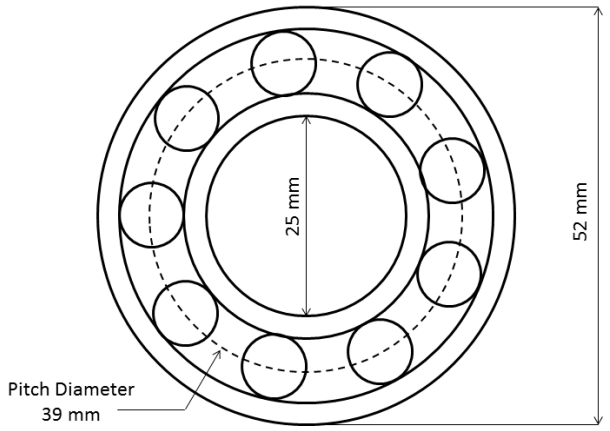

Figure 5.6. Drawing of the type 6205-2RS bearing

For the validation results, type 6205-2RS steel FAG bearings were used for testing. Four fault types were simulated on steel bearings: inner and outer race faults, rolling element fault, and cage fault (see Figure 5.7). The inner and outer race faults were generated by scratching the steel race surfaces with a diamond tip grinding wheel bit to cover the ball contact surface. The scratches on both races were about 1/16 inch wide and 1/250 inch deep. The ball fault damage was created by cutting the steel cage in one of the ball locations and then using the diamond tip grinding wheel bit to create a small dent in one of the steel balls. The dent was about 20% of the ball volume. For the cage fault, the steel cage was cut in between two ball locations. The cut was about 50% of the ball diameter. For all seeded fault tests, the bearing seal and grease was removed and replaced following the creation of the fault.

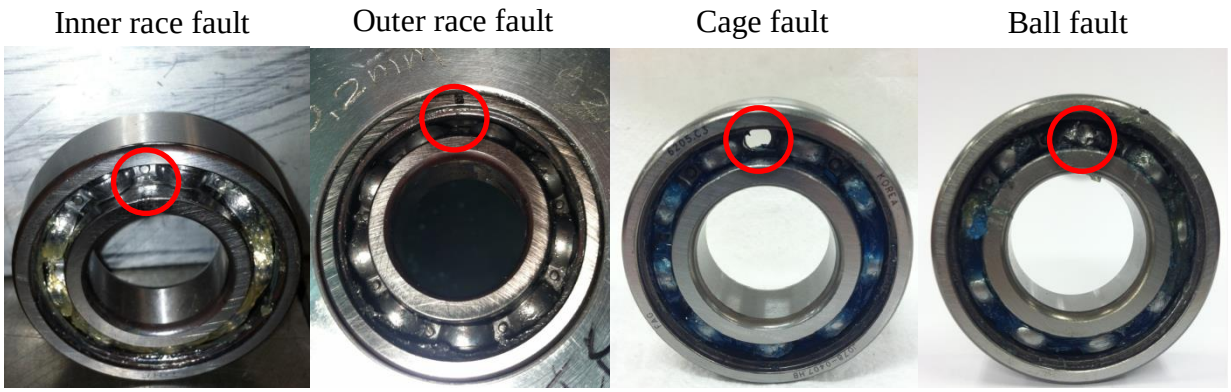

Figure 5.7. The four type 6205-2RS steel bearing seeded faults

For the type 6205-2RS steel bearings, the inner and outer races, balls, and cage are all composed of steel. The type 6205-2RS bearing dimensions are provided in Table 5.1 and fundamental fault frequencies in Table 5.2.

Table 5.1. Type 6205-2RS/6205-RS bearing parameters

Bearing Parameter	Ball Diameter	Pitch Diameter	Inside Diameter	Outside Diameter	Thickness	Number of Balls
Value	8 (mm)	39 (mm)	25 (mm)	52 (mm)	15 (mm)	9

Table 5.2. Type 6205-2RS/6205-RS bearing fundamental fault multipliers

Fundamental Frequency Type	Inner Race	Outer Race	Cage	Ball
Fundamental Frequency (Hz)	5.415	3.585	0.398	4.714

6. VALIDATION RESULTS

6.1 Experimental Data Sets Used for Validation of Methodology

Table 6.1. Shaft speed, sample duration, and number of samples collected for all steel bearings

Shaft Speed (Hz)	Sample Duration (s)	Number of Samples
30	15	5
45	12	5
60	8	5

Table 6.2. Shaft speed, sample duration, and number of samples collected for steel bearing low speed experiment

Shaft speed (Hz)	Sample Duration (s)	Number of Samples
2	100	5
4	50	5
6	33	5
8	25	5
10	20	5

6.2 UH-60A On-Aircraft Vibration Data

Test-cell experiments were conducted in the Helicopter Transmission Test Facility (HTTF) at the Patuxent River Naval Air Station in Maryland, USA. The transmission with the 82 mm planet carrier crack was tested along with a healthy transmission. A total of six accelerometers and two tachometers were used for data acquisition. Raw time domain data was collected over a range of torque levels at a sampling rate of 100 kHz for a length of 180 seconds.

The on-aircraft vibration data was acquired using the US Army VMEP system (Grabill *et al.*, 2001; Grabill *et al.*, 2002; Grabill *et al.*, 2003). At the Corpus Christ Army Depot (CCAD), the transmission with the 82 mm cracked carrier was installed and tested in a UH-60A helicopter (Aircraft X). Three unfaulted UH-60A helicopters (Aircraft A, B & C) were also tested from the Birmingham, Alabama National Guard (BNG). For safety precautions, only ground runs at 20%

and 30% torque settings were completed and each aircraft was stabilized for 5 minutes at each state before vibration acquisitions were completed. For all vibration measurements, the nose was pointed in the direction of the wind which was less than 10 knots. It is also important to note that the cyclic stick position may have varied between acquisitions.

The raw data was only acquired for Aircrafts A and X using the VMEP system. Additionally, only Accelerometers 3 and 5 from Figure 2 were recorded. The sampling rate for the raw data was 48 kHz with a bandwidth of 18.75 kHz. The acquisition lengths were 25 seconds equating to data records of 1.2 million samples per acquisition. Further information regarding planetary gear mesh vibration can be found in (Blunt and Keller, 2006).

6.3 AE Based Fault Diagnosis Results 6205-2RS Steel Bearing

(The results in this section are previously published as Van Hecke, B., Qu, Y., and He, D., 2014, "Bearing fault diagnosis based on a new acoustic emission sensor technique", *Proceedings of the Institution of Mechanical Engineers Part O: Journal of Risk and Reliability*, Vol. 229, No. 2, DOI: 10.1177/1748006X14558900.)

This section presents the validation results for the seeded fault tests conducted on the bearing test rig. After heterodyne, the AE data was digitized at a sampling rate of 100 kHz. The AE signal was acquired simultaneously with the tachometer signal which was a record of the shaft rotation. Provided in Figure 6.1 is the tachometer and raw AE signal from the seeded inner race fault bearing recorded at a shaft speed of 30 Hz.

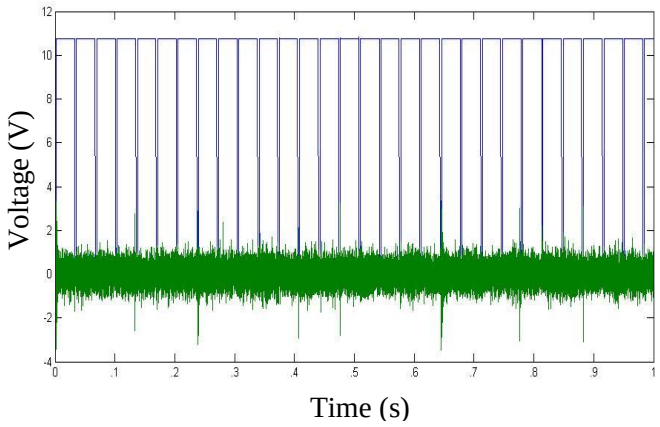

Figure 6.1. Inner race fault raw AE and tachometer signal at 30 Hz shaft speed

Before the spectral average of the AE signal could be computed, the bearing signals were band pass filtered. Upon examining the frequency spectrums, it was observed that the fundamental fault frequencies could not be identified. Thus, the calculated fault frequencies could not be used as the basis for band pass filter selection. However, to choose a proper filter band, Shannon's entropy was computed on the resulting healthy bearing signals after the implementation of different filter bands. Figure 6.2 presents an example of this technique applied to a healthy bearing signal. Provided is the value of entropy or average amount of information in the signals for each filter band tested. As shown in Figure 6.2, the highest level of entropy is observed with the use of a 5 kHz to 20 kHz filter band.

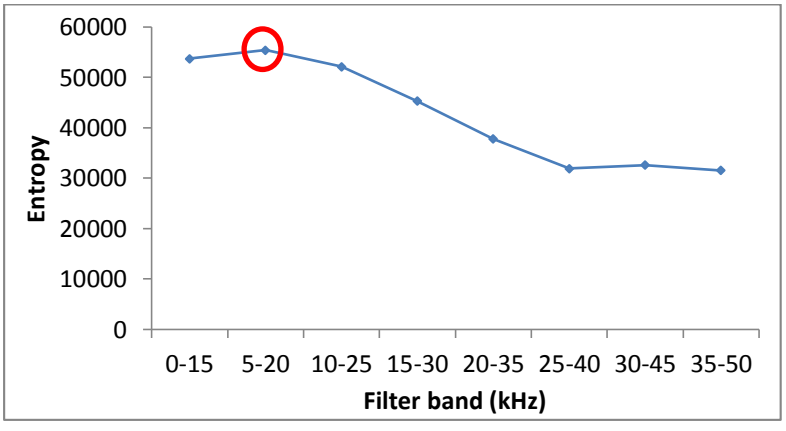

Figure 6.2. Entropy of band pass filtered healthy bearing signal at 45 Hz shaft speed

Based on the results shown in Figure 6.2, a filter band of 5 kHz to 20 kHz was selected and utilized for the results presented in this section. Thus, the AE signal was band pass filtered, time synchronously resampled, and spectrally averaged using the signal information contained between ZCT of the shaft. Finally, the CIs were computed after the time domain representation of the spectral average result was acquired.

Although a total of 10 CIs were tested, two were found to be effective: RMS and peak. Additionally, for comparison purposes and to exemplify the effectiveness of the selected filter band, results are presented for signals with and without the implementation of a band pass filter before additional processing. Figure 6.3 presents the RMS CI results for all collected samples without the use of a band pass filter and Figure 6.4 presents the RMS CI results for all collected data samples after using the aforementioned filter band selection criteria. Samples 1-5 correspond to a shaft speed of 30 Hz, while samples 6-10 correspond to a shaft speed of 45 Hz and samples 11-15 correspond to a shaft speed of 60 Hz.

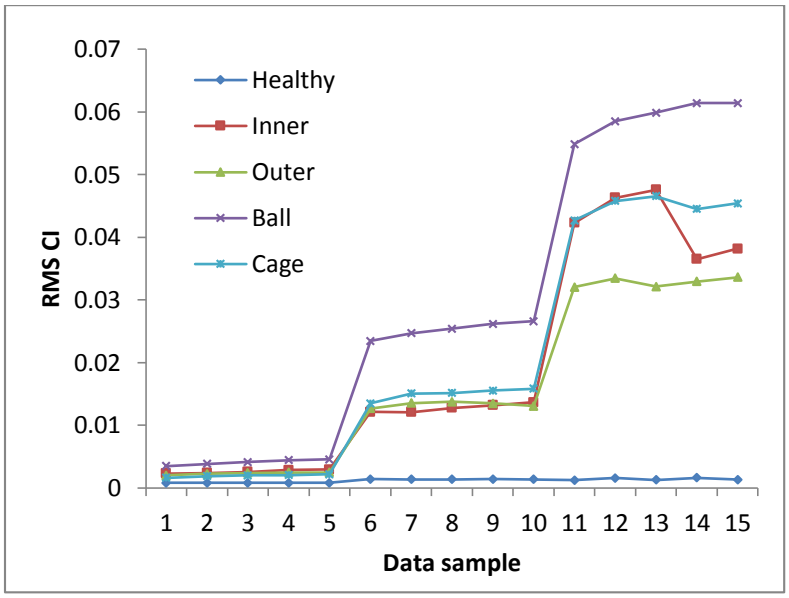

Figure 6.3. Steel bearing AE signal RMS by sample number without filter

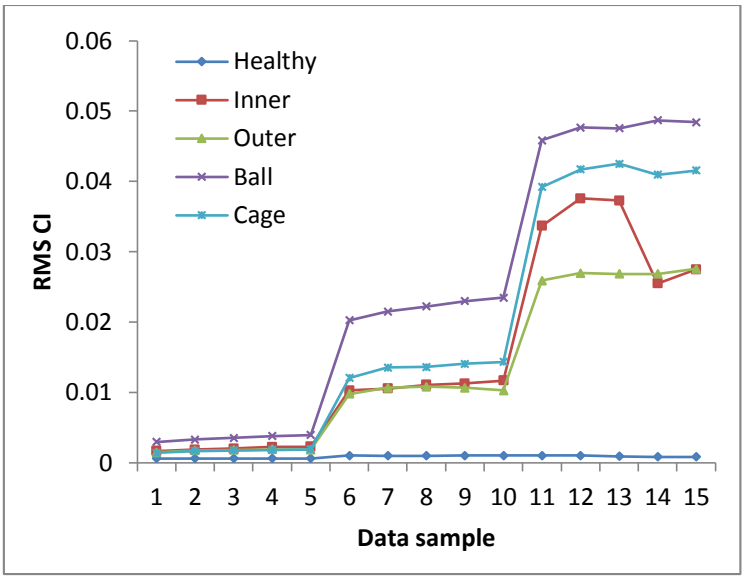

Figure 6.4. Steel bearing AE signal RMS by sample number with filter

It should be noted that for the faulty bearing signals, the RMS CI value increases with shaft speed, regardless of fault type and whether or not a filter was utilized. Additionally, there is clear differentiation of any of the faulty bearing signals when compared to the healthy case for all acquisitions. However, it should be noted that with the use of a filter, greater separation is observed between the cage and inner race results for samples 11 – 13 at the 60 Hz shaft speed. Additionally, a decrease in separation was observed at samples 14 and 15. Moreover, at the 45 Hz shaft speed, the filtered result provided better separation of the cage fault signal from inner and outer race fault signals. The least amount of separation was observed at the 30 Hz shaft speed regardless of whether or not the filter was implemented. To determine the diagnostic ability of the methodology, the RMS CI values for all signals were averaged and plotted versus shaft speed. The results for both the non-filtered and filtered data samples are presented in Figure 6.5 and Figure 6.6 respectively.

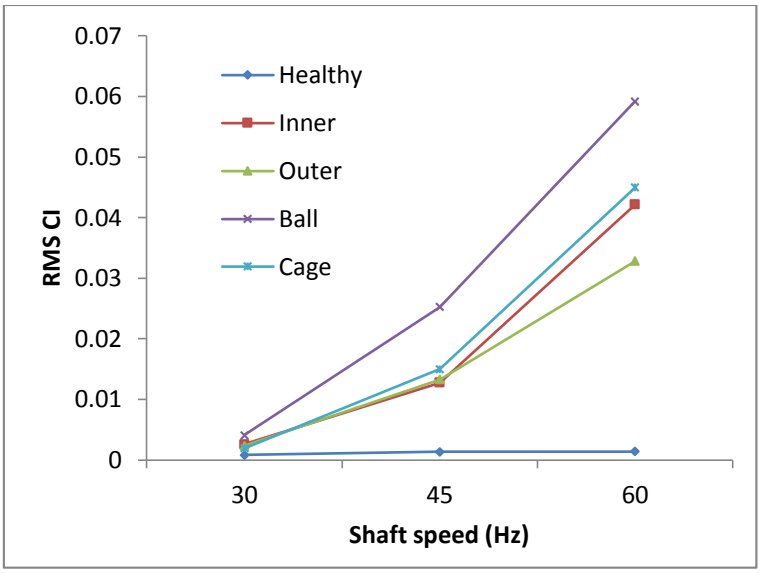

Figure 6.5. Steel bearing AE signal average RMS by shaft speed without filter

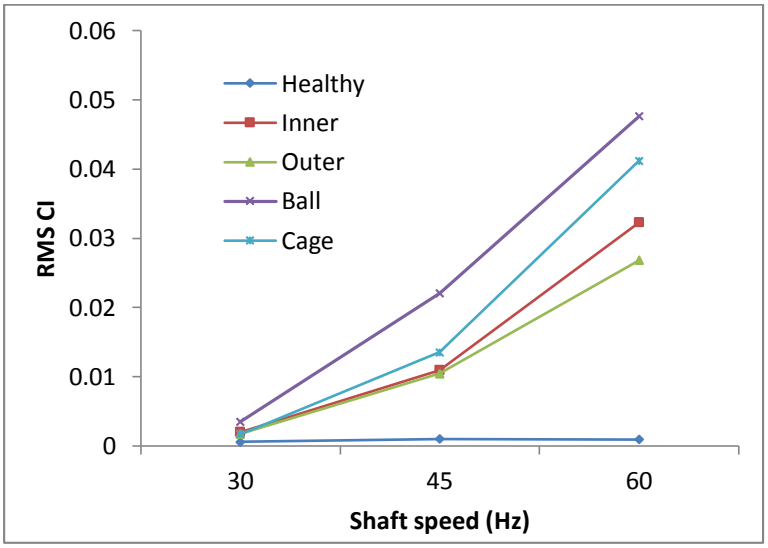

Figure 6.6. Steel bearing AE signal average RMS by shaft speed with filter

The results in Figure 6.5 and Figure 6.6 indicate that RMS is an effective CI at the tested shaft speeds. All fault types can be differentiated from each other and the healthy bearing case. The averaged results further exemplify the previously mentioned observations. With the implementation of a band pass filter before spectral averaging, a greater separation of the results

is observed at the 60 Hz shaft speed. Additionally, without filtering the inner and outer race average switches at the 45 Hz shaft speed which was not problematic for the case when a band pass filter was utilized. Similar results were observed for the peak CI and are shown in Figure 6.7 and Figure 6.8.

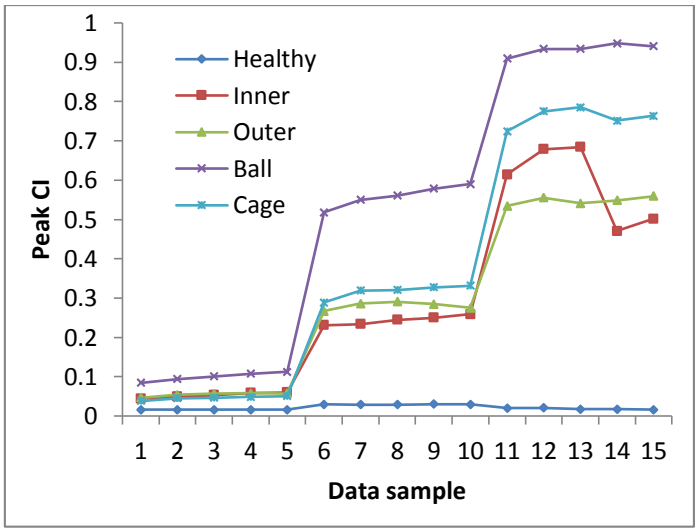

Figure 6.7. Steel bearing AE signal Peak by sample number without filter

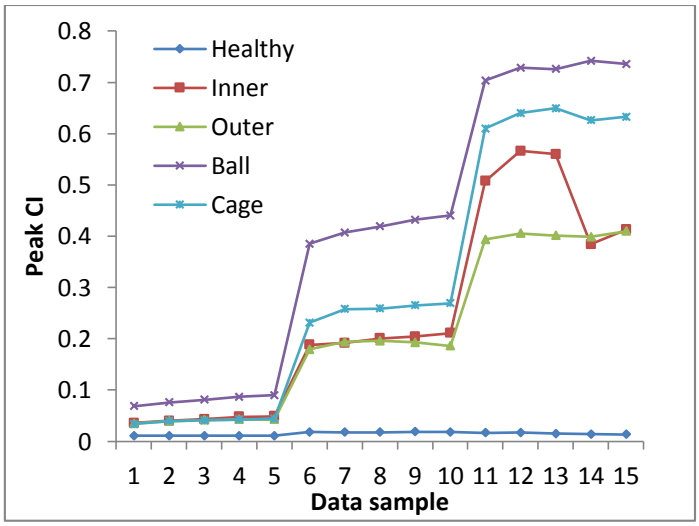

Figure 6.8. Steel bearing AE signal peak by sample number with filter

As shown above, the peak CI also effectively differentiates the faulty bearing signals from the healthy case. Although the results appear similar, the average of the peak value versus shaft speed provides a better view for comparison. The peak CI results are presented in Figure 6.9 and Figure 6.10 respectively.

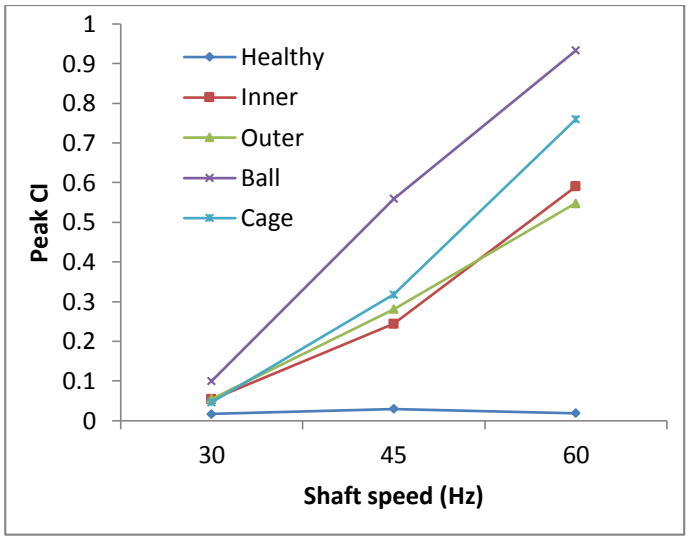

Figure 6.9. Steel bearing AE signal average peak by shaft speed without filter

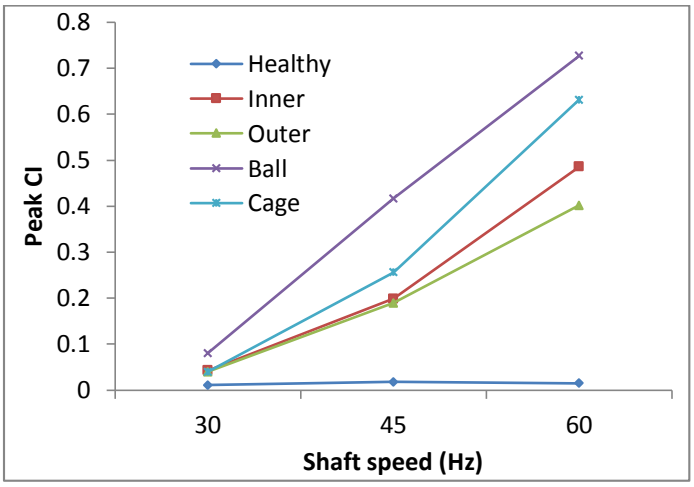

Figure 6.10. Steel bearing AE signal average peak by shaft speed with filter

As with the average RMS CI results, the average peak CI also is effective in differentiating the faulty bearing cases from each other and the healthy case. Additionally, it should be noted that the separation of cage and inner race faults when using the peak CI is greater than when using RMS, suggesting that peak value is a more effective CI for bearing fault diagnosis using this methodology. Also, the previously mentioned switch of inner and outer race results at the 45 Hz shaft speed is distinct for the results obtained without filtering. As with RMS, when the filtered results are utilized, this phenomenon did not occur. Moreover, as with the previous case, the faulty results are clearly separable from the healthy case, with ball fault results indicating the largest level of separation. However, it should be noted that although the inner race, outer race and cage faulty results are differentiated from the healthy bearing case, the separation from each other cannot be seen as distinctly as with the 45 and 60 Hz shaft speeds. Note that in Figure 6.6 and Figure 6.10, one can observe that the CI values of the faults are ranked in an increasing order as follows: outer race fault, inner race fault, cage fault, and ball fault. This observed trend can be explained as following. In the test rig, the bearing inner race moves with the shaft while the outer race is stationary. Thus, as the components rotate, the outer race impacts are the least likely to occur, which is why the RMS and Peak CI values for the outer race acquisitions were the lowest amongst the failure modes. Since the inner race is moving with the shaft, there are more opportunities for inner race impacts when compared to the outer race case which results in higher CI values. This phenomenon is exaggerated with the cage fault bearing. As the inner race rotates, the cage fault causes uncharacteristic movement of the cage and an increase in behavior in the AE signal which results in a higher value of both the RMS and peak value in the acquisitions when compared to the both of the bearing races. On that note, the rolling elements are constantly spinning as the inner race rotates, so the missing ball volume in

seeded fault provides more opportunities for impacts and results in the ball fault bearing having highest observed RMS and Peak values amongst the acquisitions. Conversely, the healthy bearing contains an absence of fault, so there were not any excitations in the signals that result in increasing RMS and Peak value with increments in shaft speed.

In summary, the RMS and peak features extracted from the spectral average results effectively differentiate all four fault types from each other and from the healthy bearing case, which has not been presented in the literature. Thus, the use of the TSR based spectral averaging approach exemplifies the effectiveness of implementing an AE based approach. Additionally, the presented approach requires the computation of a single average, eliminating the need for multiple averages for each bearing component. Hence, the results indicate that the presented technique is an effective and efficient approach to AE based bearing fault diagnostics.

6.4 Vibration Based Fault Diagnosis Results 6205-2RS Steel Bearing

(The results in this section are previously published as Van Hecke, B., Qu, Y., He, D., and Bechhoefer, E., 2014, "A new spectral average-based bearing fault diagnostic approach", *Journal of Failure Analysis and Prevention*, Vol. 14, No. 3, pp. 354– 362.)

This section presents the validation results for the seeded fault test conducted on the bearing test rig. The vibration signals were digitized at a rate 102,400 kHz simultaneously with the tachometer signal which was a record of the shaft rotation. Figure 6.11 shows a 1 second acquisition of a tachometer and raw vibration signal from the seeded cage fault bearing recorded at a shaft speed of 30 Hz.

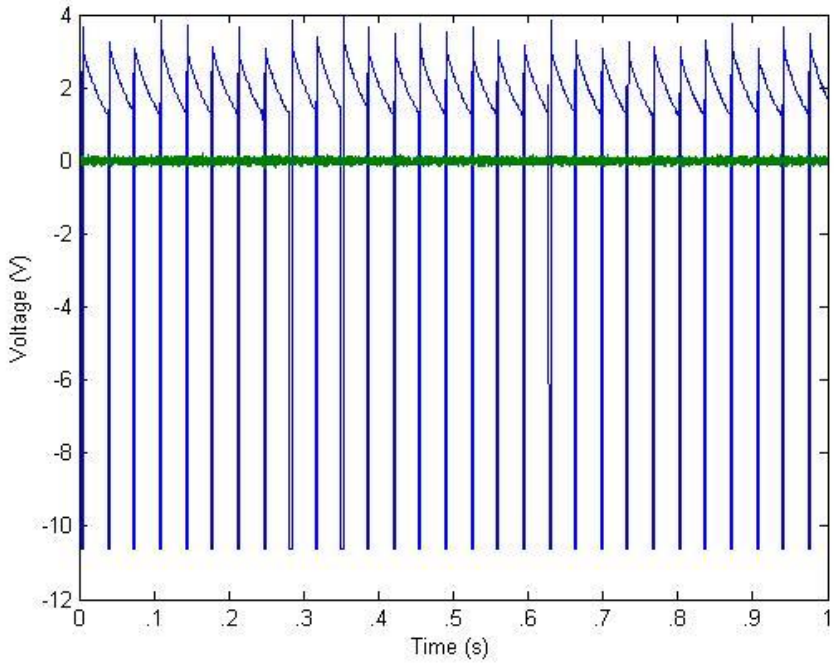

Figure 6.11. Cage fault raw vibration and tachometer signal at 30 Hz shaft speed

Before the SA of the vibration envelope signal could be computed, the faulty bearing signals were band pass filtered. Upon examination of the spectrums of the faulty bearing signals, it was observed that due to noise in the system, the fundamental fault frequencies could not be observed. Thus, the aforementioned fundamental frequencies could not be used as the basis for filter band selection. However, it was observed that the majority of the energy related to the signal was contained below 15 kHz. Thus, a filter band of 1 Hz to 15 kHz was applied before the spectral average computation to extract the signal information related to the bearing defects. Provided in Figure 6.12 is an example spectrum for each faulty bearing type at a shaft speed of 60 Hz.

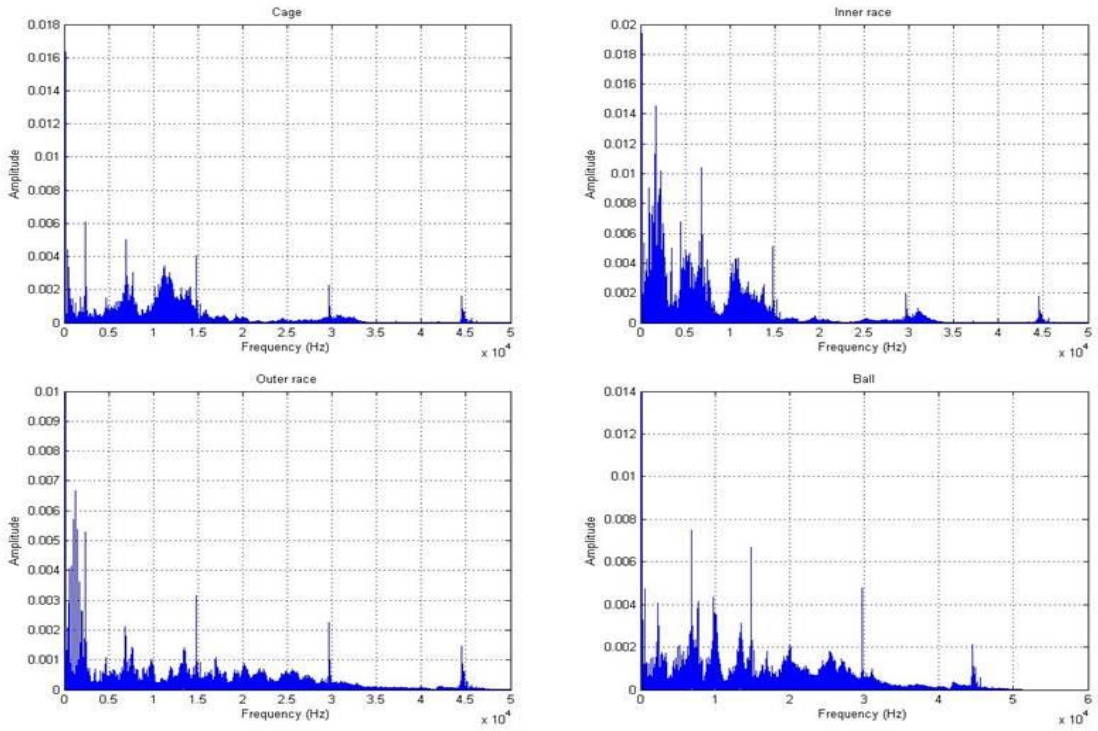

Figure 6.12. Vibration frequency spectrums for cage, inner race, outer race, and ball bearings

Once the raw signal was band pass filtered, it then was enveloped, time synchronously resampled, and spectrally averaged using the signal information contained between ZCT of the shaft. Then, after the time domain representation of the spectral average result was acquired, numerous CIs were computed. Although a total of 10 CIs were tested, two were found to be effective: RMS and peak value. Provided in Figure 6.13 is the RMS CI results for all collected data samples. Samples 1-5 correspond to a shaft speed of 30 Hz, while samples 6-10 correspond to a shaft speed of 45 Hz, and samples 11-15 correspond to a shaft speed of 60 Hz.

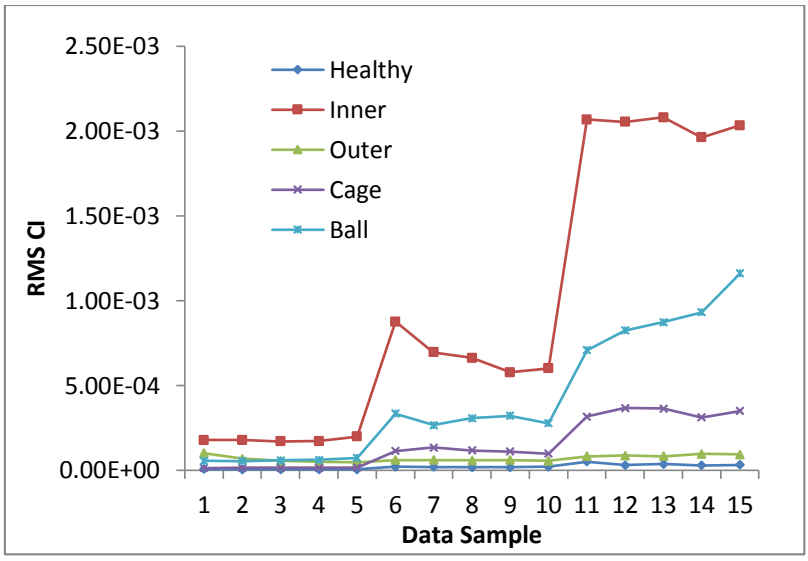

Figure 6.13. Steel bearing vibration signal RMS by sample number

As shown in Figure 6.13, the RMS value for inner race, ball, and cage fault bearings increase with shaft speed. This results in an increase of separation of the faulty from the healthy bearing case. However, it should be noted that although a separation of the outer race fault bearing to the healthy case is observed, the increase in RMS is subtle compared to the other seeded fault bearing results. Additionally, at the shaft speed of 30 Hz, the RMS values for ball, cage, and outer race fault bearings are close and do not follow the same level of separation observed at the 45 Hz and 60 Hz shaft speeds. To determine the effectiveness of the RMS CI, the average values by shaft speed (Hz) are presented in Figure 6.14.

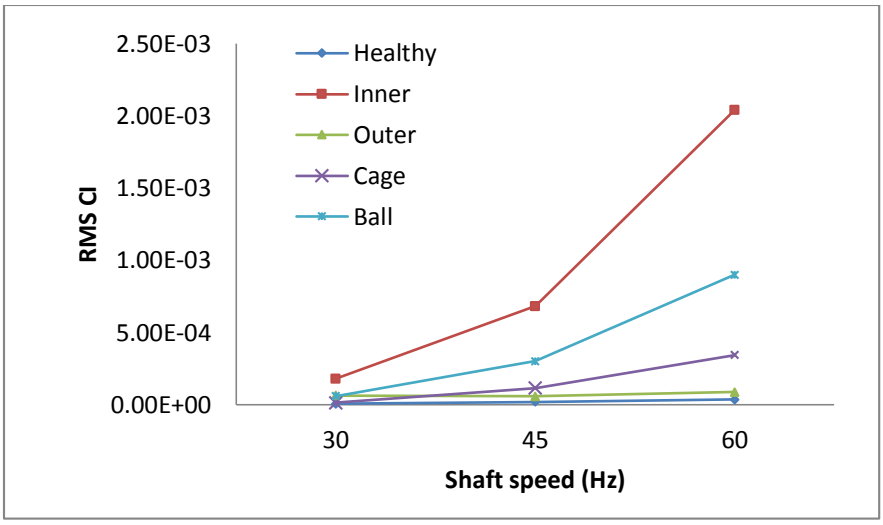

Figure 6.14. Steel bearing vibration signal average RMS by shaft speed

In Figure 6.14, it is observed that clear diagnosis of all four fault types can be accomplished at both the 45 Hz and 60 Hz shaft speeds. Additionally, because the outer race faulty bearing RMS separation level is not as significant as the other faulty bearing cases; the lowest differentiation from the healthy bearing result is observed. However, the peak CI proved to be a more effective CI than RMS and the result is shown in Figure 6.15.

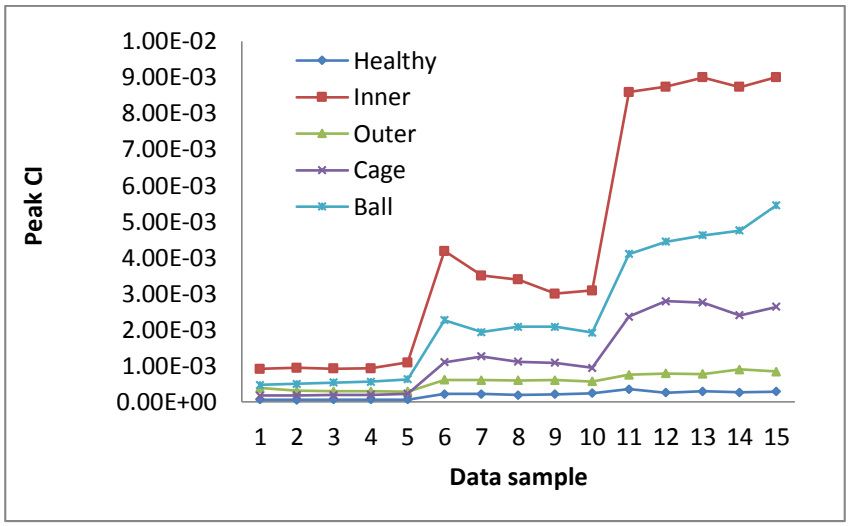

Figure 6.15. Steel bearing vibration signal peak by sample number

As observed in Figure 6.15, it should be noted that for the faulty bearing signals, the peak CI value increases with shaft speed, regardless of fault type. Similar to the RMS results, the outer race signals provided the lowest increase in peak value as the shaft speed increased. However, separation of the faulty bearing results from the healthy case is observed. Additionally, the faulty bearing average peak values are separable from each other for all samples except for a switch of the cage and outer race results at the shaft speed of 30Hz. As with the RMS CI, to determine the diagnostic ability of the methodology, the peak CI values for all signals were averaged and plotted versus shaft speed. This result is presented in Figure 6.16.

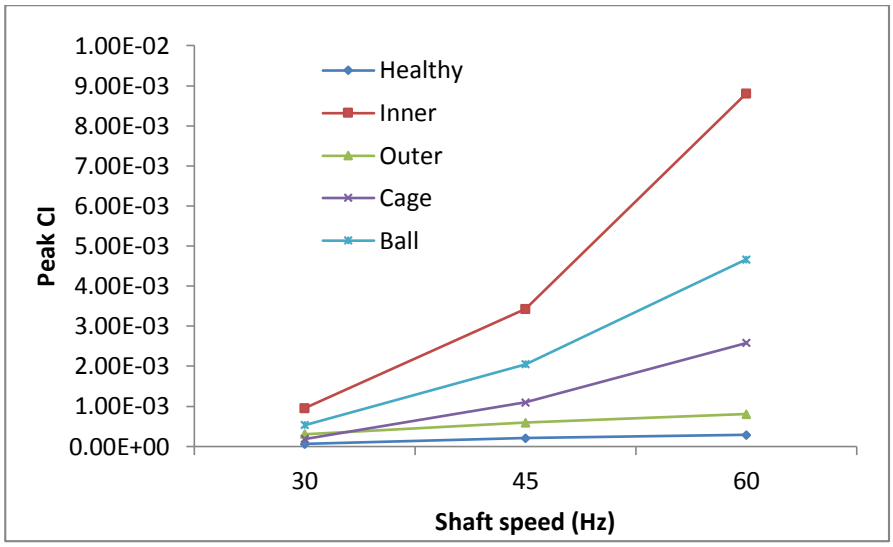

Figure 6.16. Steel bearing vibration signal average peak by shaft speed

The results in Figure 6.16 indicate that peak value is an effective CI at the tested shaft speeds. All fault types can be differentiated from each other and the healthy bearing case at all shaft speeds, except at 30 Hz, where the outer race peak value is higher than the cage peak value. Furthermore, the peak value provided a better result than RMS.

In summary, the results presented indicate that the use of RMS and peak value as CIs can accomplish bearing fault diagnosis with implementation of the presented methodology. It was observed that although fault detection can be accomplished at the shaft speed of 30 Hz, the cage fault and outer race fault results cannot be distinguished. However, at the shaft speeds of 45 Hz and 60 Hz, clear separation of all four fault types from the healthy bearing case and from each other is observed, providing merit for the diagnostic ability of the presented methodology. Thus, the use of a TSR based spectral averaging approach results in the effective diagnosis of all four fault types from each other and from the healthy bearing case, which has not been reported in the literature.

6.5 A Comparison Between Spectral Averaging and the Traditional Envelope Analysis Technique

(The results in this section are previously published as Van Hecke, B., He, D., and Qu, Y., 2014, "On the use of spectral averaging of acoustic emission signals for bearing fault diagnostics", *ASME Journal of Vibration and Acoustics*, Vol. 136, No. 6, DOI: 10.1115/1.4028322.)

The envelope analysis technique has been well established for vibration based bearing fault diagnostics. Thus, before implementing the presented methodology, the envelope analysis technique was applied to the AE signals for comparison. For comparison purposes, Figure 6.17 presents a visual representation of the presented methodology and how it compares to the traditional envelope analysis technique. For envelope analysis, the path on the right is followed, where the AE signal envelope is the next step following band pass filtering. Conversely, the presented methodology follows the path on the left where time synchronous resampling is the next step after band pass filtering.

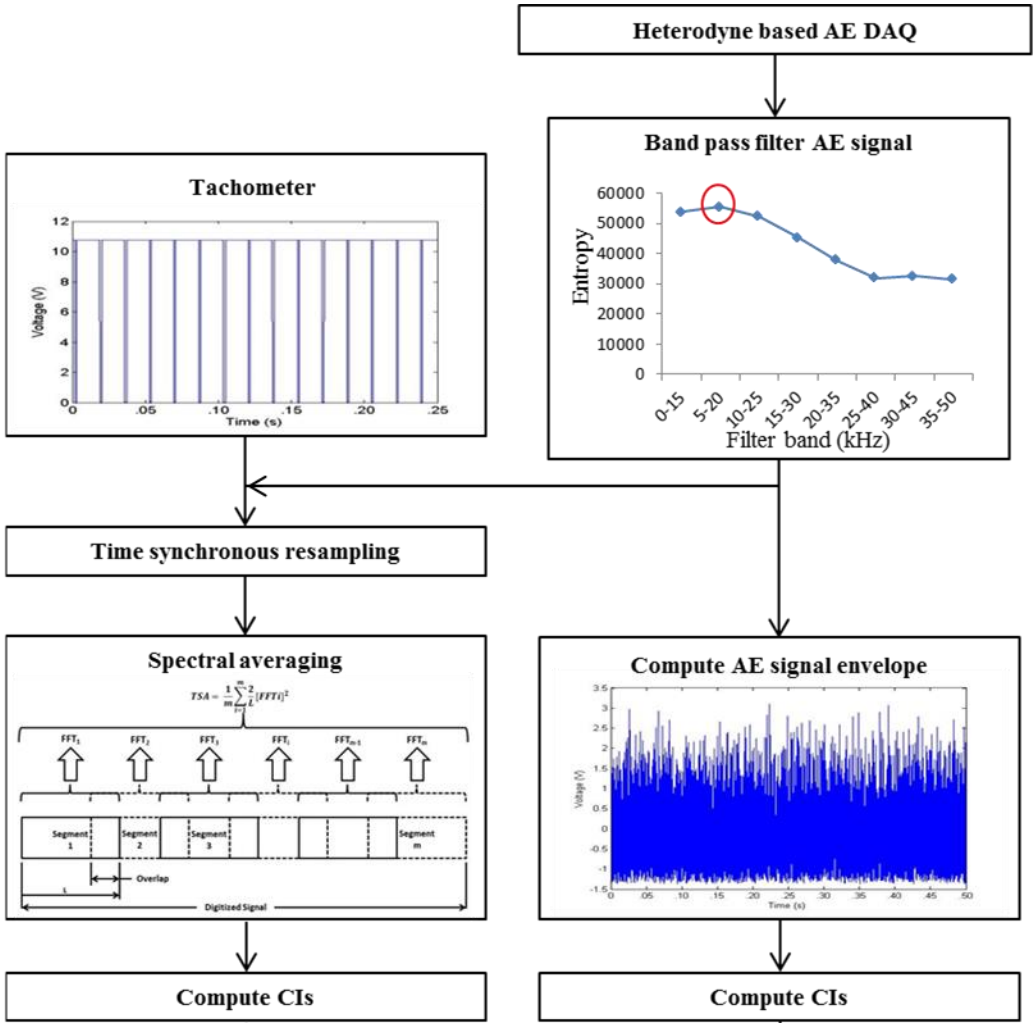

Figure 6.17. Comparison of the spectral averaging and envelope analysis techniques

When applying the methodology to the AE data, the signal envelope of the band pass filtered signal appeared to hinder the result. Thus, for spectral averaging of the AE signals, time synchronous resampling was accomplished after filtering. After selecting the filter band, the signal acquisitions were band pass filtered, synchronously resampled, and spectrally averaged using the signal information contained between ZCTs of the shaft. Then, after the time domain representation of the spectral average was acquired, numerous CIs were computed and evaluated. Although a total of 10 CIs were tested for both the spectral average and envelope analysis

results, two were found to be effective: RMS and peak. Figure 6.18 presents the RMS CI results for all collected AE data samples using the presented methodology and the envelope analysis technique.

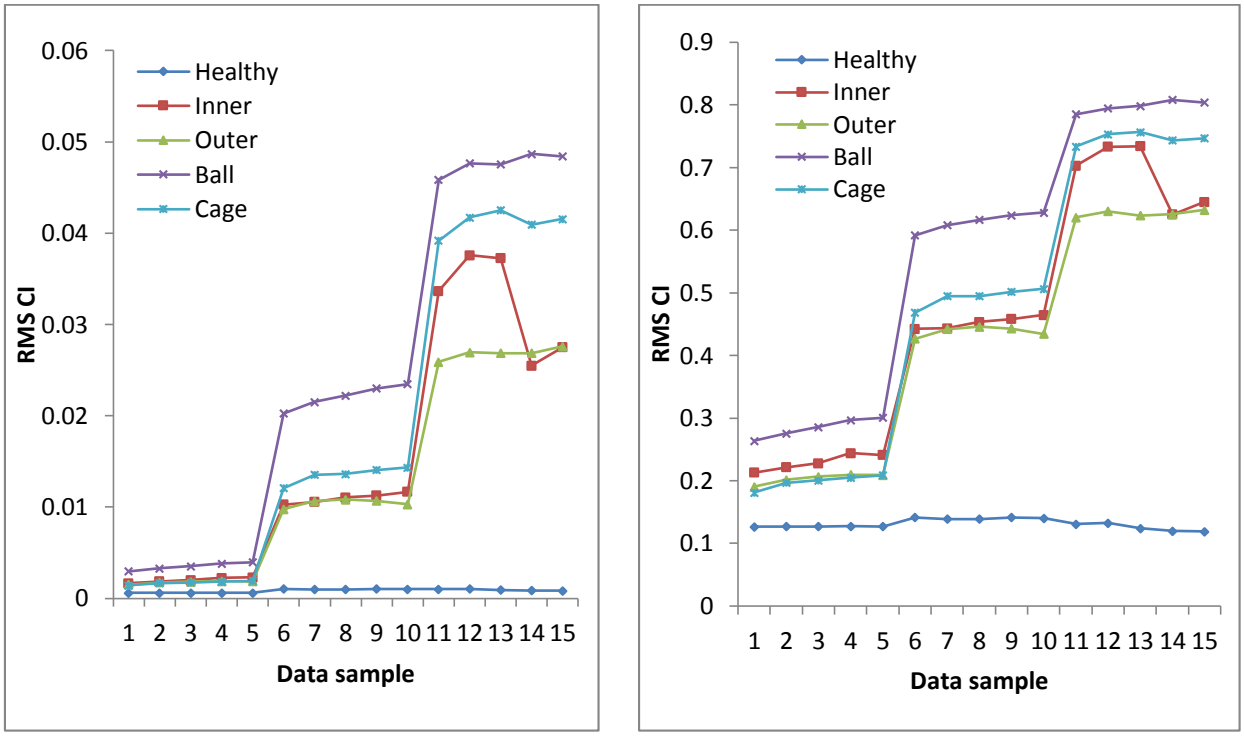

Figure 6.18. AE RMS by sample number using spectral average (left) and envelope analysis (right)

As shown in Figure 6.18, samples 1-5 correspond to a shaft speed of 30 Hz, while samples 6-10 correspond to a shaft speed of 45 Hz, and samples 11-15 correspond to a shaft speed of 60 Hz. It should be noted that for the faulty bearing signals, the RMS CI value increases with shaft speed, regardless of fault type or which methodology was applied. There are some additional observations to mention regarding the RMS CI results. Namely, as shown on the right in Figure 6.18, although envelope analysis can effectively separate the faulty bearing signals from the healthy case, the faulty signal separation at the 60 Hz shaft speed appears to be

less significant than the AE based spectral average results. Moreover, for the envelope analysis results, switching of the outer race, inner race, and cage signals were observed at the shaft speed of 30 Hz. Although the switching occurred for the spectral average results, the switching of levels was less significant. The best separation among faulty bearing types is at the 60 Hz shaft speed for both AE centered methodologies. However, the separation of the faulty signals from each other and from the healthy case appeared to be more significant when using the spectral averaging approach. To determine the diagnostic ability of the methodology, the RMS CI values for all signals were averaged and plotted versus shaft speed. The respective results are presented in Figure 6.19.

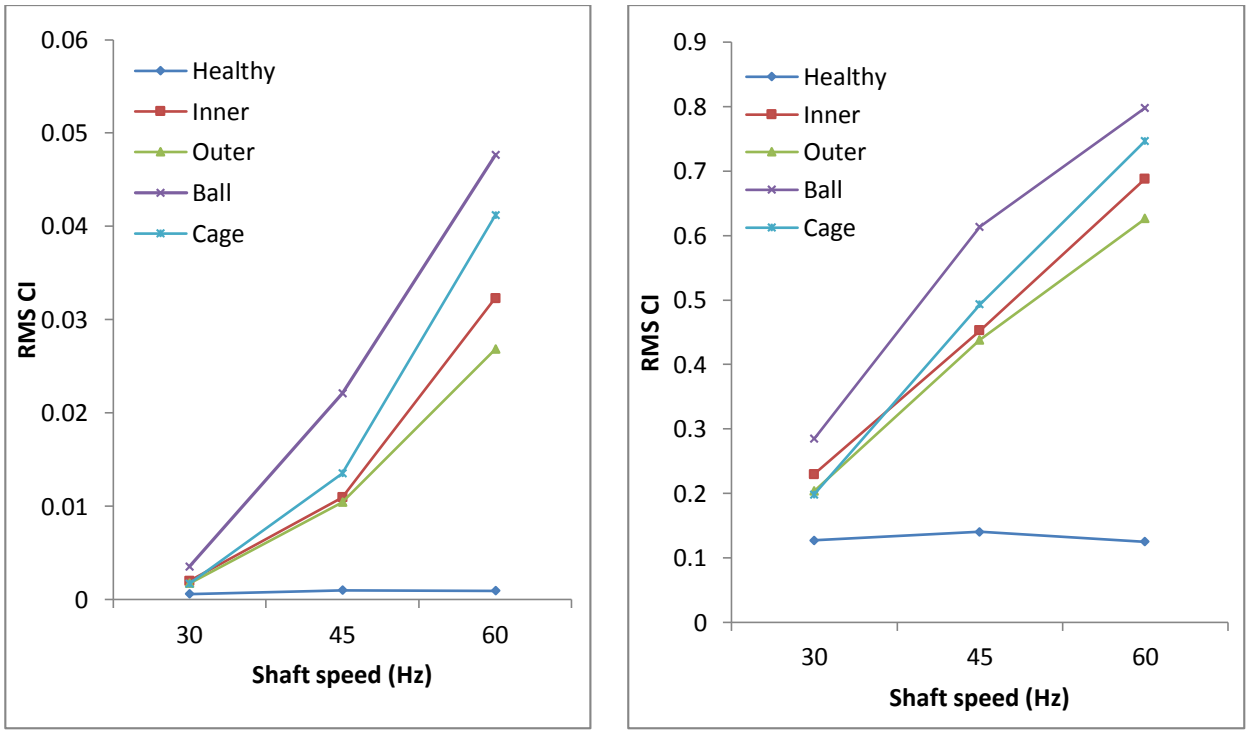

Figure 6.19. AE average RMS by shaft speed using spectral average (left) and envelope analysis (right)

The results in Figure 6.19 indicate that RMS is an effective CI at the tested shaft speeds. The AE centered envelope analysis provides the best separation of the faulty signals from the healthy. However, with that approach, the cage, inner and outer racer results are close to one another and all three appear to switch at the 30 Hz shaft speed. For the spectral average result, it should be noted that clear differentiation of the faulty signal results from each other and the healthy case is observed at both the 45 Hz and 60 Hz shaft speeds. Also, although the separation of the inner race, outer race, and cage is the least significant at the 30 Hz shaft speed, the switching of the three was not as significant as when using the envelope analysis technique. Additionally, the ball fault signal is clearly separable at all three tested shaft speeds for both methodologies. Similar results were observed for the peak CI and are presented in Figure 6.20 with data sample corresponding to shaft speed in the same fashion as in Figure 6.18.

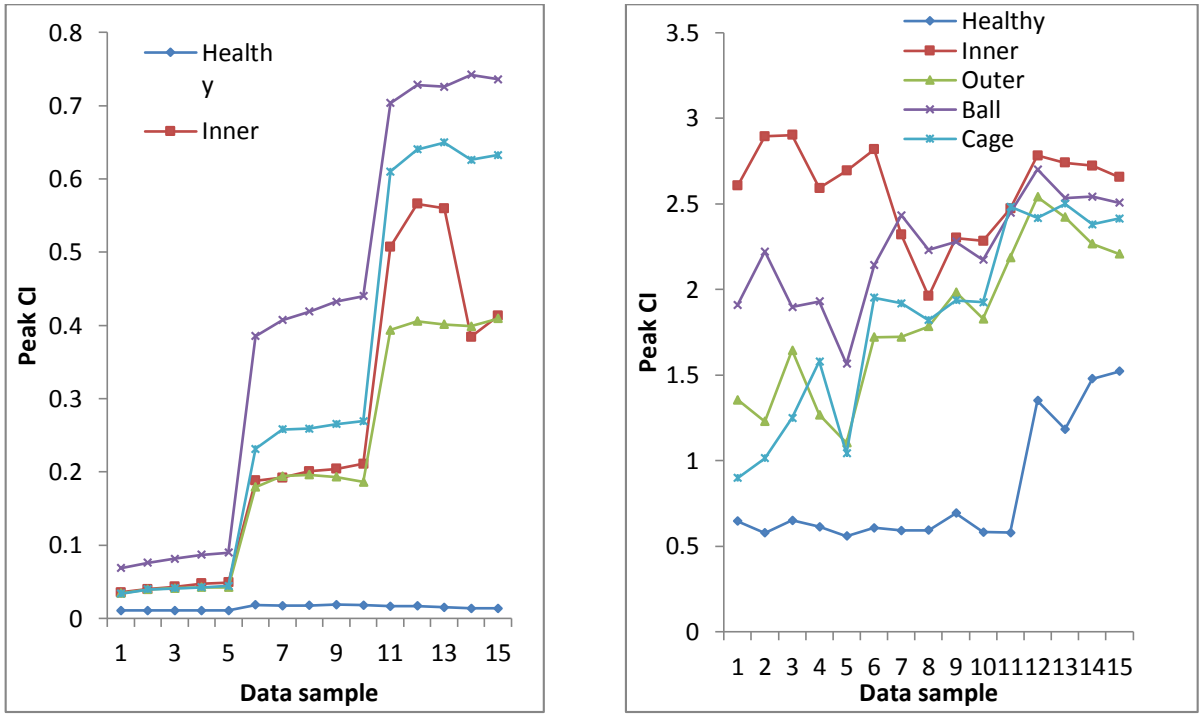

Figure 6.20. AE peak by sample number using spectral average (left) and envelope analysis (right)

As shown in Figure 6.20, the peak CI also effectively differentiates the faulty bearing signals from the healthy case. Using the AE based envelope analysis; fault detection can be made, although there is a significant amount of variability and overlap amongst the faulty signal results. As with the RMS CI, the AE spectral average result shown on the left in Figure 6.20 is the best. In this case, clear differentiation of the faulty signals from each other is apparent at the both the 45 Hz and 60 Hz shaft speed which was not observed with the AE envelope analysis results. More importantly, when using the presented approach, the highest level of separation of the faulty cases from the healthy case was also observed. It is also important to note that although the cage, inner, and outer race results are close together at the 30 Hz shaft speed, they are all separated from the healthy case, allowing fault detection to be accomplished. As with RMS, the peak CI average results are presented in Figure 6.21.

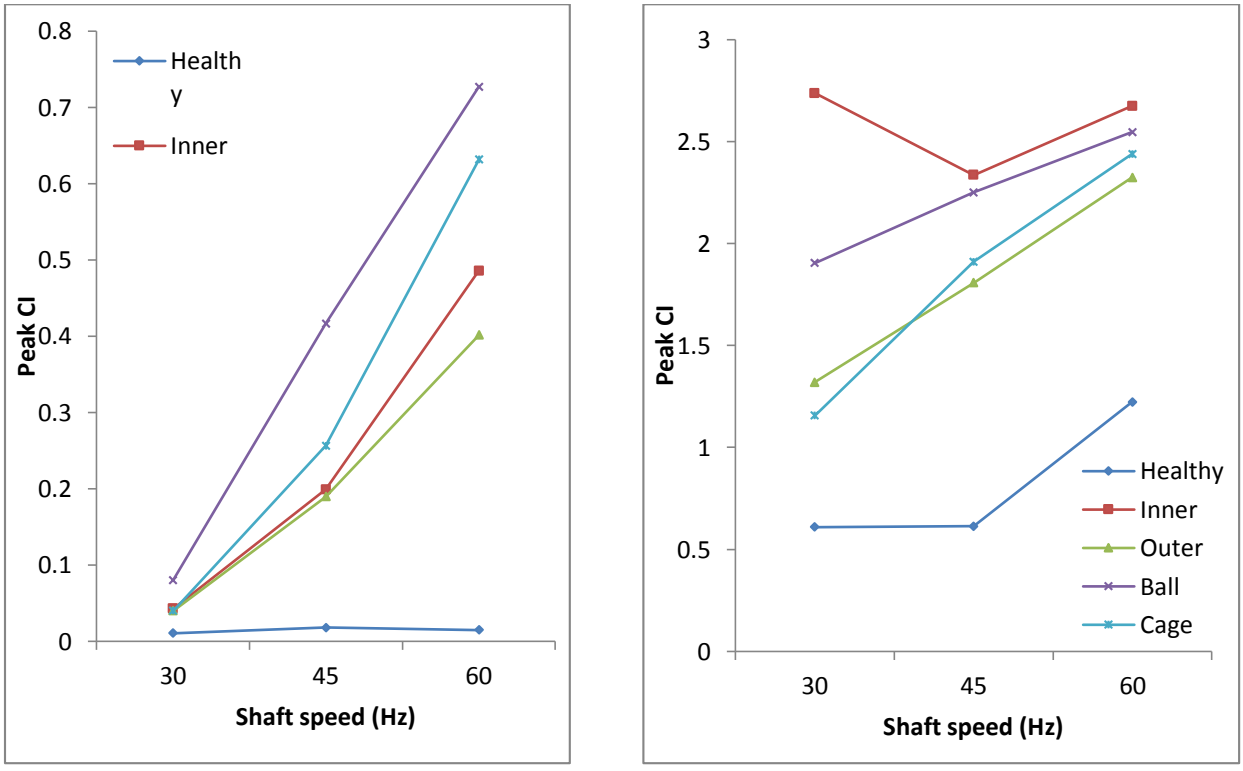

Figure 6.21. AE average peak by shaft speed using spectral average (left) and envelope analysis (right)

Similarly to the RMS CI results, the average peak CI also is effective in differentiating the faulty bearing cases from each other and the healthy case. Additionally, it should be noted that the separation of cage and inner race faults when using the peak CI is greater than when using RMS, suggesting that peak value is a more effective CI for bearing fault diagnosis using this methodology. Moreover, there is less apparent variability when using the spectral average results, suggesting a slight improvement than when applying the envelope analysis technique to the AE data.

6.6 A Comparison Between AE and Vibration Based Approaches

(The results in this section are previously published as Van Hecke, B., He, D., and Qu, Y., 2014, "On the use of spectral averaging of acoustic emission signals for bearing fault diagnostics", *ASME Journal of Vibration and Acoustics*, Vol. 136, No. 6, DOI: 10.1115/1.4028322.)

Additionally, the presented spectral averaging approach was applied to the vibration acquisitions. It was observed that for the vibration data, the utilization of the signal envelope before resampling improved the spectral average result. Hence, all vibration acquisitions were enveloped before resampling. Additionally, for comparison purposes and to exemplify the effectiveness of the presented methodology, CI results are provided using both AE and vibration data. Figure 6.22 presents the RMS CI results for the AE and vibration acquisitions.

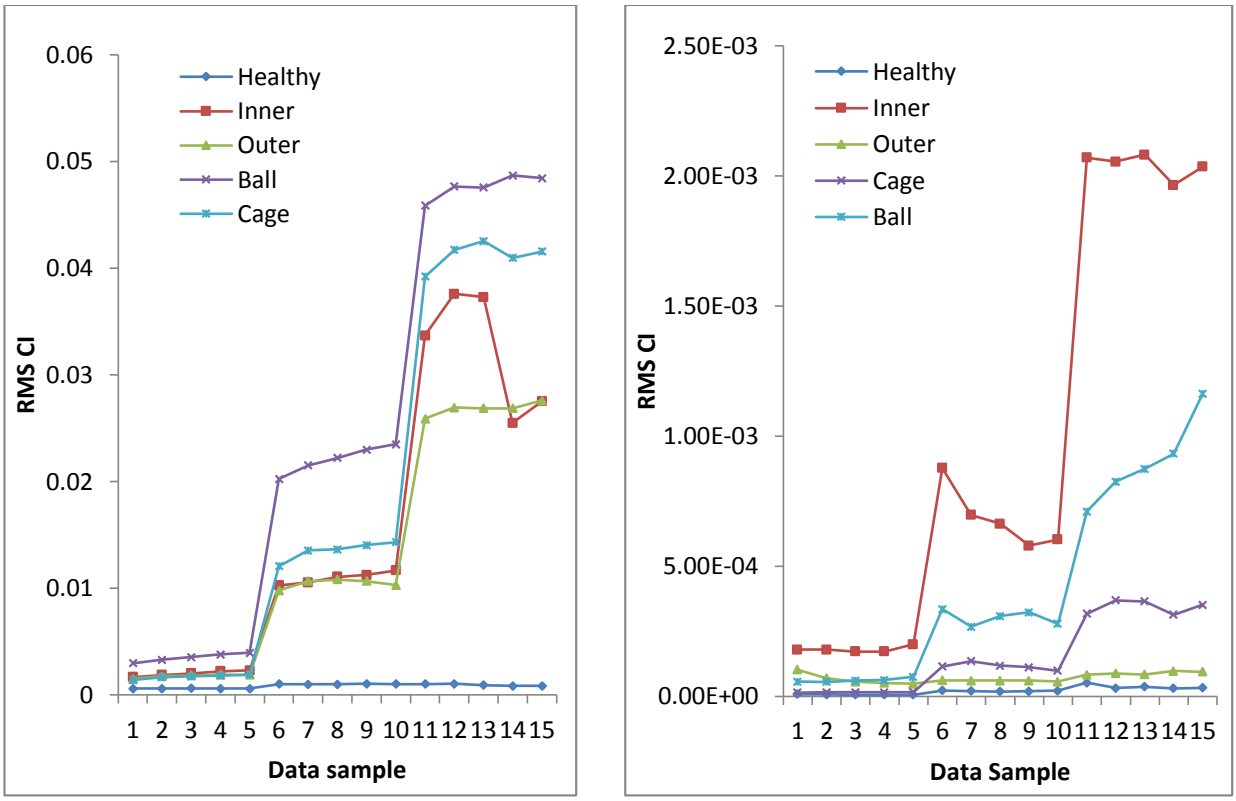

Figure 6.22. RMS by sample number for AE (left) and vibration (right) using spectral averaging

As shown in Figure 6.22, the separation for the vibration results is fair at the 45 Hz and 60 Hz shaft speeds. Additionally, it should be noted that the best separation is of the inner race signal, which is distinctly separated from the healthy and faulty bearing cases. Moreover, for vibration, the faulty bearing signals are all differentiable from each other and form the healthy case. However, the switching at the 30 Hz shaft speed is also observed as with envelope analysis results and the cage and outer race fault signals are close to the healthy at the 45 Hz and 60 Hz shaft speeds, which was not observed when using the AE based envelope analysis or spectral averaging approaches. The vibration result in Figure 6.22 shows better separation of the faulty signals from each other but the least separation of the faulty from the healthy case. It should also be noted that the separation of the faulty from the healthy bearing signals is greatest when using

the spectral averaging result. The average RMS results by shaft speed are presented in Figure 6.23.

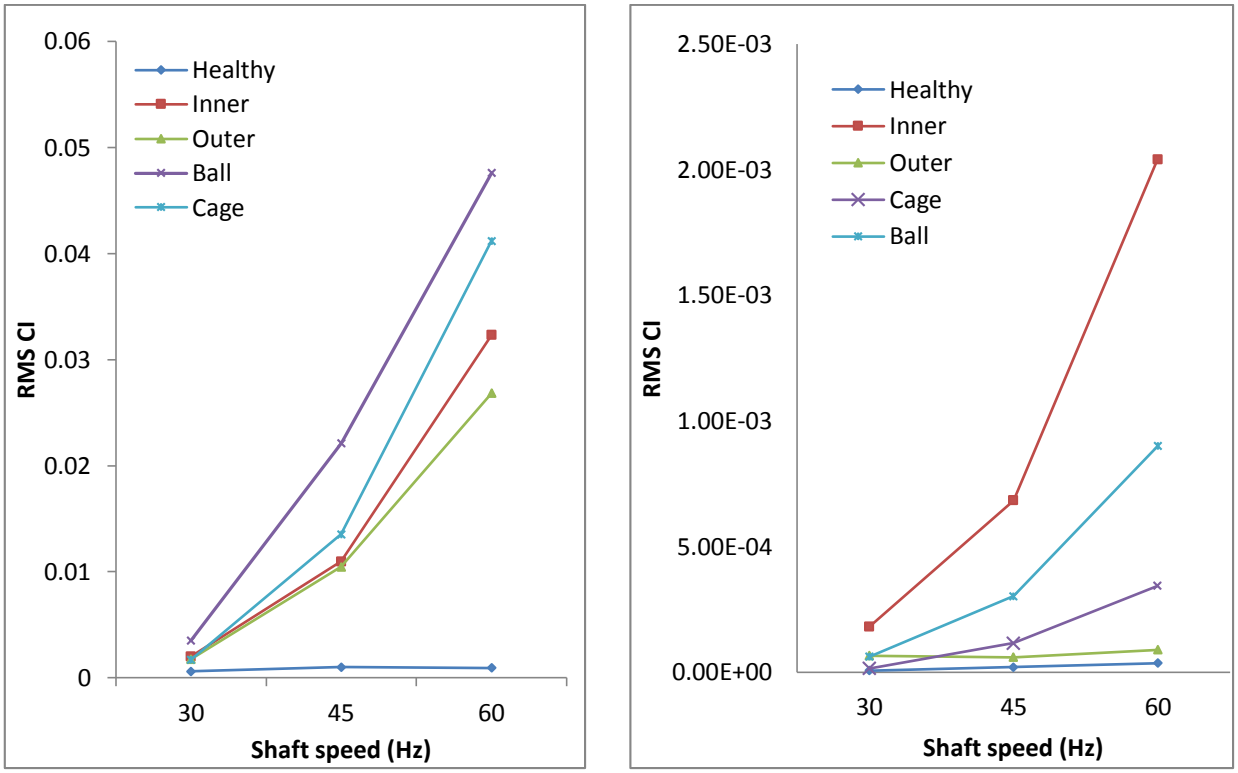

Figure 6.23. Average RMS by shaft speed for AE (left) and vibration (right) using spectral averaging

In Figure 6.23 it should be noted that the best separation of the faulty cases from the healthy case is observed at the 45 Hz and 60 Hz shaft speeds, with AE providing greater separation of the faulty signals from the healthy. Moreover, the faulty signals are clearly separable form each other at the aforementioned shaft speeds so fault diagnosis is achieved using both vibration and acoustic sensors. Additionally, switching was observed at the 30 Hz shaft speed for both data types. However, the switching is more significant for the vibration data, and switching of the cage and healthy case occurs which eliminates fault detectability at the 30 Hz

shaft speed. For AE, at the 30 Hz shaft speed, fault diagnosis is not accomplished but the separation of the faulty from the healthy allows clear fault detection. The greater separation of the faulty signal results from the healthy case in combination with the detectability of fault at the 30 Hz shaft speed suggests AE is a better approach. Next, Figure 6.24 presents the peak CI results.

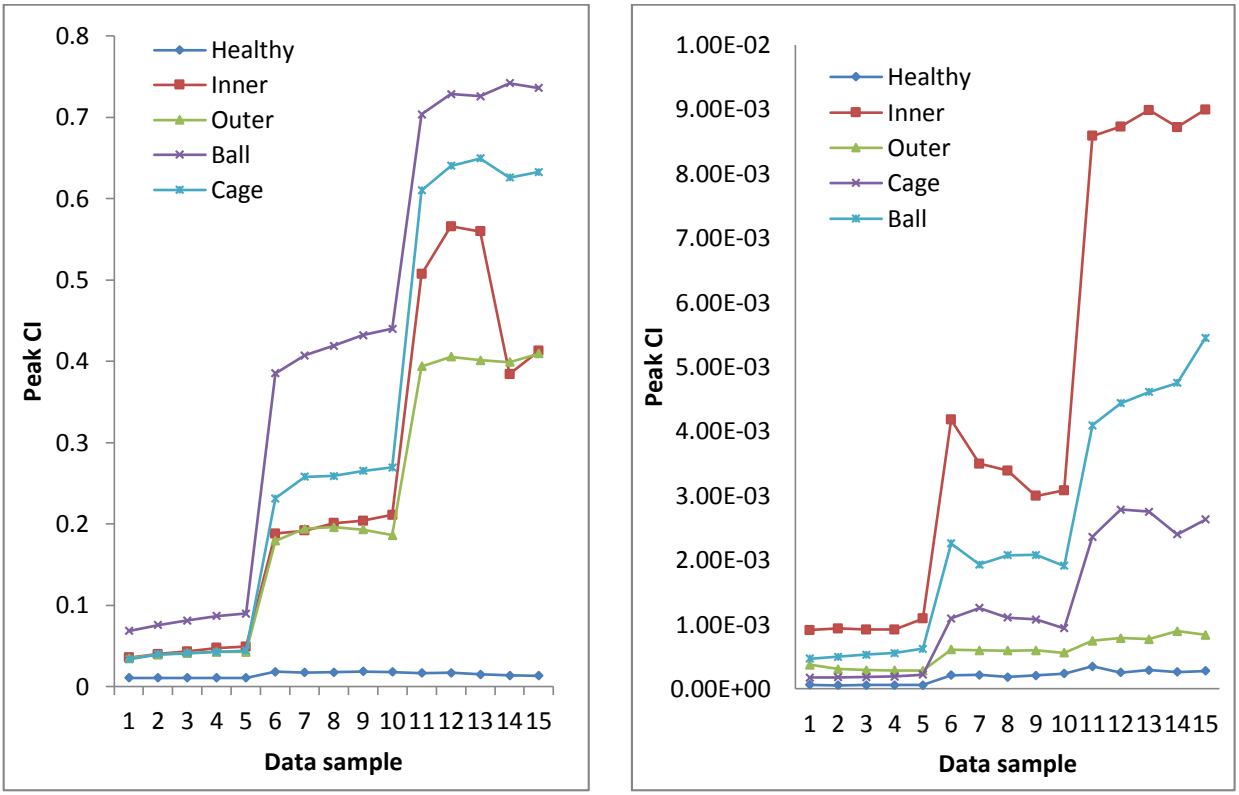

Figure 6.24. Peak by sample number for AE (left) and vibration (right) using spectral averaging

As shown in Figure 6.24, fault detection can be accomplished at all 3 tested shaft speed when applying the spectral average approach to vibration or AE acquisitions. However, it should be noted that the separation of the faulty bearing signals from the healthy case is more significant for the AE than the vibration case, suggesting that AE is a better approach when implementing the presented methodology. Moreover, the switching occurring at the 30 Hz shaft speed is more

significant for the vibration acquisitions. Additionally, the AE and vibration results obtained using the spectral average were better than the AE centered envelope analysis approach. As with the previous cases, Figure 6.25 presents the average peak results versus shaft speed.

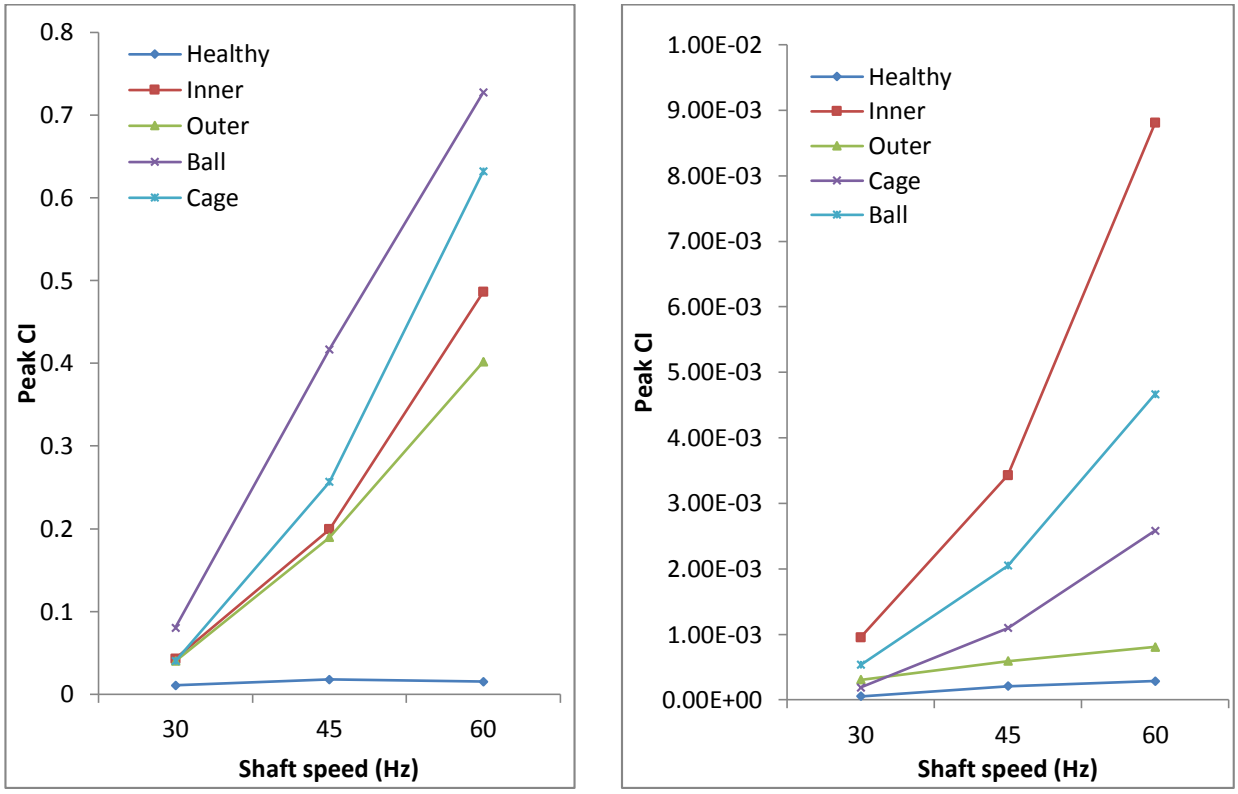

Figure 6.25. Average peak by shaft speed for AE (left) and vibration (right) using spectral averaging

As shown in Figure 6.25, the peak CI is effective for both AE and vibration when using the spectral average approach. However, AE is given a slight edge due to the greater separation of the faulty from the healthy bearing case and the less significant switch at the 30 Hz shaft speed.

In summary, the RMS and peak features extracted from the spectral average results effectively differentiate all four fault types from each other and from the healthy bearing case,

which has not been presented in the literature. Thus, the use of the TSR based spectral averaging approach exemplifies the effectiveness of implementing an AE based approach. Additionally, unlike TSA, the presented approach requires the computation of a single average, eliminating the need for multiple averages for each bearing fault type.

6.7 Low Speed AE Based Fault Diagnosis Results 6205-2RS Steel Bearing

This section presents the validation results of the conducted low speed seeded fault tests. After heterodyning, the signals were collected at a 100 kHz sampling rate. After DAQ, the signals were time synchronously resampled and spectrally averaged. The result was then used for CI computations. Although a total of 30 CIs were investigated, 4 were proven to clearly diagnose all four bearing fault types. Shown in Figure 6.26 are the averaged AM shannon's entropy CI values by shaft speed. Each point presents the average value of the 5 samples for each bearing at every tested shaft speed. Along with each average CI value is the 95% confidence error bar.

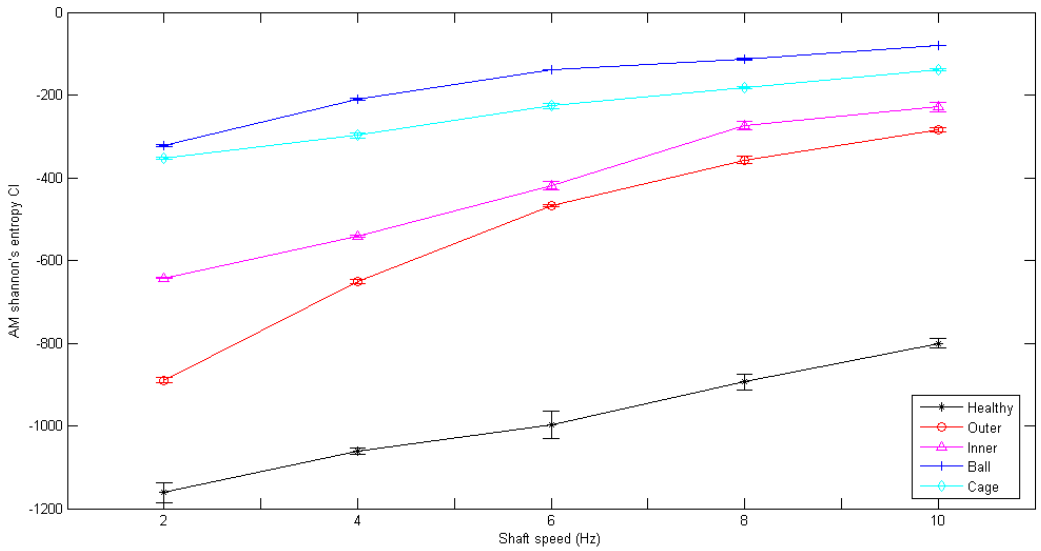

Figure 6.26. Average AM shannon's entropy by shaft speed (Hz)

As shown in Figure 6.26, the AM shannon's entropy CI clearly diagnoses all four bearing fault types. Because there is no overlap of the error bars, the separation of the failure modes from each other and the healthy bearing type is statistically validated. Additionally, all bearing signals appear to contain similar upward trending of the CI values as shaft speed is increased. Another interesting observation is that the orders of the failure modes are consistent with the high speed diagnosis results found in the previous sections. Next, Figure 6.27 presents the averaged EO shannon's entropy CI values by shaft speed.

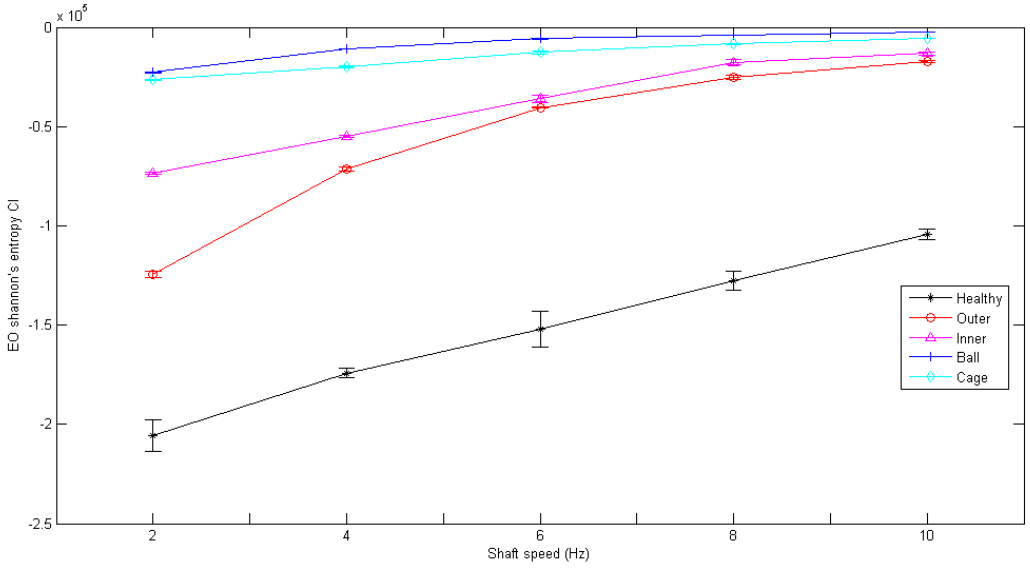

Figure 6.27. Average EO shannon's entropy by shaft speed (Hz)

The results in Figure 6.27 follow the same representation as those presented in Figure 6.26. Each point corresponds to the average CI value of the 5 acquired samples at each shaft speed, along with the 95% error bar. This result validates the capability of the EO shannon's entropy CI. There is no overlap amongst any of the error bars which confirms statistical diagnosis of the bearings types. Although diagnosis is accomplished, the separation does not

appear to be as significant as observed when using the AM shannon's entropy CI. Additionally, the bearing type order was maintained in the same fashion as Figure 6.26 as well as the aforementioned high speed bearing results. Figure 6.28 below presents the averaged Shannon's entropy results by shaft speed.

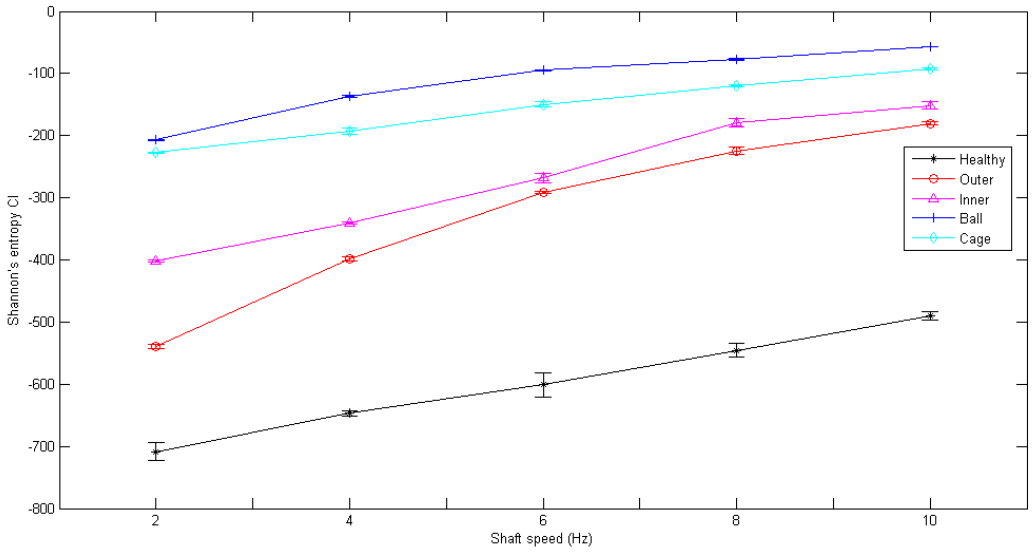

Figure 6.28. Average shannon's entropy by shaft speed (Hz)

As shown in Figure 6.28, the Shannon's entropy CI also clearly diagnoses all bearing fault types. The trending is similar to what was observed in Figure 6.26 and Figure 6.27 and the separation is statistically validated with the absence of overlap of the 95% error bars. Moreover, the appearance of the separation appears to be greater than that of the result depicted in Figure 6.27, though not as significant as the results presented in Figure 6.26. However, all three results confirm the diagnostic potential of differing forms of the Shannon entropy CI. Next, Figure 6.29 presents the average histogram lower bound results by shaft speed.

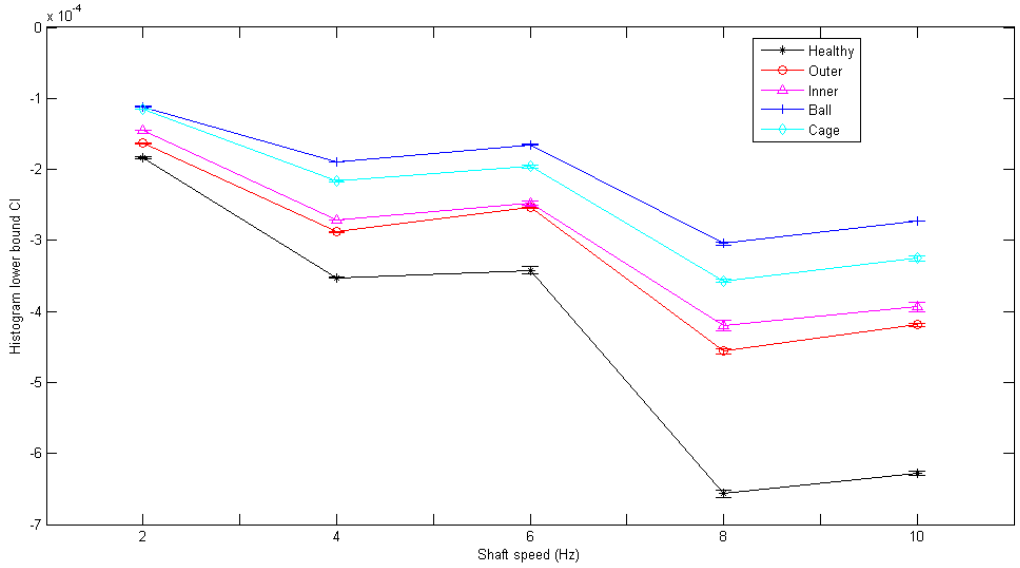

Figure 6.29. Average lower bound by shaft speed (Hz)

As shown in Figure 6.29, the histogram lower bound CI also clearly differentiates all four bearing fault types from each other and the healthy bearing case. This separation is also statistically validated by the results containing zero overlap of the error bars which was observed with the last three condition indicators. Moreover, the same order of the bearing types was observed as with the previous figures. One interesting thing to note is that the highest CI values were observed at the 2 Hz shaft speed and the trending went in the downward direction with increasing shaft speed to 10 Hz.

To summarize, Figure 6.26 to Figure 6.29 show the ability of AM shannon's entropy, EO shannon's entropy, shannon's entropy and histogram lower bound to be used for low speed bearing diagnostics when combined with a heterodyne based AE DAQ, and the presented signal processing methodology. These results confirm that the use of low sampled AE data can achieve fault diagnosis at speeds less than 10 Hz. Moreover, it should also be noted that for the shannon's entropy CI results presented in Figure 6.26 to Figure 6.28, the trending and separation

of the failure modes increases with decreasing shaft speeds. Thus, there is potential for the methodology to diagnose the bearing fault modes at shaft speeds lower than what was presented herein. Hence, a novel effective and efficient AE based low speed bearing diagnosis approach has been validated.

6.8 Detection of On-Aircraft Fatigue Crack in a UH-60A Planet Gear Carrier

First, the results for the US Army test cell data will be discussed. Of all the loading conditions, only the 20% torque test cell data for both transmissions was available for analysis. Thus, since only one acquisition of 180 seconds was available for each transmission, the data was segmented into 30 second intervals to provide more samples while ensuring enough tachometer revolutions for spectral average computations. The result was 6 segments of 30 seconds for each transmission at the aforementioned torque level and the methodology presented in Figure 4.4 was implemented. Additionally, since sensor 5 was closest to the source, it was the only sensor investigated. After the CIs were computed, 95% confidence intervals were obtained to determine the statistical significance of the CI values. It was found that 4 CIs clearly differentiated the 82 mm crack transmission from the healthy transmission. Figure 6.30 presents the average CI values for the 6 samples along with the 95% confidence intervals for sensor 5 test cell data.

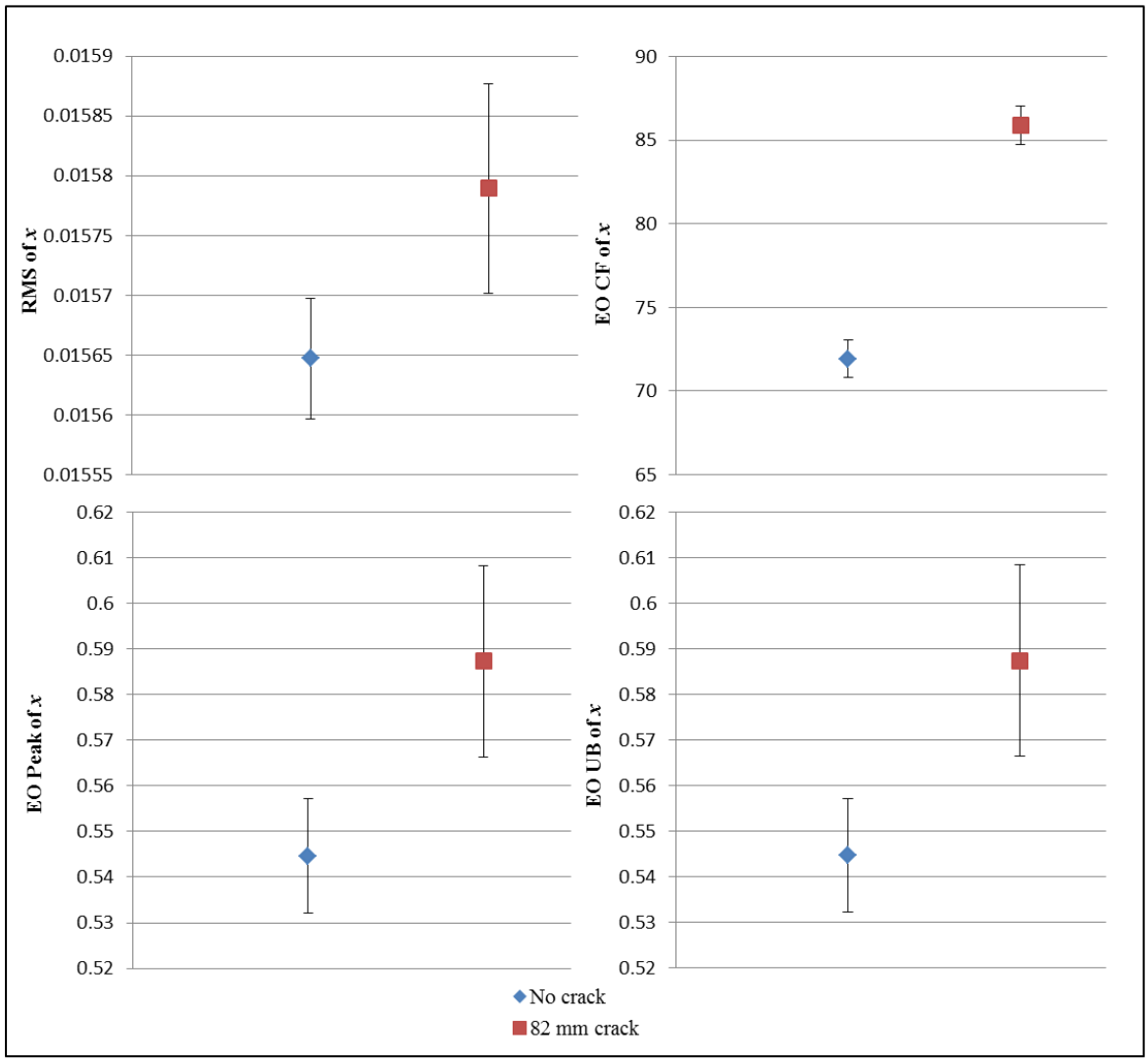

Figure 6.30. Average CI values with 95% confidence interval for sensor 5 test cell data

Next, the results of the UH-60A on-aircraft VMEP data analysis are presented. All VMEP acquisitions were processed following the methodology presented in Figure 4.4. To determine if the fatigue crack was detectable for the on-aircraft data using the presented approach, the two sample CI values at each torque setting were averaged. For sensor 3, the average CI values for each torque level are presented in Table 6.3. Once the average CI values were computed, the percent difference in the CI values between Aircraft X and Aircraft A was

calculated. For sensor 3, it was found that the 4 Aircraft X CI means were separable from Aircraft A CI means for both torque settings of 20% and 30%. Then, to examine which CIs performed better in terms of the separation, they were ranked in Table 6.3 from the highest to the lowest percent difference. It was found that the order of the CI ranking was the same for both torque settings which confirms torque independence of the CI values. For sensor 3, the best CI was EO peak with percent differences of 86.794 and 105.375 for 20% and 30% torque respectively. Figure 6.31 presents the average EO Peak CI values at the 20% and 30% torque settings for both Aircraft X and Aircraft A.

Table 6.3. Sensor 3 CI average results

	Sensor 3					
	Aircraft X	Aircraft A		Aircraft X	Aircraft A	
CI	20% torque setting		% Diff	30% torque setting		% Diff
EO Peak	5.348	2.863	86.794	5.210	2.537	105.3745
EO UB	5.348	2.863	86.793	5.210	2.537	105.3728
RMS	0.030	0.026	17.094	0.029	0.024	19.997
EO CF	90.055	87.637	2.758	90.022	86.632	3.912

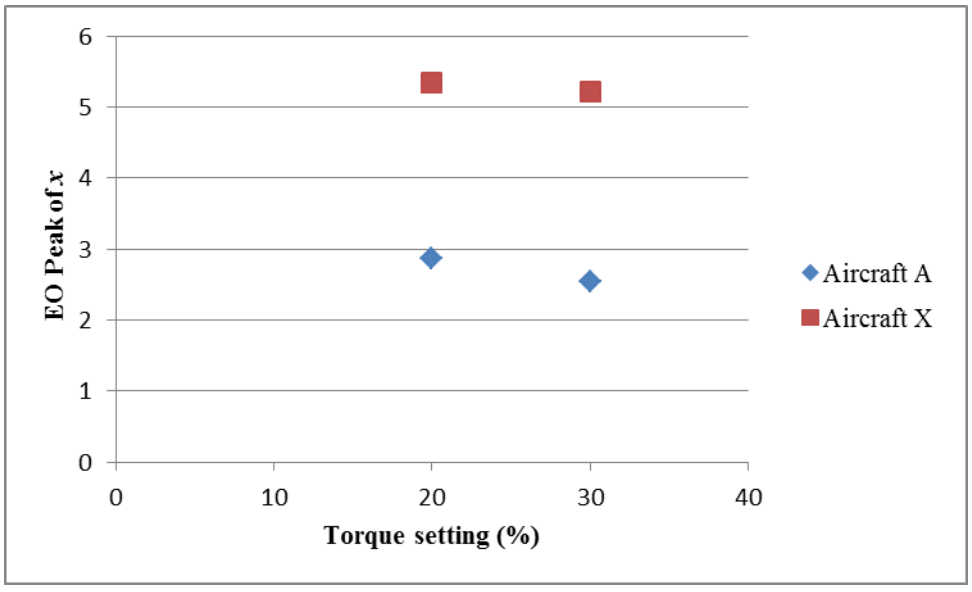

Figure 6.31. Average EO Peak CI by torque setting for sensor 3

The VMEP acquisitions for sensor 5 were processed in the same manner as sensor 3. Thus, the CI values at each torque level were averaged and percent difference between Aircraft X and Aircraft A computed. The results for the sensor 5 CIs are presented in Table 6.4. Similar to the sensor 3 results, the CI rankings were the same for both torque settings which again confirms torque independence of the CI values. Also, the best CI for sensor 5 was EO Peak. The average EO Peak CI results are shown at both torque settings for both Aircraft X and Aircraft A in Figure 6.32. It is important to note that the top 2 CIs for sensor 5 perform better than the top CI (EO Peak) for sensor 3 in terms of percent difference. The reason for the higher percent difference using sensor 5 data is likely due to the fact that sensor 5 was much closer to the planet carrier fatigue crack.

Table 6.4. Sensor 5 CI average results

			Sensor 5			
	Aircraft X	Aircraft A		Aircraft X	Aircraft A	
CI	20% torque setting		% Diff	30% torque setting		% Diff
EO Peak	3.121	1.083	188.246	3.021	1.013	198.265
EO UB	5.316	1.961	171.112	5.127	1.848	177.524
RMS	0.030	0.025	19.489	0.029	0.025	16.353
EO CF	51.556	49.045	5.119	51.646	48.360	6.795

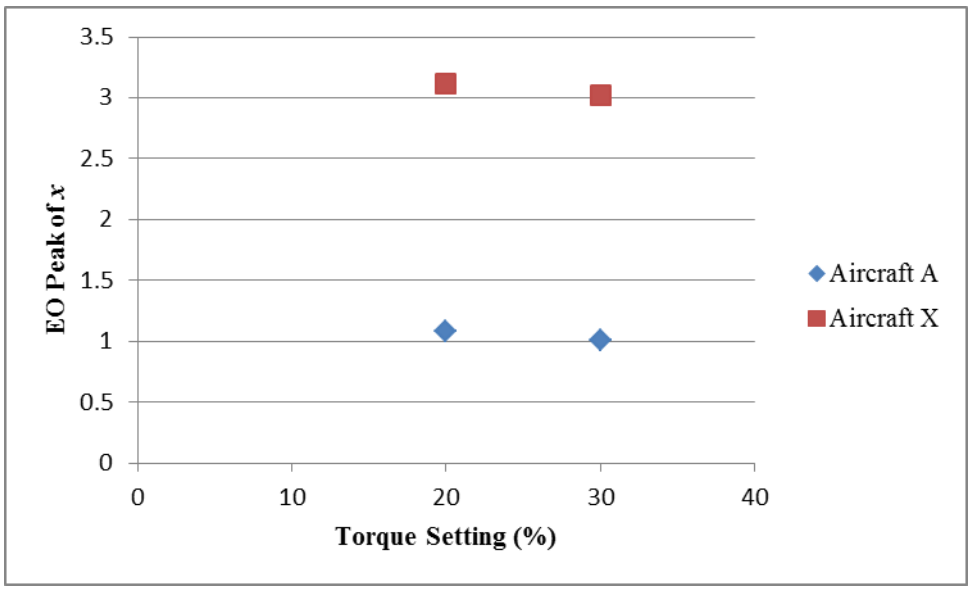

Figure 6.32. Average EO Peak CI by torque setting for sensor 5

In this section, a new method for detecting an on-aircraft fatigue crack in a planet carrier of an epicyclic transmission was presented. This method begins by time synchronously resampling vibration signals to segment the signals according to shaft crossing times such that an even number of data points are obtained to compute a spectral average. Then, the result is used to extract features and evaluate numerous CIs for planet carrier fatigue crack detection. The methodology was validated using the raw vibration test cell and on-aircraft data acquired from a number of US Army UH-60A Black Hawk helicopter main transmissions. For the test cell data, analysis was done for sensor 5 at the 20% torque setting. For the on-aircraft data, both sensor 3 and sensor 5 acquisitions were processed. For each sensor, two samples of data were analyzed for both the 20% and 30% torque settings. The results indicate that using the presented approach, a total of 4 CIs can be used to detect the fatigue crack in a planet carrier for both the test cell and on-aircraft UH-60A vibration data. The CIs were ranked in the order of percent difference of Aircraft X mean CI values from Aircraft A mean CI values. The ranking for both

sensor data was constant regardless of torque setting, indicating that the CIs are torque independent. Also, the EO Peak CI was the best for both sensors in terms of percent difference. The studies currently reported in the literature have had difficulty detecting the fatigue crack using the on-aircraft data. The results in this section indicate that the presented approach can be utilized to address the detection of fatigue cracks in a planet carrier of a UH-60A helicopter using VMEP vibration data.

7. CONCLUSIONS

In this dissertation, effective and efficient AE based techniques for bearing fault diagnostics were developed and validated using a bearing test rig and seeded fault tests. A frequency reduction hardware solution was developed based on heterodyne that lower the AE signal frequency allowing the reduction of the sampling rate from several MHz to 100kHz. Through this technique, the AE signals are demodulated and low-pass filtered to extract the useful fault frequencies needed for bearing health assessment. AE sensors offer a number of advantages over their vibration counterparts which are standard to use in industry. By reducing the sampling rate of AE sensors to a rate comparable to vibration sensors, AE can be feasibly applied in the field with much less storage and computational burden. To extract useful features from the low sampled AE signals, a signal processing method based on synchronous resampling and spectral averaging was developed. This was the first reported application of low sampled AE data in combination with a novel signal processing algorithm that was validated to diagnose all bearing fault types at both high and low speed ranges.

This research has several significant contributions. First, the sampling rate for AE sensors has been reduced to a rate comparable to vibration signals. This allows a reduction in computational burden while affording the ability to take advantage of AE benefits such as incipient fault detection and increased sensitivity. Second, the time synchronous resampling and spectral averaging combination allows a single average to be computed and effectively diagnoses all four bearing fault types. Other bearing techniques based on TSA require either multiple averages or multiple trigger signals to be computed for each bearing fault type. This further reduces computation time. Additionally, this method accounts for fluctuations in shaft speed and

bearing slippage which reduces variability amongst CI values and smearing in FFT computations.

Through seeded fault tests, the research contributions have been validated. The methodology has also been extended and validated for bearing fault diagnosis using accelerometer data. When compared with the use of vibration sensors, AE outperforms the accelerometer results. Also, this approach has been compared with and shows improvement against the widely used envelope analysis technique when applied to the collected AE signals. Additionally, low speed diagnosis of all four bearing fault types has not been presented for the 2-10 Hz shaft speed range. A modified algorithm that uses a different analysis signal and low speed condition indicators can statistically diagnosis all failure modes which has not been presented in literature. Moreover, the developed technique has been extended and validated to detect fatigue cracks on a planet gear carrier in a UH-60A helicopter using test cell and on-aircraft vibration data. Previous research has achieved results with test cell data but not with the on-aircraft data.

In summary, this research shows AE sensors can be applied in industrial settings at a low cost and reduced computational burden. Also, the new signal processing technique is effective for bearing fault diagnosis using AE and vibration sensors at low and high speed ranges. Lastly, the technique is shown to be effective for on-aircraft UH-60A planet gear carrier crack detection as well.

REFERENCES

Antoni, J., 2006, "The spectral kurtosis: a useful tool for characterizing non-stationary signals", *Mechanical Systems and Signal Processing*, Vol. 20, No. 2, pp. 282 – 307.

Antoni, J. and Randall, R. B., 2006, "The spectral kurtosis: application to the vibratory surveillance and diagnostics of rotating machines", *Mechanical Systems and Signal Processing*, Vol. 20, No. 2, pp. 308 – 331.

Applied Industrial Technologies, 2009, "Lubricant failure = bearing failure", URL http://www.machinerylubrication.com/Magazine/Issue/Machinery%20Lubrication/1/2009.

Balderston, H. L., 1969, "The detection of incipient failure in bearings", *Materials Evaluation*, Vol. 27, No. 6, pp. 121 – 128.

Bansal V., Gupta, B. C., Prakash, A., and Eshwar, V. A., 1990, "Quality inspection of rolling element bearing using acoustic emission technique", *Journal of Acoustic Emission*, Vol. 9, No. 2, pp. 142 – 146.

Bearing-news, 2014, "Global demand for bearings projected to jump 7.3% annually to 2018", URL http://www.bearing-news.com/global-demand-bearings-projected-jump-7-3-annually-2018/

Bechhoefer, E. and Kingsley, M., 2009, "A review of time synchronous average algorithms", *Annual Conference of the Prognostics and Health Management Society*, San Diego, CA, Sept. 27 – Oct. 1.

Bechhoefer, E., Van Hecke, B., and He, D., 2013, "Processing for improved spectral analysis", *Annual Conference of the Prognostics and Health Management Society*, New Orleans, LA, Oct. 14 - 17.

Bechhoefer, E., Qu, Y., Zhu, J., and He, D., 2013, "*Signal processing techniques to improve an acoustic emission sensor*", Annual Conference of the Prognostics and Health Management Society, Oct 14 – 17, New Orleans, LA.

Blunt, D.M. and Keller, J.A., 2006, "Detection of a fatigue crack in a UH-60A planet gear carrier using vibration analysis", *Mechanical Systems and Signal Processing*, Vol. 20, No. 8, pp. 2095-2111.

Bonnardot, F., El Badaoui, M., Randall, R.B., Daniere, J, and Guillet, F., 2005, "Use of the acceleration signal of a gearbox in order to perform angular resampling (with limited speed fluctuation)", *Mechanical Systems and Signal Processing*, Vol. 19, No. 4, pp. 766 – 785.

Braun, S., 1975, "The extraction of periodic waveforms by time domain averaging", *Acustica*, Vol. 32, pp. 69 -77.

Braun, S., 2011, "The synchronous (time domain) average revisited", *Mechanical Systems and Signal Processing*, Vol. 25, No. 4, pp. 1087 – 1102.

Canada, R. G., and Robinson, J.C., 1995, "Vibration measurements on slow speed machinery", *Predictive Maintenance Technology National Conference*, Indianapolis, IN, Vol. 8, pp. 33 – 37.

Catlin Jr., J. B., 1983, "The use of ultrasonic diagnostic technique to detect rolling element bearing defects", *Proceedings of Machinery and Vibration Monitoring and Analysis Meeting, Vibration Institute*, Houston, TX, April 19 – 21, pp. 123 – 130.

Choudhury, A. and Tandon, N., 2000, "Application of acoustic emission technique for the detection of defects in rolling element bearings", *Tribology International*, Vol. 33, No. 1, pp. 39 – 45.

Christian, K. N., Mureithi, N., Lakis, A., and Thomas, M., 2007, "On the use of synchronous averaging, independent component analysis and support vector machines for bearing fault diagnosis", *First International Conference on Industrial Risk Engineering*, Montreal, QC, Canada, Dec. 17 – 19.

Combet, F. and Gelman L., 2007, "An automated methodology for performing time synchronous averaging of a gearbox signal without a speed sensor", *Mechanical Systems and Signal Processing*, Vol. 21, No. 6, pp. 2590 – 2606.

Cong, F., Chen, J., Dong, G., and Pecht, M., 2013, "Vibration model of rolling element bearings in a rotor-bearing system for fault diagnosis", *Journal of Sound and Vibration*, Vol. 332, No. 8, pp. 2081 – 2097.

Cui, L., Wang, J., and Lee, S., 2014, "Matching pursuit of an adaptive impulse dictionary for bearing fault diagnosis", *Journal of Sound and Vibration*, Vol. 333, No. 10, pp. 2840 – 2862.

Decker, H., 2002, "Crack detection for aerospace quality spur gears", *58th International Annual Forum and Technology Display sponsored by American Helicopter Society*, Montreal, Quebec, Canada, Jun 11 – 13.

Dong, M., He, D., Banerjee, P., and Keller, J.A., 2004, "Equipment health diagnosis and prognosis using advanced hidden Markov models", *58th Meeting of the Machinery Failure Prevention Technology Society*, Virginia Beach, Virginia, Apr 26 - 30.

Dwyer, R., 1984, "Use of the kurtosis statistic in the frequency domain as an aid in detecting random signals", *IEEE Journal of Oceanic Engineering*, Vol. 9, No. 2, pp. 85 – 92.

Eftekharnejad, B., Carrasco, M. R., Charnley, B., and Mba, D., 2011, "The application of spectral kurtosis on acoustic emission and vibrations from a defective bearing", *Mechanical Systems and Signal Processing*, Vol. 25, No. 1, pp. 266 – 284.

Eitzen, D., Breckenridge, F. R., Millerand, R. K., and McIntire, P. (Eds.), 1987, "Nondestructive testing handbook, acoustic emission testing", second ed., *American Society for Non-destructive Testing*, vol. 5, pp. 120–134.

El Badaoui, M., Antoni, J., Guillet, F., and Daniere, J., 2001, "Use of the moving cepstrum integral to detect and localise tooth spalls in gears", *Mechanical Systems and Signal Processing*, Vol. 15, No. 5, pp. 873 – 885.

Elforjani, M. and Mba, D., 2010, "Accelerated natural fault diagnosis in slow speed bearings with acoustic emission", *Engineering Fracture Mechanics*, Vol. 77, No. 1, pp. 112 - 127.

Elforjani, M. and Mba, D., 2011, "Condition monitoring of slow-speed shafts and bearings with acoustic emission", *Strain*, Vol. 47, No. 2, pp. 350 – 363.

Felten, D., 2003, "Understanding bearing vibration frequencies", *Mechanical Field Service Department, L&S Electric, Inc., Schofield, Wisconsin*, pp. 1 – 3.

Freedonia, 2010, "World bearing industry", URL http://www.reportlinker.com/p091960-summary/World-Bearings-Market.html.

Gong, X. and Qiao, W., 2013, "Bearing fault diagnosis for direct-drive wind turbines via current-demodulated signals", *IEEE Transactions on Industrial Electronics*, Vol. 60, No. 8, pp. 3419 – 3428.

Grabill, P., Berry, J., Grant, L., and Porter, J., 2001, "Automated helicopter vibration diagnostics for the US army and national guard", *American Helicopter Society 57th Annual Forum*, Washington, DC, May 9 - 11.

Grabill, P., Brotherton, T., Berry, J., and Grant, L., 2001, "The US army and national guard vibration management enhancement program (VMEP): data analysis and statistical results", *American Helicopter Society 58th Annual Forum*, Montreal, Canada, Jun 11 -13.

Grabill, P., Brotherton, T., Berry, J., Branhof, B., and Grant, L., 2003, "Rotor smoothing and vibration monitoring results for the US army VMEP", *American Helicopter Society 59th Annual Forum,* Phoenix, AZ, May 6 - 8.

Hawman, M. W. and Galinaitis, W. S., 1988, "Acoustic emission monitoring of rolling element bearings", *IEEE Ultrasonics Symposium Proceedings*, Chicago, IL, Oct 2 – 5.

Hayes, M. H., 2012, *Schaum's outlines, digital signal processing, second edition, McGraw-Hill Companies Inc.,* USA.

He, D., Li, R., and Zhu, J., 2013, "Plastic bearing fault diagnosis based on a two-step data mining approach", *IEEE Transactions on Industrial Electronics*, Vol. 60, No. 8, pp. 3429 – 3440.

He, D., Li, R., Zhu, J., and Zade, M., 2011a, "Data mining based full ceramic bearing fault diagnostic system using AE sensors", *IEEE Transactions on Neural Networks*, Vol. 22, No. 12, pp. 2022 – 2031.

He, D., Li, R., Zade, M., and Zhu, J., 2011b, "Development and evaluation of ae based condition indicators for full ceramic bearing fault diagnosis", *IEEE International Conference on Prognostics and Health Management*, Denver, CO, June 20 – 23.

He, D., Li, R., and Zhu, J., 2012a, "Plastic bearing fault diagnosis based on a two-step data mining approach", *IEEE Transactions on Industrial Electronics*, Vol. 60, No. 8, pp. 3429 – 3440.

He, Q., Li, P., and Kong, F., 2012b, "Rolling bearing localized defect evaluation by multiscale signature via empirical mode decomposition", *Journal of Vibration and Acoustics*, Vol. 134, No. 6.

He, Q., Wang, J., Hu, F., and Kong, F., 2013, "Wayside acoustic diagnosis of defective train bearings based on signal resampling and information enhancement", *Journal of Sound and Vibration*, Vol. 332, No. 21, pp. 5635 – 5649.

He, Y., Zhang, X., and Friswell, M., 2009, "Defect diagnosis for rolling element bearings using acoustic emission", *Journal of Vibration and Acoustics*, Vol. 131, No. 6.

He, Y. and Zhang, X., 2012, "Approximate entropy analysis of the acoustic emission from defects in rolling element bearings", *Journal of Vibration and Acoustics*, Vol. 134, No. 6.

Hong, H. and Liang, M., 2009, "Fault severity assessment for rolling element bearings using the Lempel-ziv complexity and continuous wavelet transform", *Journal of Sound and Vibration*, Vol. 320, No. 2, pp. 452 – 468.

Hou, S., Li, Y., Wang, Z., and Liang, M., 2010, "A new low-frequency resonance sensor for low speed roller bearing monitoring", *Journal of Vibration and Acoustics*, Vol. 132, No. 1.

Jamaludin, N., Mba, D. and Bannister R.H., 2001, "Condition monitoring of slow-speed rolling element bearings using stress waves", *Proceedings of the Institution of Mechanical Engineeers, Part E: Journal of Process Mechanical Engineering*, Vol. 215, No. 4, pp. 245 – 271.

Jin, X., Zhao, M., Chow, T., and Pecht, M., 2014, "Motor bearing fault diagnosis using trace ratio linear discriminant analysis", *IEEE Transactions on Industrial Electronics*, Vol. 61, No. 5, pp. 2441 – 2451.

Kappaganthu, K. and Nataraj, C., 2011, "Feature selection for fault detection in rolling element bearings using mutual information", *Journal of Vibration and Acoustics*, Vol. 133, No. 6.

Keller, J.A. and Grabill, P., 2003, "Vibration monitoring of UH-60A main transmission planetary carrier fault", *American Helicopter Society 59th Annual Forum*, Phoenix, AZ, May 6 -8.

Kilundu, B., Chiementin, X., Duez, J., and Mba, D., 2011, "Cyclostationarity of acoustic emissions (ae) for monitoring bearing defects", *Mechanical Systems and Signal Processing*, Vol. 25, No. 6, pp. 2061 -2072.

Kim, E., Tan, A., Yang, B. and Kosse, V., 2007, "Experimental study on condition monitoring of low speed bearings: time domain analysis", *The 5th Australasian Congress on Applied Mechanics*, Brisbane, Australia, Dec 10 – 12.

Lei, Y., He, Z., and Zi, Y., 2008, "Application of a novel hybrid intelligent method to compound fault diagnosis of locomotive roller bearings", *Journal of Vibration and Acoustics*, Vol. 130, No. 3.

Li, R., He, D., and Zhu, J., 2012, "Investigation on full ceramic bearing fault diagnostics using vibration and ae sensors", *IEEE International Conference on Prognostics and Health Management: Enhancing Safety, Efficiency, Availability, and Effectiveness of Systems Through PHM Technology and Application*, Denver, CO, June 18 – 21.

Li, B., Chow, M., Tipsuwan, Y., and Hung, J., 2000, "Neural-network-based motor rolling bearing fault diagnosis", *IEEE Transactions on Industrial Electronics*, Vol. 47, No. 5, pp. 1060 – 1069.

Li, C. and Li, S. Y., 1985, "Acoustic emission analysis for bearing condition monitoring", *Wear*, Vol. 185, No. 1, pp. 67 – 74.

Liu, X., Wu, X., and Liu, C., 2011, "A comparison of acoustic emission and vibration on bearing fault detection", *International Conference on Transportation, Mechanical, and Electrical Engineering*, Changchun, China, Dec 16 – 18.

Liu, X., Bo, L., He, X., and Veidt, M., 2012, "Application of correlation matching for automatic bearing fault diagnosis", *Journal of Sound and Vibration*, Vol. 331, No. 26, pp. 5838 – 5852.

Loparo, K., Adams, M., Lin, W., Abdel-Magied, M., and Afshari, N., 2000, "Fault detection and diagnosis of rotating machinery", *IEEE Transactions on Industrial Electronics*, Vol. 47, No. 5, pp. 1005 – 1014.

Lu, W., Jiang. W., Wu, H., and Hou, J., 2012, "A fault diagnosis scheme of rolling element bearing based on near-field acoustic holography and gray level co-occurrence matrix", *Journal of Sound and Vibration*, Vol. 331, No. 15, pp. 3663 – 3674.

Mathews, J. R., 1983, *Acoustic emission*, *Gordon and Breach Science Publishers Inc.*, New York, NY.

Mba, D., 2003, "Acoustic emissions and monitoring bearing health", *Tribology Transactions*, Vol. 46, No. 3, pp. 447 – 451.

Mba, D. and Rao, R., 2006, "Development of acoustic emission technology for condition monitoring and diagnosis of rotating machines; bearings, pumps, gearboxes, engines and rotating structures", *The Shock and Vibration Digest*, Vol. 38, No. 1, pp. 3 – 16.

Mba, D., 2008, "The use of acoustic emission for estimation of bearing defect size", *Journal of Failure Analysis and Prevention*, Vol. 8, No. 2, pp. 188 – 192.

McFadden, P. D. and Smith J. D., 1984, "The vibration monitoring of rolling element bearings by the high-frequency resonance technique – a review", *Tribology International*, Vol. 17, No. 1, pp. 3 – 10.

McFadden, P. D., 1984, "Model for the vibration produced by a single point defect in a rolling element bearing", *Journal of Sound and Vibration*, Vol. 96, No. 1, pp. 69 – 82.

McFadden, P. D., 1985, "The vibration produced by multiple point defects in a rolling element bearing", *Journal of Sound and Vibration*, Vol. 98, No. 2, pp. 263 – 273.

McFadden, P. D., 1987a, "A revised model for the extraction of periodic waveforms by time domain averaging", *Mechanical Systems and Signal Processing*, Vol. 1, No. 1, pp. 83 – 95.

McFadden. P. D., 1987b, "Examination of a Technique for the Early Detection of Failure in Gears by Signal Processing of the Time Domain Average of the Meshing Vibration", *Mechanical systems and Signal Processing*, Vol. 1, No. 2, pp. 173 – 183.

McFadden, P.D., 1989, "Interpolation techniques for time domain averaging of gear vibration", *Mechanical Systems and Signal Processing*, Vol. 3, No.1, pp. 87 – 97.

McFadden, P.D., 1991, "A technique for calculating the time domain averages of the vibration of the individual planet gears and the sun gear in an epicyclic gearbox", *Journal of Sound and Vibration*, Vol. 144, No. 1, pp. 163 – 172.

McFadden, P. D. and Toozhy, M. M., 2000, "Application of synchronous averaging to vibration monitoring of rolling element bearings", *Mechanical Systems and Signal Processing*, Vol. 14, No. 6, pp. 891 – 906.

McInerny, S.A., Hardman, W., Keller, J.A., and Bednarczyk, R., 2003, "Detection of a cracked planet carrier", *10th International Congress on Sound and Vibration*, Stockholm, Sweden, Jul 7 – 10.

Mechefske, C. F., and Mathew, J., 1992, "Fault detection and diagnosis in low speed rolling element bearings, part II: the use of parametric spectra", *Mechanical Systems and Signal Processing*, Vol. 6, No. 4, pp. 297 – 307.

Miettinen, J., and Pataniitty, P., 1999, "Acoustic emission in monitoring extremely slowly rotating rolling bearing", *Proceedings of COMADEM '99*, Coxmoor, Oxford, pp. 289 – 297.

Morhain, A. and Mba, D., 2003, "Bearing defect diagnosis and acoustic emission", *Proceedings of the Institution of Mechanical Engineers, Part J: Journal of Engineering Tribology*, Vol. 217, No. 4, pp. 257 – 272.

Nienhaus, K., Boos, F.D., Garate, K., and Baltes, R., 2012, "Development of acoustic emission (ae) based defect parameters for slow rotating roller bearings", *Journal of Physics: Conference Series*, Vol. 364, No. 1, Huddersfield, UK, June 18 – 20.

Pan, J., Wang, H. Q., Wang, F., Yang, J. F., and Liu, W. B., 2012, "Intelligence diagnosis method for roller bearings using features of ae signal", *Journal of Physics: Conference Series*, Vol. 364, No. 1, Huddersfield, UK, June 18 – 20.

Prieto, M., Cirrincione, G., Espinosa, A., Ortega, J., and Henao, H., 2013, "Bearing fault detection by a novel condition-monitoring scheme based on statistical-time features and neural networks", *IEEE Transactions on Industrial Electronics*, Vol. 30, No. 8, pp. 3398 – 3407.

Proakis, J. and Manolakis, D., 2007, *Digital signal processing: principles, algorithms, and applications, 4th edition*, *Pearson Education Inc.*, Upper Saddle River, NJ.

Qu, Y., Van Hecke, B., He, D., Yoon, J., Bechhoefer, E., and Zhu, J., 2013, "Gearbox fault diagnostics using AE sensors with low sampling rate", *Journal of Acoustic Emission*, Vol. 31, No. 1, pp. 67 – 90.

Qu, Y., He, D., Yoon, J., Van Hecke, B., Bechhoefer, E. and Zhu, J., 2014, "Gearbox tooth cut fault diagnostics using acoustic emission and vibration sensors – a comparative study", *Sensors*, Vol. 14, No. 1, pp. 1372 - 1393.

Qu, Y., Bechhoefer, E., He, D., Zhu, J., 2013, "A new acoustic emission sensor based gear fault detection approach", *International Journal of Prognostics and Health Management*, Vol. 4, Sp. 2, pp. 1 – 14.

Qu, Y., Zhu, J., He, D., Qiu, B., and Bechhoefer, E., 2013, "Time synchronous average based acoustic emission signal analysis on gear fault detection", *IEEE International Conference on Prognostics and Health Management*, Gaithersburg, MD, June 24 – 27.

Raharjo, P., Tesfa, B., Gu, F., and Ball, A. D., 2012, "A comparative study of the monitoring of a self aligning spherical journal using surface vibration, airborne sound and acoustic emission", *Journal of Physics: Conference Series*, Vol. 364, No. 1, p. 012035. IOP Publishing.

Randall, R. and Antoni, J., 2011, "Rolling element bearing diagnostics – a tutorial", *Mechanical Systems and Signal Processing*, Vol. 25, No. 2, pp. 485 – 520.

Rogers, L. M., 1979, "The application of vibration signature analysis and acoustic emission source location to on-line condition monitoring of anti-friction bearings", *Tribology International*, Vol. 12, No. 2, pp. 51 – 58.

Sako, T. and Yoshie, O., 2010, "Diagnostic method of low speed rolling element bearing using ae envelope waveform", *IEEE Region 10 Annual International Conference*, Fukuoka, Japan, Nov 21 – 24.

Sawalhi N. and Randall, R., 2004, "The application of spectral kurtosis to bearing diagnostics", *Acoustics Conference*, Sydney, Australia, Nov 3 – 5.

Saxena, A., Wu, B., and Vachtsevanos, G., 2005, "A methodology for analyzing vibration data from planetary gear systems using complex Mortlet wavelets", *American Control Conference*, Portland, Oregon, Jun 8 - 10.

Sawalhi, N., Randall, R., Endo, H., 2007, "The enhancement of fault detection and diagnosis in rolling element bearings using minimum entropy deconvolution combined with spectral kurtosis", *Mechanical Systems and Signal Processing*, Vol. 21, No. 6, pp. 2616 – 2633.

Shirioshi, J., Li, Y., Liang, S., Kurfess, T., and Danyluk, S., 1997, "Bearing condition diagnostics via vibration and acoustic emission measurements", *Mechanical Systems and Signal Processing*, Vol. 11, No. 5, pp. 693 – 705.

Siegel, D., Al-Atat, H., Shauche, V., Liao, L., Snyder, J., and Lee, J., 2012, "Novel method for rolling element bearing health assessment – A tachometer-less synchronously averaged envelope feature extraction technique", *Mechanical Systems and Signal Processing*, Vol. 29, No. 1 , pp. 362 – 376.

Smith, J.D., 1982, "Vibration monitoring of bearings at low speeds", *Tribology International*, Vol. 15, No. 3, pp. 139 – 144.

Tan, C. C., 1990, "Application of acoustic emission to the detection of bearing failures", *International Tribology Conference*, Brisbane, Australia, Dec 3 – 5.

Tandon, N. and Choudhury, A., 1999, "A review of vibration and acoustic measurement methods for the detection of defects in rolling element bearings", *Tribology International*, Vol. 32, No. 8, pp. 469 – 480.

Tandon, N. and Nakra, B. C., 1990, "Defect detection in rolling element bearings by acoustic emission method", *Journal of Acoustic Emission*, Vol. 9, No. 1, pp. 25 – 28.

Tandon, N. and Nakra, B. C., 1992, "Comparison of vibration and acoustic measurement techniques for the condition monitoring of rolling element bearings", *Tribology International*, Vol. 25, No. 3, pp. 205 – 212.

Teager, H. M., and Teager S. M., 1992, "Evidence for nonlinear sound production mechanisms in the vocal tract", *Speech Production and Speech Modeling Symposium, Time Frequency and Time-Scale Analysis*, Victoria, British Columbia, Canada, pp. 345 – 348.

Tse, P, Peng, Y., and Yam, R., 2001, "Wavelet analysis and envelope detection for rolling element bearing fault diagnosis – their effectiveness and flexibilities", *Journal of Vibration and Acoustics*, Vol. 123, No. 3, pp. 303 – 310.

Van Hecke, B., Yoon, J., and He, D., 2015, "On the use of acoustic emission sensors with low sampling rate for low speed bearing fault diagnostics", *Joint Conference: MFPT 2015 and ISA's 61st International Instrumentation Symposium*, May 12 – 14, Huntsville, AL.

Van Hecke, B., He, D., and Qu, Y., 2014a, "On the use of spectral averaging of acoustic emission signals for bearing fault diagnostics", *ASME Journal of Vibration and Acoustics*, Vol. 136, No. 6, doi:10.1115/1.4028322

Van Hecke, B., Qu, Y., and He, D., 2014b, "A new acoustic emission sensor based bearing fault diagnostic technique", *MFPT Conference*, May 20 – 22, Virginia Beach, VA, pp. 61 – 81.

Van Hecke, B., Qu, Y., He, D., and Bechhoefer, E., 2014c, "A new spectral average-based bearing fault diagnostic approach", *Journal of Failure Analysis and Prevention*, Vol. 14, No. 3, pp. 354– 362.

Van Hecke, B., Qu, Y., and He, D., 2014d, "Bearing fault diagnosis based on a new acoustic emission sensor technique", *Journal of Risk and Reliability*, Vol. 229, No. 2, DOI: 10.1177/1748006X14558900.

Van Hecke, B., Bechhoefer, E., Qu, Y., and He, D., 2014e, "Bearing fault diagnosis using a spectral average based approach", *70th AHS Annual Forum*, May 20 – 22, Palais des Congrès, Montréal, Canada.

Večeř, P. Kreidl, M., and Šmid, R., 2005, "Condition indicators for gearbox condition monitoring systems", *Acta Polytechnica*, Vol. 45, No. 6, pp. 35 – 43.

Vrabie, V. D., Granjon, P., and Serviere, C., 2003, "Spectral kurtosis: from definition to application", *IEEE Workshop on Nonlinear Signal and Image Processing*, Grado, Italy, June 8 -11.

Wang, G., Liu, C., and Cui, Y., 2012, "Clustering diagnosis of rolling element bearing fault based on integrated autoregressive/autoregressive conditional heteroscedasticity model", *Journal of Sound and Vibration,* Vol. 331, No. 19, pp. 4379 – 4387.

Wang, D., Shen, W., and Tse, P. W., 2013, "A novel adaptive wavelet stripping algorithm for extracting the transients caused by bearing localized faults", *Journal of Sound and Vibration,* Vol. 332, No. 25, pp. 6871 – 6890.

Wang, J. and He, Q., 2014, "Exchanged ridge demodulation of time-scale manifold for enhanced fault diagnosis of rotating machinery", *Journal of Sound and Vibration,* http://dx.doi.org/10.1016/j.jsv.2014.01.006.

Wang, Y.F. and Kootsookos, P.J., 1998, "Modeling of low shaft speed bearing faults for condition monitoring", *Mechanical Systems and Signal Processing*, Vol. 12, No. 3, pp. 415 – 426.

Wei, D. and Zhan-Sheng, L., 2009, "Genetic integration of different diagnosis methods and/or fault features for improvement of diagnosis accuracy", *Journal of Vibration and Acoustics*, Vol. 131, No. 1.

Welch, P., 1967, "The use of fast fourier transform for the estimation of power spectra: a method based on time averaging over short, modified periodograms", *IEEE Transactions on Audio and Electroacoustics*, Vol. AU-15, No. 2, pp. 70 – 73.

Widodo, A., Kim, E. Y., Son, J. D., Yang, B. S., Tan, A. C. C., Gu, D. S., Choi, B. K., and Mathew, J., 2009, "Fault diagnosis of low speed bearing based on relevance vector machine and support vector machine", *Expert Systems with Applications*, Vol. 36, No. 3, pp. 7252 – 7261.

Wu, B., Saxena, A., Khawaja, T.S., Patrick, R., Vachtsevanos, G., and Sparis, P., 2004, "An approach to fault diagnosis of helicopter planetary gears", *IEEE Autotestcon,* San Antonio, Texas, Sept 20 - 23.

Wu, B., Saxena, A., Patrick, R., and Vachtsevanos, G., 2005, "Vibration monitoring for fault diagnosis of helicopter planetary gears", *16th IFAC World Congress*, Prague, Jul 3 - 8.

Yan, R., Gao, R., and Wang, C., 2009, "Experimental evaluation of a unified time-scale-frequency technique for bearing defect feature extraction", *Journal of Vibration and Acoustics*, Vol. 131, No. 4.

Yoon, J., Van Hecke, B., and He, D., 2015a, "Planetary gearbox fault detection using an acoustic emission sensor", *Joint Conference: MFPT 2015 and ISA's 61st International Instrumentation Symposium*, May 12 – 14, Huntsville, AL.

Yoon, J., He, D., Van Hecke, B., Nostrand, T., Zhu, J., Bechhoefer, E., 2015b, "A spectral averaging based planetary gearbox fault diagnostics using a single vibration sensor", *AWEA Wind Power 2015 Conference*, May 18 – 21, Orlando, FL.

Yoon, J., He, D., and Van Hecke, B., 2014, "A PHM approach to additive manufacturing equipment health monitoring, fault diagnosis, and quality control", *Annual PHM Conference*, Sept. 29 – Oct. 2, Fort Worth, TX.

Yoon, J. M., He, D., nad Qiu, B., 2013, "Full ceramic bearing fault diagnosis using lamstar neural network", *IEEE PHM Conference Proceedings*, Gaithersburg, MD, June 24 – 27.

Yoshioka, T. and Fujiwara, T., 1982, "A new acoustic emission source locating system for the study of rolling contact fatigue", *Wear*, Vol. 81, No. 1, pp. 183 – 186.

Yoshioka, T. and Fujiwara, T., 1984, "Application of acoustic emission technique to detection of rolling bearing failure", *American Society of Mechanical Engineers, Production Engineering Division Publication*, Vol. 14, pp. 55 – 76.

Yoshioka, T., 1992, "Detection of rolling contact subsurface fatigue cracks using acoustic emission technique", *Lubrication Engineering*, Vol. 49, No. 4, pp. 303 – 308.

Yoshioka, T., Korenaga, A., Mano, H., and Yamamoto, T., 1999, "Diagnosis of rolling bearing by measuring time interval of ae generation", *Journal of Tribology,* Vol. 121, No. 3, pp. 468 – 472.

Yu, J., 2012, "Local and nonlocal preserving projection for bearing defect classification and performance assessment", *IEEE Transactions on Industrial Electronics,* Vol. 59, No. 5, pp. 2363 – 2376.

Zhang, Y., Liang, M., Li., C., and Hou, S., 2013, "A joint kurtosis-based adaptive bandstop filtering and iterative autocorrelation approach to bearing fault detection", *Journal of Vibration and Acoustics,* Vol. 135, No. 5.

Zhou, W., Habetler, T., and Harley, R., 2008, "Bearing fault detection via stator current noise cancellation and statistical control", *IEEE Transactions on Industrial Electronics,* Vol. 55, No. 12, pp. 4260 – 4269.

APPENDIX

Dear Prof. Van Hecke,

It is our pleasure to grant you permission to publish **any part or all of** the ASME paper "On the Use of Spectral Averaging of Acoustic Emission Signals for Bearing Fault Diagnostics," by Brandon Van Hecke; David He; Yongzhi Qu J. Vib. Acoust.. 2014, 136(6), as cited in your letter in a dissertation entitled Development of Novel Acoustic Emission Based Methodology and Tools for Bearing Fault Diagnostics to be published by University of Illinois at Chicago.

Permission is granted for the specific use as stated herein and does not permit further use of the materials without proper authorization. Proper attribution must be made to the author(s) of the materials. **Please note:** if any or all of the figures and/or Tables are of another source, permission should be granted from that outside source or include the reference of the original source. ASME does not grant permission for outside source material that may be referenced in the ASME works.

As is customary, we request that you ensure proper acknowledgment of the exact sources of this material, the authors, and ASME as original publisher. Acknowledgment must be retained on all pages printed and distributed.

Many thanks for your interest in ASME publications.

Sincerely,

Beth Darchi

Publishing Administrator

ASME

2 Park Avenue, 6th Floor

New York, NY 10016-5990

Tel 1.212.591.7700

darchib@asme.org

SPRINGER LICENSE
TERMS AND CONDITIONS

May 19, 2015

This is a License Agreement between Brandon Van Hecke ("You") and Springer ("Springer") provided by Copyright Clearance Center ("CCC"). The license consists of your order details, the terms and conditions provided by Springer, and the payment terms and conditions.

All payments must be made in full to CCC. For payment instructions, please see information listed at the bottom of this form.

License Number	3632631463490
License date	May 19, 2015
Licensed content publisher	Springer
Licensed content publication	Journal of Failure Analysis and Prevention
Licensed content title	A New Spectral Average-Based Bearing Fault Diagnostic Approach
Licensed content author	Brandon Van Hecke
Licensed content date	Jan 1, 2014
Volume number	14
Issue number	3
Type of Use	Thesis/Dissertation
Portion	Full text
Number of copies	1
Author of this Springer article	Yes and you are the sole author of the new work
Order reference number	None
Title of your thesis / dissertation	Development of Novel Acoustic Emission Based Methodology and Tools for Bearing Fault Diagnostics
Expected completion date	Jun 2015
Estimated size(pages)	130
Total	0.00 USD
Terms and Conditions	

Introduction

The publisher for this copyrighted material is Springer Science + Business Media. By clicking "accept" in connection with completing this licensing transaction, you agree that the following terms and conditions apply to this transaction (along with the Billing and Payment terms and conditions established by Copyright Clearance Center, Inc. ("CCC"), at the time that you opened your Rightslink account and that are available at any time at http://myaccount.copyright.com).

Limited License

With reference to your request to reprint in your thesis material on which Springer Science and Business Media control the copyright, permission is granted, free of charge, for the use indicated in your enquiry.

Licenses are for one-time use only with a maximum distribution equal to the number that

you identified in the licensing process.

This License includes use in an electronic form, provided its password protected or on the university's intranet or repository, including UMI (according to the definition at the Sherpa website: http://www.sherpa.ac.uk/romeo/). For any other electronic use, please contact Springer at (permissions.dordrecht@springer.com or permissions.heidelberg@springer.com).

The material can only be used for the purpose of defending your thesis limited to university-use only. If the thesis is going to be published, permission needs to be re-obtained (selecting "book/textbook" as the type of use).

Although Springer holds copyright to the material and is entitled to negotiate on rights, this license is only valid, subject to a courtesy information to the author (address is given with the article/chapter) and provided it concerns original material which does not carry references to other sources (if material in question appears with credit to another source, authorization from that source is required as well).

Permission free of charge on this occasion does not prejudice any rights we might have to charge for reproduction of our copyrighted material in the future.

Altering/Modifying Material: Not Permitted
You may not alter or modify the material in any manner. Abbreviations, additions, deletions and/or any other alterations shall be made only with prior written authorization of the author(s) and/or Springer Science + Business Media. (Please contact Springer at (permissions.dordrecht@springer.com or permissions.heidelberg@springer.com)

Reservation of Rights
Springer Science + Business Media reserves all rights not specifically granted in the combination of (i) the license details provided by you and accepted in the course of this licensing transaction, (ii) these terms and conditions and (iii) CCC's Billing and Payment terms and conditions.

Copyright Notice:Disclaimer
You must include the following copyright and permission notice in connection with any reproduction of the licensed material: "Springer and the original publisher /journal title, volume, year of publication, page, chapter/article title, name(s) of author(s), figure number(s), original copyright notice) is given to the publication in which the material was originally published, by adding; with kind permission from Springer Science and Business Media"

Warranties: None

Example 1: Springer Science + Business Media makes no representations or warranties with respect to the licensed material.

Example 2: Springer Science + Business Media makes no representations or warranties with respect to the licensed material and adopts on its own behalf the limitations and disclaimers established by CCC on its behalf in its Billing and Payment terms and conditions for this licensing transaction.

Indemnity
You hereby indemnify and agree to hold harmless Springer Science + Business Media and CCC, and their respective officers, directors, employees and agents, from and against any

and all claims arising out of your use of the licensed material other than as specifically authorized pursuant to this license.

No Transfer of License
This license is personal to you and may not be sublicensed, assigned, or transferred by you to any other person without Springer Science + Business Media's written permission.

No Amendment Except in Writing
This license may not be amended except in a writing signed by both parties (or, in the case of Springer Science + Business Media, by CCC on Springer Science + Business Media's behalf).

Objection to Contrary Terms
Springer Science + Business Media hereby objects to any terms contained in any purchase order, acknowledgment, check endorsement or other writing prepared by you, which terms are inconsistent with these terms and conditions or CCC's Billing and Payment terms and conditions. These terms and conditions, together with CCC's Billing and Payment terms and conditions (which are incorporated herein), comprise the entire agreement between you and Springer Science + Business Media (and CCC) concerning this licensing transaction. In the event of any conflict between your obligations established by these terms and conditions and those established by CCC's Billing and Payment terms and conditions, these terms and conditions shall control.

Jurisdiction
All disputes that may arise in connection with this present License, or the breach thereof, shall be settled exclusively by arbitration, to be held in The Netherlands, in accordance with Dutch law, and to be conducted under the Rules of the 'Netherlands Arbitrage Instituut' (Netherlands Institute of Arbitration).***OR:***

All disputes that may arise in connection with this present License, or the breach thereof, shall be settled exclusively by arbitration, to be held in the Federal Republic of Germany, in accordance with German law.

Other terms and conditions:

v1.3

Questions? customercare@copyright.com or +1-855-239-3415 (toll free in the US) or +1-978-646-2777.

Gratis licenses (referencing $0 in the Total field) are free. Please retain this printable license for your reference. No payment is required.

VITA

NAME: Brandon E. Van Hecke

EDUCATION:

B.S. Industrial Engineering, University of Illinois at Chicago, IL, 2010

Ph.D., Industrial Engineering and Operation Research, University of Illinois at Chicago, IL, 2015

PROFESSIONAL EXPERIENCE:

Job Title: University Instructor Date: January 2015 – May 2015

Employer: University of Illinois at Chicago Location: Chicago, IL

Job Description: Instructed an Operations Research II course for the spring 2015 semester. Responsibilities included preparation and presentation of all course lectures as well as development of all homework assignments and exam questions. Topics covered included dynamic programming, integer programming, nonlinear programming, metaheuristics and decision analysis.

Job Title: Research Assistant Date: January 2011 – May 2015

Employer: University of Illinois at Chicago Location: Chicago, IL

Job Description: Conducted research in the Intelligent Systems Modeling and Development Laboratory. Involved in the development of novel acoustic emission (AE) and vibration based health assessment methodologies; development of signal processing algorithms to aid in the extraction of fault signals related to bearing and gear health degradation; implementation and validation of novel industrial data acquisition systems and sensor evaluation; PhD dissertation preparation.

Job Title: Teaching Assistant Date: August 2010 – December 2014

Employer: University of Illinois at Chicago Location: Chicago, IL

Job Description: Various duties included the facilitation of lectures/review sessions; weekly designation of time devoted to assisting and tutoring students; creation and grading of homework assignments and labs; proctoring/grading examinations and course projects.

JOURNAL PUBLICATIONS:

Papers Published:

Van Hecke, B., Qu, Y., and He, D., 2014, "Bearing fault diagnosis based on a new acoustic emission sensor technique", *Proceedings of the Institution of Mechanical Engineers Part O: Journal of Risk and Reliability*, Vol. 229, No. 2, DOI: 10.1177/1748006X14558900.

Van Hecke, B., He, D., and Qu, Y., 2014, "On the use of spectral averaging of acoustic emission signals for bearing fault diagnostics", *ASME Journal of Vibration and Acoustics*, Vol. 136, No. 6, DOI: 10.1115/1.4028322.

Van Hecke, B., Qu, Y., He, D., and Bechhoefer, E., 2014, "A new spectral average-based bearing fault diagnostic approach", *Journal of Failure Analysis and Prevention*, Vol. 14, No. 3, pp. 354– 362.

Qu, Y., Van Hecke, B., He, D., Yoon, J., Bechhoefer, E., and Zhu, J., 2013, "Gearbox fault diagnostics using AE sensors with low sampling rate", *Journal of Acoustic Emission*, Vol. 31, No. 1, pp. 67 – 90.

Qu, Y., He, D., Yoon, J., Van Hecke, B., Bechhoefer, E. and Zhu, J., 2014, "Gearbox tooth cut fault diagnostics using acoustic emission and vibration sensors – a comparative study", *Sensors*, Vol. 14, No. 1, pp. 1372 - 1393.

Yoon, J., He, D., and Van Hecke, B., 2015, "On the use of a single piezoelectric strain sensor for wind turbine planetary gearbox fault diagnosis", *IEEE Transactions on Industrial Electronics*, DOI: 10.1109/TIE.2015.2442216.

Papers Submitted:

Van Hecke, B., Yoon, J., and He, D., "Low speed bearing fault diagnosis using acoustic emission sensors", *Journal of Applied Acoustics*.

Yoon, J., He, D., Van Hecke, B., Nostrand, T., Zhu, J., and Bechhoefer, E., "Vibration based wind turbine planetary gearbox fault diagnosis using spectral averaging", *Wind Energy*.

Van Hecke, B., Yoon, J., and He, D., "On detection of on-aircraft fatigue cracks in a UH-60A planet carrier using spectral averaging", *Insight – Non-Destructive Testing and Condition Monitoring*.

CONFERENCE PUBLICATIONS:

Van Hecke, B., Yoon, J., and He, D., 2015, "On the use of acoustic emission sensors with low sampling rate for low speed bearing fault diagnostics", *Joint Conference: MFPT 2015 and ISA's 61st International Instrumentation Symposium*, May 12 – 14, Huntsville, AL.

Van Hecke, B., Bechhoefer, E., Qu, Y., and He, D., 2014, "Bearing fault diagnosis using a spectral average based approach", *70th AHS Annual Forum*, May 20 – 22, Palais des Congrès, Montréal, Canada.

Van Hecke, B., Qu, Y., and He, D., 2014, "A new acoustic emission sensor based bearing fault diagnostic technique", *MFPT Conference*, May 20 – 22, Virginia Beach, VA, pp. 61 – 81.

Yoon, J., Van Hecke, B., and He, D., 2015, "Planetary gearbox fault detection using an acoustic emission sensor", *Joint Conference: MFPT 2015 and ISA's 61st International Instrumentation Symposium*, May 12 – 14, Huntsville, AL.

Qu, Y., Van Hecke, B., He, D., Yoon, J., Bechhoefer, E., and Zhu, J., 2014, "A study on comparing acoustic emission and vibration sensors for gearbox fault diagnostics", *MFPT Conference*, May 20 – 22, Virginia Beach, VA, pp. 455 – 480.

Bechhoefer, E., Van Hecke, B. and He, D., 2013, "Processing for improved spectral analysis", *Annual PHM Conference*, Oct. 14–17, New Orleans, LA.

Yoon, J., He, D., Van Hecke, B., Nostrand, T., Zhu, J.,and Bechhoefer, E., 2015, "A spectral averaging based planetary gearbox fault diagnostics using a single vibration sensor", *AWEA Wind Power 2015 Conference*, May 18 – 21, Orlando, FL.

Yoon, J., He, D., and Van Hecke, B., 2014, "A PHM approach to additive manufacturing equipment health monitoring, fault diagnosis, and quality control", *Annual PHM Conference*, Sept. 29 – Oct. 2, Fort Worth, TX.

Yoon, J., He, D., Van Hecke, B., Nostrand, T., Zhu, J., and Bechhoefer, E., 2014, "Planetary gearbox fault diagnosis using a single piezoelectric strain sensor", *Annual PHM Conference*, Sept. 29 – Oct. 2, Fort Worth, TX.

AWARDS AND VOLUNTEER ACTIVITIES:

2nd Author of MFPT Society Runner-up Best Student Paper Award, May 2015

UIC Department of Mechanical and Industrial Engineering Professor Faydor Litvin Graduate Honor Award, June 2014.

2nd Author of MFPT Society Best Student Paper Award, May 2014.

UIC Graduate Student Council Travel Award, June 2014.

Volunteer member of the 2014 PHM society conference management team.

Prognostics and Health Management Society Doctoral Consortium Award, October 2013.

Peer reviewer for the Journal of Intelligent Manufacturing, Journal of Mechanical Engineering Science, IEEE Transactions on Industrial Electronics, IEEE PHM conference, and PHM society conference, April 2011- May 2015